ÉCOLE DE TECHNOLOGIE SUPÉRIEURE
UNIVERSITÉ DU QUÉBEC

DESIGN, DEVELOPMENT AND TESTS IN REAL TIME OF CONTROL
METHODOLOGIES FOR A MORPHING WING IN WIND TUNNEL

BY
Michel Joël TCHATCHUENG KAMMEGNE

MANUSCRIPT-BASED PRESENTED TO ÉCOLE DE TECHNOLOGIE SUPÉRIEURE
IN PARTIAL FULFILLMENT FOR THE DEGREE
OF DOCTOR OF PHILOSOPHY
Ph.D.

MONTREAL, JULY 28TH 2016

BOARD OF EXAMINERS

THIS THESIS HAS BEEN EVALUATED

BY THE FOLLOWING BOARD OF EXAMINERS

Dr. Ruxandra Mihaela Botez, Thesis Supervisor
Department of Automated Production Engineering at École de technologie supérieure

Dr. Martine Dubé, President of the Board of Examiners
Department of Mechanical Engineering at École de technologie supérieure

Dr. Vincent Duchaine, Member of the jury
Department of Automated Production Engineering at École de technologie supérieure

Dr. Franck Cazaurang, External Evaluator
Université de Bordeaux

THIS THESIS WAS PRENSENTED AND DEFENDED

IN THE PRESENCE OF A BOARD OF EXAMINERS AND THE PUBLIC

MONTRÉAL JUNE 21ST 2016

AT ÉCOLE DE TECHNOLOGIE SUPÉRIEURE

ACKNOWLEDGMENTS

VIII

least my dearest son Joseph Junior, for his pretty smile which helped me to stand up during all these challenges.

CONCEPTION, DEVELOPPEMENT ET TESTS DE LOIS DE COMMANDE EN TEMPS RÉEL POUR UNE AILE DÉFORMABLE EN SOUFFLERIE

Michel Joël TCHATCHUENG KAMMEGNE

RÉSUMÉ

Dans le souci de laisser aux générations futures un espace environnemental plus propre, c'est-à-dire moins pollué, la communauté internationale se mobilise afin de trouver des solutions écologiques, adéquates, efficaces et réalisables dans tous les secteurs d'activité. Cette thèse est .écrite dans le cadre du projet MDO505. Les principaux objectifs de ce projet sont : la fabrication et la conception d'un démonstrateur ayant un extrados rigide et déformable sous l'effet de force d'actionneur, l'extension et du contrôle de la zone laminaire au-dessus de l'extrados et comparer les effets aérodynamiques de l'aileron rigide et déformable. L'extension de la région laminaire a pour avantage de réduire la traînée en repoussant la région de transition au maximum vers le bord de fuite. La position de la région transition dépend des cas de vol et est contrôlée indirectement au travers de la position des actionneurs installés à l'intérieur de l'aile. De ce fait, le travail présenté ici se focalise sur le contrôle de la position des actionneurs.

Cette thèse rapporte essentiellement la modélisation, l'instrumentation, et les réalisations expérimentales en soufflerie. Trois phases de tests avec différentes valeurs d'angle de déflection de l'aileron, d'angle d'attaque et du nombre de Mach ont été réalisées dans la soufflerie subsonique du Conseil National de la Recherche du Canada (CNRC) sur un profil d'aile trapézoïdal. Le profil d'aile utilisé est constitué de plusieurs longerons, raidisseurs, nervure, d'une peau supérieure flexible faite en matériaux composite (fibre de carbone de verre), d'un aileron rigide capable balayer une plage d'angle allant de +/-6 degrés. L'envergure du démonstrateur mesure 1.5 m et la corde mesure 1.5 m.

Des analyses structurales ont été faites pour déterminer l'orientation des plis et le nombre de couches de fibres de verre nécessaires pour la peau en composite. Ces analyses ont permis aussi de déterminer les forces utiles à apporter par les actionneurs pour déformer l'extrados. Les profils aérodynamiques optimisés ainsi que la localisation optimale de la zone de transition pour chaque cas de vol ont été obtenus par le solveur XFoil en 2D et par Fluent en 3D. La combinaison des résultats des équipes aérodynamique et structurale ont permis de déterminer les actionneurs et capteurs à intégrer dans le profil d'aile.

Les actionneurs (4 au total) sont attachés sur les nervures et placés à l'intérieur de l'aile afin de déformer son extrados. Les actionneurs ont été commandés par un contrôleur dont les gains ont été obtenus avec différentes méthodologies. Les capteurs de pression (32 au total) fixés dans l'extrados permettent d'évaluer la zone de transition à partir des valeurs mesurées, analysées. Le code d'évaluation a été conçu par le LARCASE à l'aide du logiciel Matlab/Simulink.

X

Mots Clés: Soufflerie, commande, modélisation, simulation, actionneurs, conception, transition, aile, aileron.

DESIGN, DEVELOPMENT AND TESTS IN REAL TIME OF CONTROL METHODOLOGIES FOR A MORPHING WING IN WIND TUNNEL

Michel Joël TCHATCHUENG KAMMEGNE

ABSTRACT

In order to leave a cleaner environmental space to future generations, the international community has been mobilized to find green solutions that are effective and feasible in all sectors. The CRIAQ MDO505 project was initiated to test the morphing wingtip (wing and aileron) technology as one of these possible solutions. The main objectives of this project are: the design and manufacturing of a morphing wing prototype, the extension and control of the laminar region over the extrados, and to compare the effects of morphing and rigid aileron in terms of lift, drag and pressure distributions. The advantage of the extension of the laminar region over a wing is the drag reduction that results by delaying the transition towards its trailing edge. The location of the transition region depends on the flight case and it is controlled, for a morphing wing, via the actuators positions and displacements. Therefore, this thesis work focuses on the control of the actuators positions and displacements.

This thesis presents essentially the modeling, instrumentation and wind tunnel testing results. Three series of wind tunnel tests with different values of aileron deflection angle, angle of attack and Mach number have been performed in the subsonic wind tunnel of the IAR-NRC. The used wing airfoil consisted of stringers, ribs, spars and a flexible upper surface mad of composite materials (glass fiber carbon), a rigid aileron and flexible aileron. The aileron was able to move between +/-6 degrees. The demonstrator's span measures 1.5 m and its chord measures 1.5 m.

Structural analyses have been performed to determine the plies orientation, and the number of fiberglass layers for the flexible skin. These analyses allowed also to determine the actuator's forces to push and pull the wing upper surface. The 2D XFoil and 3D solvers Fluent were used to find the optimized airfoil and the optimal location of the transition for each flight case. Based on the analyses done by the aerodynamic and structural teams in the MDO5050 project, the most efficient actuators and pressure sensors to integrate inside the wing were selected.

The actuators (4 in total) are attached to the ribs and placed inside of the wing to deform the upper surface thereof. The actuators are controlled by a controller whose gains were obtained with different methodologies. Pressure sensors (32 in total) were fixed in the wing upper surface in order to estimate the transition zone from the measured and analyzed data. The evaluation code for raw pressure sensors data was designed at the LARCASE using the Matlab / Simulink software.

XII

TABLE OF CONTENTS

LIST OF TABLES

LIST OF FIGURES

Page

XXII

LIST OF ABREVIATIONS

ABS   Acrylonitrile butadiene styrene

CRIAQ   Consortium for Research and Innovation in Aerospace in Quebec

DARPA   Defense Advanced Research Projects Agency

DAQ   Data Acquisition

DC   Direct Current

FEM   Finite Element Method

FFT = Fast Fourier transform

IAR-NRC   Institute for Aerospace Research – Canadian National Research Center

IATA   International Air Transport Association

ICAO   International Civil Aviation Organization

LARCASE   Laboratory of Applied Research in Active Control, Avionics and Aeroservoelasticity

LVDT   Linear Variable Differential Transducer

PID   Proportional Integral Derivative

MDO   Multi-Disciplinary Optimization

mf   =   membership function

NASA   National Aeronautics and Space Administration

SMA   Shape Memory Alloy

STD   =   Standard Deviation

LIST OF SYMBOLS AND UNITS OF MEASUREMENTS

i_M	motor's winding current
U	motor's voltage
R	motor'S winding resistor
L	motor's winding inductance
e	induced voltage (back EMF)
k_e	speed constant
k_T	torque constant
ω_m	mechanical motor's speed
T_e	motor's torque
T_L	Load torque
J_{eq}	Total system inertia
i_M	motor current
k_e	angular speed constant
k_f	friction coefficient
k_t	torque constant
$C_i(s)$	current controller transfer function
$G(s)$	angular speed over voltage transfer function
$G_i(s)$	current over voltage transfer function
$G_{po}(s)$	open loop transfer function of the system controlled in current
$H(s)$	actuator transfer function

J	inertia
K_p	proportional gain in current controller
K_{pd}	proportional gain in position controller
L	motor inductance
M	Mach number
N	factor for transition positioning using the e^n method in XFoil code
$P_d(s)$	position controller transfer function
R	motor resistance
T_d	derivative time constant in position controller
T_e	motor torque
T_i	integral time constant in current controller
T_L	load torque
V	motor voltage
w_m	motor angular speed
α	angle of attack
ϕ	angular position of the actuator
B	friction coefficient
$E(s)$	PD position controller transfer function
E_k	induced voltage (back EMF) in the kth winding
F	function in back EMF equation
i_k	current of the kth phase
I	motor current
J	inertia

k_e	angular speed constant
k_t	torque constant
K_c	critical gain
K_e	back EMF constant
K_p	proportional gain in position controller
L	motor inductance
L_k	inductance of the kth winding
P_e	electric power
R	motor resistance
R_k	resistance of the kth winding
T_c	oscillation period
T_d	derivative time constant in position controller
T_e	electromagnetic torque
U	motor voltage
V_{ik}	line-to-line voltage
V_k	voltage of the kth phase
w	motor angular speed
θ	electrical rotor angular position
ω	rotor speed
dY_{opt}	desired vertical displacements of the optimized airfoil at the actuation points
dY_{real}	real vertical displacements at the actuation points
M	Mach number
α	angle of attack

XXX

δ	aileron deflection angle
a, b, c	parameters of the triangular membership functions
a_1^i	parameters of the linear function $f(x_1)$
A	fuzzy set in the antecedent
A_1^i	associated individual antecedent fuzzy sets of input variable
b_0^i	scalar offsets
B	friction coefficient of the load bearing
dY_{opt}	desired vertical displacements of the optimized airfoil at the actuation points
dY_{real}	real vertical displacements at the actuation points
e	back EMF
f	frequency
$f(x_1)$	polynomial function
$G_e(s)$	transfer function of the electrical part of the motor
$G_i(s)$	transfer function of the current controller
$G_m(s)$	transfer function of the mechanical part of the motor
$G_p(s)$	transfer function of the position based encoder controller
J	inertial load of the output motor shaft
k_e	angular speed constant
k_t	torque constant
K_{dp}	derivative gain in position controller
K_{it}	integral gain in torque controller
K_{pp}	proportional gains in position controller
K_{pt}	proportional gains in torque controller

L	motor inductance
M	Mach number
R	motor resistance
T_e	motor torque
T_L	load torque
u	voltage command
M	Mach number
α	angle of attack
δ	aileron deflection angle
ω_m	angular speed of the motor output shaft
x	independent variable on the universe of discourse
x_1	individual input variable
y	crisp function in the consequent
y^j	First-order polynomial function in the consequent
α	angle of attack
δ	aileron deflection angle
ω	pulsation
τ_e	electrical time constant of the motor
τ	constant
θ	motor shaft angular position
M	Mach number
α	angle of attack

δ aileron deflection angle

W_{to} Take-Off Gross Weight

INTRODUCTION

Air transport is a key factor, and one of the most used means of transportation of people and goods. In the Annual Report of Aviation Climate Solutions, it was specified that the airline industry supports the transport of close to 3.3 billion passengers annually, and an increase of 3 % is expected by 2050, which will be equivalent to around 4 billion. This increase is illustrated graphically in Figure 0.1. The growth in passenger numbers in air transportation has direct consequences from an environmental perspective.

Figure 0.1 Total regular traffic between 2002-2011
(Taken from ICAO council annual report 2011)

0.1 Environmental impact of aviation

Human actions release harmful gases to the environment from a number of different actions, including:

- Flaring (burning natural gas flares), producing electricity by burning fossil fuels or other fuel sources,
- Fires in forests during hot weather,
- Large-scale livestock (methane),
- Transportation (air, land, sea, etc.).

In its 2007 Report the IPCC (Intergovernmental Panel on Climate Change) estimated the amount of carbon dioxide (CO_2) emitted by the aviation sector to be approximately 2% of the

total CO_2 emitted annually. In the same report, the IPCC states that this amount will increase up to 3% in 2050.

0.2   Technological advancement

With the goal of preserving a healthy environment for future generations, a number of governments, in collaboration with industrial partners, research centers, and universities meet in numerous seminars and conferences to find new solutions or to enhance existing solutions, and to set common objectives for short, medium and long term research in these areas.

The development or improvement of technology in the previous decades has also benefited the aviation sector by allowing the aviation industry to save up to 35% in terms of fuel consumption reduction according to The IATA Technology Roadmap Report issued in June 2009. The study conducted between 1990 and 2008 showed a reduction of about 4.1 billion tons of CO_2, and thus a significant drop in fuels burnt, as reported in IATA Technology Roadmap 4th Edition in June 2013.

The IATA Technology Roadmap Report presented an estimated time frame for technological progress, and the different methods of fuel consumption reduction for the aviation sector. In the same report, the fuel reduction percentage estimation was presented for each technology. Table 0.1 shows the estimated fuel economy for the following technologies: Natural Laminar Flow, Advanced Fly-by-Wire, Electric Airplanes, and Morphing Material.

Table 0.1: Technology available for new aircraft designed before 2020
(Adapted from IATA Technology Roadmap, issued in June 2009)

Technologies	Fuel reduction
Laminar Natural Flow	5-10%
Advanced Fly-by-wire	1-3%
Morphing material	1-5%

The technologies presented in Table 0.1 were selected due to their similarities with the technologies presented in this thesis. The report recommended by IATA estimated that for a

passenger aircraft with 120 seats, and a takeoff weight of 60,000 kg, a full tank containing 24,000 liters would give a saving of 1% fuel (240 liters or 200 kg). The CO_2 reduction would offer significant financial savings over the long term.

In association with aircraft manufacturers and aviation service providers, IATA has fixed two main objectives: Reducing by 1.5% per year the amount of CO_2 starting from 2009 and continuing to 2020, and Halving the CO_2 amount for 2050 horizon from its 2005 level.

0.3   Morphing Potential Benefits

The "morphing wing" concept can be understood as the ability of a wing to change its initial shape in real time depending of the flight conditions. The targeted objective for using the morphing wing concept is to increase its aerodynamic performance.

The conventional aircraft wings are designed to be efficient during cruise. They are equipped with different control surfaces such as slats, flaps, spoilers and ailerons. These control surfaces are not considered as integral parts of the wing. They are attached to the wing with hinges; these hinges actually create discontinuities, and lower the aerodynamic efficiency of the wing because they induce turbulence in the air flow over the wing.

Morphing wings concepts require generally actuators or actuation mechanisms, sensors and a flexible skin. The power of the actuator, its force, weight, volume and size are important parameters to take into account in the wing design phase. The actuators not only support a structural load, but also an aerodynamic load, which is why they have to be self-locking.

Using the morphing concept, classical geometry-variation control surfaces (slats, flaps and ailerons) could be replaced by a flexible structure, an integral part of the wing, capable of producing a smooth variation of the wing's geometry. The morphing wing technique might give benefits in terms of significant drag reduction.

Studies realized at NASA (Sridhar, Osborn et al.) evaluated the saving cost for the U.S fleet of wide-body transport aircraft to be 140 million USD for a drag reduction of more than 1%. The amount of fuel cost saving is dependent of course on the flight distance.

0.4   Presentation of the CRIAQ MDO 505 project

Reduction of carbon emissions is one of the most important subjects, and is approached from different sectors. Each sector is required to find its appropriate technological solutions. In the aeronautical field, different paths could be followed to achieve the common goal of reducing fuel consumption:

- More efficient propulsion systems,
- Integration of light weight materials in aircraft manufacturing,
- Improved aircraft flight trajectories.

According to the classification proposed in the IATA report, some of these technologies need to be integrated into future aircraft. This integration becomes a great challenge for airplane manufacturers as they face issues of compatibility, reliability, profitability and certification for their systems. The ideal consensus for solving these problems is the manufacturing of a large-scale prototype, which can be tested and validated by experimental wind tunnel testing and further by flight tests. Thus, the CRIAQ MDO505 project was launched in 2012 and brought together students, researchers, and industrial experts to achieve the common goal of reducing aircraft fuel consumption by reducing its drag through an active morphing structure. Drag reduction was further validated experimentally by wind tunnel tests. The wing drag reduction was achieved by moving the laminar/turbulent flow transition region towards the wing trailing edge. The delaying of the flow transition allowed to obtain an extended laminar flow on the upper surface. Changes of the configuration of the wing airfoil had effects on the lift, and drag loads, as well as on the flow transition region. The turbulent flow was minimized as much as possible, thus less drag, and fuel consumption are obtained.

The CRIAQ MDO505 project was funded by both government and industry. The Canadian participating industrial companies were Bombardier Aerospace, Thales Canada, and the Canadian Research Institute IRA-NRC. This multidisciplinary project was international as it took place in collaboration with Italy. The Italian partners were Alenia, University of Naples and CIRA. The multidisciplinary aspect of this project was marked at the academic level in Canada by the collaboration between different teams at the ÉTS in Controls, Aerodynamics, Structures and AeroServoElasticity areas, and at the École Polytechnique in Montreal. The

flow diagram shown in figure 0.2 represents the contributions of all partners. The Italian team specific contribution was to design, manufacture and control a morphing aileron to increase its lift. The Italian team contributions are not included in this flow diagram.

Figure 0.2 Simplified flow diagram

The respective tasks were assigned to different teams early in the project, and are detailed forthwith. The structural team at the ETS and at the IAR-NRC were in charge of designing and manufacturing the wing and the rigid aileron. The LARCASE team, lead by Dr. Botez, the project leader, was in charge of the design and implementation of the control laws in open and closed loop, and of developing and conducting the aerodynamic studies for the characterisation and calibration of the pressure sensors installed on the morphing area of the wing upper surface. Aerodynamic studies were carried out at LARCASE to determine the desired aerodynamic airfoils shapes and the required displacements to be implemented by the actuators for the flight conditions for the experimental wind tunnel test; the team of IRA-NRC team was in charge of coordinating the wind tunnel tests at their wind tunnel facility, of

performing infrared measurements and loads measurements by use of their balance (''weighting system''). The tasks assigned to the Italian team were similar to those of the Canadian team, but they were applied to the morphing aileron. These tasks concerned the design, manufacturing and control of the morphing aileron.

For this project, an industrial trapezoidal wing demonstrator with a root chord of 1.5 m, a span of 1.5 m and a leading edge sweep angle of 8 degrees was designed and manufactured. It was also equipped of ribs and spars, two actuation lines located at **32%** and **48%** of the chord, respectively, and a trailing edge on which a morphing or rigid aileron was attached. The ailerons hinge is located at **72%** of the chord. The rigid inner part of the wing is manufactured essentially of aluminum, while a portion of the wing upper surface between **20%** and **65%** of the chord is made of a flexible skin. This flexible skin has been optimized, and was manufactured essentially of composite materials by the structures team at the ÉTS. It has been optimized to withstand structural tensile, compressive forces, and aerodynamic loads in the IAR-NRC wind tunnel. Thus, aero-structural research was carried out. Bench tests were also performed for 1 g loads in the absence of aerodynamic loads following Bombardier team requirements. Three sets of tests were conducted on the demonstrator at the IAR-NRC subsonic wind tunnel in Ottawa.

0.5   Overview of the subsonic wind tunnel where the tests were performed

The IAR-NRC wind tunnel is a closed circuit subsonic wind tunnel whose maximum speed is 140 m /s. The chamber of the test section measures 1.9 m x 2.7 m x 5.2 m (width x height x length). The turbulence rate was fixed at 0.14%. It is equipped with a cooling flow system during testing, which has a data acquisition and control system. This facility is also leased by other industrial and university partners.

The IAR-NRC wind tunnel is provided with a weighting system (balance) to measure all the aerodynamic forces and moments acting on the model installed in its test chamber. Thanks to the pressure taps installed in the test chamber, its static pressure can be measured. The information given in this subsection is provided by the website of the IRA-NRC (www.nrc-cnrc.gc.ca).

0.6   Objectives and originality of the controller

The global goal of the project is to extend the laminarity area over the upper surface of the wing. The extension of the flow laminarity is accomplished by changing the flexible skin shape of the wing upper surface. Actuators used for the wing upper surface shape change are controlled to maintain its desired shape position for any given flight condition.

To achieve the global objective of the project, the research work presented in this thesis is aimed to design and test a real time controller of the actuator displacements under any flight conditions. The actuators fixed on the ribs have to provide the necessary force to push/to pull on the skin and modify its aerodynamic airfoil shape that will be optimized for increase of aerodynamic performance of the wing. Different control laws were designed and experimentally validated in the IAR-NRC wind tunnel on the morphing wing.

The originality of the thesis consists in the numerical and experimental control of in-house electrical actuators used to change the morphing wing airfoil shape by use of different control methodologies. Two types of ailerons (conventional and morphing) were attached to the wing during three sets of wind tunnel tests. A set of thirty-two Kulite pressure sensors were integrated on the upper surface of the morphing wing to acquire the pressure fluctuation over the wing. Besides, the final adopted control architecture took into account the dynamic of the actuator's motor voltage amplifier. The objective is not only to compensate actuator's backlash, but also to synchronise both position sensors ("encoder" measuring the motor's shaft position and linear "position sensor" measuring the morphing skin displacement).

0.7   Issues of the research

The main challenge of the global project is to design and manufacture a reliable active demonstrator that fulfills the desired requirements: the aerodynamic efficiency (drag reduction, laminar flow extension or improvement) of the morphing wing should be improved.

The operating control system of the actuators used in the research project was entirely designed and manufactured at the ÉTS and is presented in this thesis. The development of a

control law for such an actuator control system with a precision of +/- 0.1 mm was in itself a significant challenge due to the presence of plays accumulated in the system after its assembly.

Regarding the system calibration there was a need to verify that the morphing skin moved exactly with the requested displacements set point. The dial indicators were installed outside the wing, as illustrated in Figure 0.3. Collected values of dial indicators, linear position sensors and skin set point requested or desired over time have shown that due to the flexibility of the entire system, dial indicators and linear position sensors values were different. The calibration of the system for each flight case by adjusting the linear position sensor set point was performed to overcome these issues. Another challenge constraint was the dedicated space available for the actuator's installation inside the wing.

Figure 0.3 Dial indicator fixed on the wing

0.8   Contributions

The main contributions in this thesis were mainly in the:

- Actuator Model Design,
- Control Schematics Architecture Experimental Validation during the bench tests at the ÉTS and during the wind tunnel tests at the IAR-NRC and at the LARCASE (Price-Païdoussis wind tunnel),
- Graphical User Interface (GUI) Programming to control the entire system, and
- System Integration to ensure the interaction between different software and hardware (control, communication, database) for wing and aileron.

Different methods were used to realize each step of these contributions. The actuator designed used in the thesis consisted essentially of two components: one electrical and one mechanical. The electrical component consisted in a motor with a gearbox, while the mechanical component included a gearing system, screw and nut. For the actuator model design, its electrical component was firstly designed, and secondly its mechanical component was added.

Figure 0.4 Equivalent model of the
actuator's motor and its Load

A brushless direct current motor was used in the actuator. This kind of motor has no brush and the commutation occurs through electronic commutation occurs. This definition is often referred in the literature as ''Electronically Commutated Motor''. The commutation board is made of a transistor or a Thyristor Bridge. The current flow through the switches is controlled by the digital output (0 or 1) of hall sensors fixed on the motor stator. The motor's rotor position is sensed by hall sensors.

Brushless direct current motors have the same behaviour as a direct current motor when two motor phases are conducting. Therefore, this motor can be modeled as a direct current machine having the equivalent circuit shown in Figure 0.4. The equations of the circuit shown in Figure 0.4 are the following:

$$J_{eq}\omega(t) + B\omega_m(t) = T_e(t) - T_L \tag{0.1}$$

$$u(t) = Ri(t) + L\frac{di}{dt} + e(t) \tag{0.2}$$

where J_{eq} is the total system (motor and load) inertia, B is the motor friction, ω is the motor's mechanical speed, R is motor's winding resistor, L is the motor's winding inductance, e is the electromotive force. The Laplace transformations of equations (0.1) and (0.2) can be expressed as follows:

$$J_{eq}\omega(s) + B\omega_m(s) = T_e(s) - T_L \tag{0.3}$$

$$U(s) = RI(s) + LsI(s) + E(s) \tag{0.4}$$

Then, the block diagram is obtained in the Laplace domain and is further shown in Figure 0.5. The steps used to obtain this block diagram are explained in details in the articles

inserted in this thesis. The load torque given in equation (0.1) is neglected in order to simplify the control design.

Figure 0.5 Motor block diagram

Equations (0.1) to (0.2) are used mainly to obtain the linear model of the actuator. This model is validated based on a comparison between the static values obtained in the simulation and those given by the datasheet of the manufacturer.

Different methodologies were developed in Matlab/Simulink to control the actuator, but not all of them were validated in both bench and wind tunnel tests. As mentioned above, because of the fact that the motor of the actuator is a brushless DC motor, it is equipped with a hall sensor that senses the rotor position. The motor position sensor is not enough to use as feedback signal for the position control for the skin displacement with the presence of plays inside the actuator. For this reason, **L**inear **V**ariable **D**ifferential **T**ransducer (LVDT) is coupled with the actuator to sense the skin displacement, and to reduce the influence of the plays.

A cascade structure with three different loops is chosen to be implemented as control architecture. The three distinct loops are: the innermost loop (first loop), that is the torque loop followed by the position controller (second loop) based on a hall sensor. Because of the fact that an accurate control position of the skin is needed, the outermost position (third loop) loop based on the LVDT is superposed on the hall sensor position loop

The controllers designed in this thesis are: a Proportional Integral (PI) controller for torque control, a Proportional Derivative for position control based on an encoder and two different Fuzzy Controllers for Position control based on Linear Variable Differential Transducer.

Fuzzy controllers are non-linear and, they were developed firstly in 1974. They are called "rule-based" controllers in the literature, because this control strategy describes a control protocol by means of rules. The rules describe the system behaviour observed by the machine operator. With the increase in the power of processors, this kind of controller is now being used in of different domains such as automotive, robotics and transportation. Fuzzy controllers consist of a Fuzzifier, an Inference system or a knowledge based system, and a Defuzzier. The Fuzzifier converts the crisp values (controller input) in its corresponding membership grade in the antecedent fuzzy sets. A Fuzzy set is composed by elements that are linguistic variables or linguistic terms. The output of the Fuzzifier uses rules stored in the knowledge based system to calculate the necessary input value for the Defuzzifier. The Defuzzifier's role remains converting the fuzzified values into a crisp signal or into process values, as shown in Figure 0.6.

Figure 0.6 Fuzzy Controller Components

In general, for a fuzzy control it is recommended to consider with three linguistic terms for each of its fuzzy inputs. The corresponding number of linguistic variables for the output is given by $2X - 1$, where X is the number of membership function of the input variables.

For the Proportional Derivative Fuzzy Controller, the interval considered for the error, and the error rate is [-12, 12] as shown in Figure 0.7, while the fuzzy rule is shown in Table 0.2. The linguistic terms for the inputs are: Negative Large (NL), Negative (N), Zero (Z), Positive (P) and Positive Large (PL).

Figure 0.7 Error Membership Functions

Table 0.2 Fuzzy rules table

	Error rate				
Error	**Negative Lage**	**Negative**	**Zero**	**Positive**	**Positive Lage**
Negative Lage	Positive very large	Positive large	Positive medium	Positive small	Zero
Negative	Positive large	Positive medium	Positive small	Zero	Negative small
Zero	Positive medium	Positive small	Zero	Negative small	Negative medium
Positive	Positive small	Zero	Negative small	Negative medium	Negative large
Positive Lage	Zero	Negative small	Negative medium	Negative large	Negative very large

The control surface shown in Figure 0.8 was generated after fixing the Fuzzy rules. The system behaviour constrained the controller to produce a linear shape. Because of its lower rise and settling time, as illustrated in Figure 0.9, compared to the Proportional Fuzzy Controller, only the latter Fuzzy logic control was validated experimentally in the wind tunnel.

Figure 0.8.Control surface for the PD-Fuzzy control

Figure 0.9 Comparison of PD- and P-Fuzzy control

Differential pressure sensors were used to measure the pressures on the wing upper surface. Some of the attractive properties of these pressure sensors are their light weight (0.2 g), their robustness in electromagnetic fields, and their amplified output signals with high precision (±0.5% of maximum measurement range) and resolution (0.1 Pounds per square inch (PSI)). The aim of these sensors is to identify the presence of the Tollmien-Schlichting waves in the flow that characterizes the laminar-to-turbulent flow transition. The piezoelectricity principle

is used in manufacturing these sensors and in the generation of an electrical signal at the output of the piezoelectric material when a mechanical effort is applied to it. The measurement range of the selected pressure measurement for transition is 5 PSI. This limit was chosen following aerodynamic calculations, where the maximum pressure was found to be for a morphing wing less than 5 PSI. The natural oscillation frequency is 150 kHz and the signal bandwith is 20 kHz. The characterization of the piezoelectric Kulite pressure sensors was realized by Manuel Flores Salinas.

Flutter analyses were performed by the aerodynamic team to ensure that no critical frequencies could appear during wind tunnel testing. To monitor the different frequencies when the wind was blowing, two accelerometers (one installed on the wing tips, and the other installed within the rigid aileron) were used. The program used to post-process the sensor data was written in Labview with the aid of Master students Vincent Rault and Yvan Tondji.

Following the introduction, the contributions, a literature review will be presented, that will show the evolution of the concept of the morphing wing in time. The literature review will be followed by published and submitted articles, written during this thesis. This thesis ends with a conclusion and recommendation for future work.

Chapter 2: Literature review.

This chapter presents a review of the state of the art in this field. An evolution of the morphing wing technology, description of actuators used for wing deformation, control strategies and materials used by various authors for morphing wing.

Chapter 3: Article 1.

Before the official start of the CRIAQ MDO505 project, another morphing wing type project has been initiated at the LARCASE laboratory. One of its objectives was to prepare and familiarize students with the following subjects for the CRIAQ MDO505 project:

- Morphing wing design,
- Theory of control logic,
- Actuator theory,

- Controller design, implementation and validation,
- Wind tunnel calibration,
- Data processing.

For this project, after manufacturing the test wing model, and after conducting wind tunnel calibration, the designed controller for the actuator was tested in the Price-Païdoussis subsonic wind tunnel located at ETS LARCASE in Montreal.

Chapter 4: Article 2

This paper presents the model of the actuator and its control methodology for the CRIAQ MDO505 project. In parallel, an experimental bench test was manufactured, and further used to validate the experimental controller. The experimental control was designed to be used in wind tunnel facility. The experimental results showing the controller's functionality were demonstrated. During the bench tests at the LARCASE no aerodynamic load was applied on the skin. The structure of control validated on the bench at LARCASE is illustrated in Figure 0.10. Due to the system repeatability the offsets values are determined to compensate the permanent static error. The offset values are not the same for all flight cases. The LVDT values are added to the controller's output in order to maintain the reference values (pink color in Figure 0.10) constant for the control architecture within the motor voltage amplifier.

Figure 0. 10 Control architecture on bench test at LARCASE

Chapter 5: Article 3

This paper explains the experimental results of the controller in terms of infrared measurements obtained at the IAR-NRC wind tunnel facility. Aerodynamic loads were applied on the model in this context. Thirty eight flight cases were tested. The Mach number varies between 0.15 to 0.25, angle of attack from -3 to +3 degrees, and aileron angle deflection from -6 to +6 degrees.

Chapter 6: Article 4

Article 4 focuses on the design of the linear model and its control. The proposed model represents the exact architecture, also as well as the simplified architecture of the control software tested in wind tunnel. The validation of the actuator numerical model was carried out by comparing numerical with experimental data. Besides, further wind tunnel results in terms of infrared measurements are shown.

Chapter 7 Article 5

The reasons for developing a parallel control system for position control were illustrated. The methodology used to post-process the wind tunnel acquired data was explained and comparisons in term of transition point position detected between pressure sensor and infrared tests were pointed out.

CHAPTER 1

RESEARCH APPROACH AND THESIS ORGANIZATION

1.1   Thesis research approach

In this thesis, research was performed in two multidisciplinary projets at the LARCASE, called ''ATR-42 morphing wing'' and '' MDO505''. The thesis concentrates on the research done by the control team in the frame of these multidisciplinary aero-structure-control projects.

The global objective of the research in the frame of the CRIAQ MDO505 project, is to enhance aerodynamic performances by controlling the wing shape in real time according to flight conditions, and it achieved by division of the research into 5 phases:

- Determining the most suitable actuator and actuation mechanism for the morphing wing;

- Actuator and its controller design,

- System integration and calibration,

- Controller validation on the bench test with no aerodynamic load; and

- Controller validation in a wind tunnel.

Before the official start of the CRIAQ MDO505 project, the ''ATR-42 morphing wing'' project, on the realization of the adaptive upper surface morphing concept for the ATR-42 wing , was initiated at the LARCASE in 2011.

In both multidisciplinary projects work was performed on the controller in collaboration with aerodynamics and structural teams. In both projects, in which the aerodynamic studies were performed firstly by the aerodynamic team to determine the optimal wing shape configuration and the actuator displacements. In parallel to the aerodynamic optimization, an aero-structural optimization method was developed. The goal of this optimization procedure was to reduce the composite skin weight while ensuring a good approximation of the targeted aerodynamic shapes. The skin optimization process aimed to respect the industrial partners'

requirements. Analytical validation methods used to test the structural integration were able to determine the stiffness, the bucking and strength of the morphing wing.

The CRIAQ MDO505 project is essentially a continuation of the ATR-42 and CRIAQ 7.1 projects, focusing on extending the laminarity over a flexible wing upper surface where an actuation mechanism combined with four actuators are integrated inside the wing. To determine the actuator for the MDO 505 project feasibility studies and constraints analyses were performed by the structural team. The constraints analysis made it possible to determine the minimal height of the actuator to best fit inside the wing. The minimal height is the smallest distance between the inner and upper surfaces. The required actuator force was evaluated by the structural team during its static linear analyses with HyperMesh. Adding a security factor of 1.5 the value of 1500N was established. Studies were done by LARCASE and the structural team to select the best motor and gearbox for the actuator, that were designed and manufactured by David Barry (Master student). Figure 1.1 shows the actuator assembled with no **L**inear **V**ariable **D**ifferential **T**ransducer (LVDT).

Figure 1.1 Manufactured in-house actuator

Subsequently, the capacity of the actuator to support at least the maximum load was validated in a traction/compression test apparatus at ETS as illustrated in figure 1.2.

Figure 1.2 Actuator during robustness test at the ETS

To validate our actuator's performance, a series of four tests were conducted, and an automatic cyclic program to move the actuator between +/- 3 mm was coded in Labview. During the first series of tests, the machine pulled on the actuation moving at 16% of its nominal speed with a force from 750 N to 1500 N. Wear has been observed inside the screw, but the actuator resisted well to the applied load. These results proved the robustness of the actuator and its ability to be integrated inside the wing in order to obtain aerodynamic optimized shapes for each flight case.

In a first approach, a nonlinear numerical model (due to the shape of the back emf) of the actuator, and its control were realized, based mainly on the data provided by the manufacturer in the datasheet. This approach was not validated experimentally because the annual licence cost for the software to use in conjunction with the corresponding hardware was too high and we couldn't buy it. This approach would have offered a very good algorithm validation with the dedicated hardware. But after some experimentation it was observed that much time would be required to replace the shipped BLDC motor with one of

the morphing actuator and to write the necessary code. Additionally it was required also to develop LVDT interface and necessary code for data acquisition.

In a second approach, a linear model of the actuator and its control was developed. Different control logic concepts were tested, and further validated experimentally on a bench test in the absence of wind, and in a wind tunnel. The disadvantage of this approach resides in the consideration of constraints on designing a linear control imposed by the hardware (motor's voltage amplifier). A configurable linear cascade control architecture (controller's gains could be changed) was implanted by the hardware (motor's voltage amplifier) provider. This architecture made it possible for different existing linear methods such as Bode diagram, Ziegler Nichols, and pole cancellation to be adapted for the morphing wing application. These methods were further utilized to obtain the appropriate gains for the controllers. The following parameters were assumed for the control modeling:

- Maximum steady state error of 0.1 mm,
- Rise time between 1 and 2 seconds),
- No load disturbance,
- Unity feedback, and
- Total inertia that consists in the sum of motor and gearbox inertia.

The software and hardware integration was carried out at the LARCASE. A number of different functions were developed and compiled, and a large amount of code was generated for the software integration. Subsequently, the compiled functions were deployed into the real time target. A total of 5 different codes were generated, and linked with each other.

Bench tests in the absence of winds, at the LARCASE, and wind tunnel tests were conducted to verify the controller's performance, to assess the system and software integration, and to test the system's response in the extreme conditions. The wind tunnel tests took place in the Price-Païdoussis wind tunnel at the LARCASE ETS in the frame of the ''ATR-42 morphing wing'', and in the IAR-NRC wind tunnel in Ottawa.

1.2 Thesis Organization

Several journal articles and conference papers are published, accepted for publication, and under review based on the methodologies and results obtained in the bench and wind tunnel tests and simulations. Five articles were submitted in peer-review journals. Two of the journal articles have been published, and three other articles are under review. Chapters 3 to 7 each present one of these journal articles.

Dr. Ruxandra Mihaela Botez, as co-author of all journal and conference papers supervised the progress and the realization of the research. In all five papers, co-author Lucian Grigorie contributed with his experience acquired in the previous CRIAQ 7.1 project as postdoctoral fellow in terms of constructive discussions on control issues. In chapter 3, co-author Andreea Koreanschi PhD student created the aerodynamic shapes with the corresponding actuator displacements by use of XFoil code. In Chapters 6 and 7, co-authors Mahmoud Mamou and Youssef Mébarki from IAR_NRC coordinated the interactions between all teams during the wind tunnel tests, and they also performed and post-processed the infrared and load (lift, drag. moments) measurements. Co-author Yvan Tondji (Master student) assisted in the pressure sensor data (Kulite) post-processing and in its interpretation, by using its in-house software coded with Matlab/Simlink. On paper (see section 2.2.1) was published on the ATR-42 project, and the other four papers were published on the CRIAQ MDO505 project.

1.2.1 First journal paper "Design and Wind Tunnel Experimental Validation of a Controlled New Rotary Actuation System for a Morphing Wing Application"

Presented in Chapter 3 and published in the *Proceedings of the Institution of Mechanical Engineers Part G Journal of Aerospace Engineering*, this paper concentrates on the design and implementation of a controller for a rotary actuator, and its experimental validation on a morphing ATR-42 wing. The comparison between the numerical pressures calculated by the 2D solver XFoil, and the experimental pressures is also performed.

In this paper, the model of the actuator was considered to be linear with the aim to simplify the design of the controllers. A cascade loop was designed, and further implemented. The torque loop is followed by the position control loop. Current controller gains were obtained

with the Bode diagram method, while Ziegler-Nichols method was used to compute the position controller gains. The relationship between the actuator's displacement in degrees and the vertical displacement in millimeters was measured with a Coordinate Measuring Machine (CMM) at ÉTS. Pressure taps installed on the wing were used to measure the static pressures over the wing, while the wind tunnel static pressure was measured with a Pitot tube. The pressure taps were connected to a signal processing unit which displayed the pressure values, and the pressure coefficient values were using Excel. Experimental results were presented Mach number equal to 0.2 and for different angles of attack between -1 and 1 degree.

1.2.2 Second journal paper "Design, numerical simulation and experimental testing of a controlled electrical actuation system in a real aircraft morphing wing model"

Inserted in Chapter 4 of this thesis, this paper was published in *the Aeronautical Journal* on September 2015. It explained a nonlinear model of the actuator and its control that was not validated on a bench test. It presented also the experimental bench test results in the absence of winds by using the non-linear model of the controller that was turned essentially based on the system's behaviour. Thirty-eight flight cases were tested and for each flight an offset was obtained and used to modulate the requested actuator position. The offset values were permanently the same due to the system's repeatability. The modulation purpose of the requested set points was to eliminate the static error for each flight case. This approach was improved later by considering the encoder signal in the control.

1.2.2 Third journal paper "Experimental Validation of a Morphing Wing Control System in Open Loop"

Presented in Chapter 5, this paper has been submitted to the *Chinese Journal of Aeronautics* and is currently under review. For the first series of wind tunnel tests, a number of 38 flight cases were tested. The real time system was installed on the wind tunnel balance which was connected with the morphing wing demonstrator. This journal paper presents essentially the results obtained during the first wind tunnel tests. The results were expressed in terms of Fast Fourier Transformation (FFT) and Root Mean Square (RMS) for the pressure sensors, and

infrared measurements. In general, it has been observed that the flow as laminar flow extended closer to the trailing edge. Based on the observations during the first set of wind tunnel tests, it was recommended that for the second series of wind tunnel tests, the extension of the infrared recording time for each flight case (flow stabilization) and the increase of the number of flight cases tests.

1.2.3 Fourth journal paper "Control of the morphing actuation mechanism integrated in a full-scaled portion of an aircraft wing"

Presented in Chapter 6, this paper has been submitted to the *Aerospace Science and Technology*, and is currently under review. In the second paper journal (Chapter 4), a nonlinear model of the actuator was shown, which was not validated experimentally because of the expensive license cost and additional work to accomplish on the dedicated hardware (CM408F DSP). To address these lacunae, the fourth paper proposes a linear model of the actuator with its control. The control architecture (triple loops) represents exactly the architecture used in the wind tunnel. The model has been validated experimentally on a bench test with the dedicated hardware. Wind tunnel results for the second test series are presented, for the suggestions after the first wind tunnel test were taken into account. A slight improvement in terms of infrared measurement results was observed. For the second series of wind tunnel tests for the flight case 68, pressure sensors revealed a transition delayed of 9 % of the chord. The transition for the non-morphed case was detected at 44% of the chord and at 53 % of the chord.

1.2.4 Fifth journal paper "Morphing wing demonstrator tested in a subsonic wind tunnel in open loop configuration"

Presented in Chapter 7, this paper has been submitted to the *Aerospace Science and Technology*, and is currently under review. In the control architecture presented in the fourth article (chapter 6), two loops were focused on position control by use of an encoder and a LVDT. This paper denotes in details the reasons that led to the development of two position loops instead of a speed and position loop as it was implemented in conventional motor drives. LVDT was selected as a solution to measure the skin displacement and to compensate backlash (play) inside the actuation. The post-processing of the pressure sensors data

collected during was done with software developed at the LARCASE. The details regarding the software code were explained in details in this article and infrared measurements for the second set of flight cases have been also presented. For the second series of wind tunnel tests for the flight case 70, pressure sensors revealed a transition delayed of 8 % of the chord. The transition for the non-morphed case was detected at 43% of the chord and at 51 % of the chord.

CHAPTER 2

LITERATURE REVIEW

This chapter briefly summarizes the different works that have been done on the morphing wing, including its development and testing over the last ten years. The basics of the boundary layer concept (essential in aerodynamics) are presented first. The origins of the morphing, the different types of morphing in terms of geometry, the various methods of control of the boundary layer are presented, as well as the actuators and materials used in the realization of wing morphing.

2.1　　Boundary layer (basic concept)

Aerodynamics basic principles were mainly defined in the boundary layer studies. The boundary layer is defined as the area where there is fluid flow between a solid body, for which the flow velocity is zero and the other speed of the fluid flow at infinity. It was described analytically by Prandtl in 1905. The boundary layer is the flow attached close to the wing of an airplane. Inside the boundary layer, the velocity of fluid flow rapidly varies from zero to the free flow speed, while the effects of fluid viscosity are greater. Figure 2.1 shows a flow over a plate where the boundary layer shown is exaggerated for clarity.

Figure 2.1: Flow of fluid over a plate
(Adapted from Cohen Kundu and Fluid Mechanics, 5th Edition)

Laminar flow characterized by a uniform velocity profile becomes turbulent when the Reynolds number is greater than the critical Reynolds number. Thus there is a laminar

boundary layer and a turbulent boundary layer where the frictional drag is much greater than for the laminar boundary layer. This frictional drag is undesirable for any aircraft, since it degrades the performance of its wings, and therefore of its entire structure. The area bounding the two laminar and turbulent flows is called the transition flow region.

The morphing wing concept is one solution (among many others) put forward to act against the degradation of the aerodynamic performance caused by the induced drag in the boundary layer. Using this technology, the aerodynamic performance can be improved by pushing the transition point towards the trailing edge. Wing morphing achieves this transition delay by changing the wing shape in real time according to the flight conditions.

2.2   Morphing wing origin

Work on wing morphing, especially on changing aircraft wing configurations for different missions and objectives, started with the beginning of modern aviation by the Wright brothers in the early 1900s. The cables fixed by them on the wings allowed lift variations, and improved further the controllability of the aircraft during flight, as illustrated in figure 2.2

Figure 2.2 Wright brothers airplane
(Adapted from Alban Dignat, public domain)

Following the concept introduced by the Wright brothers, the morphing wing concept has progressed significantly in the last decade in terms of research work accomplished by many other researchers in the field. From these research works, it has been observed that two categories of concepts can be distinguished: 'morphing wings with radical geometry change'

and 'morphing wings with smooth geometry change'. Both categories target the same objective: to increase the wing performance and aircraft maneuverability over the whole flight envelope. Thanks to the more recent technological advances, most of these studies have been focused on the second category.

2.3   Morphing Wing airplane with radical surface change

A drastic change of wing configuration makes it possible to increase or improve aircraft flying performance over the flight envelope. Such variations facilitate the adaptation to a new mission. This kind of morphing requires a large-scale change of parameters such as the span, wing area and sweep angle. (Jha and Kudva 2004) revealed that NASA and Defense Advanced Research Projects Agency (DARPA) initiated a program with the aim to accomplish different missions during a single flight. The designers focused on achieving a wing structure capable of a 200% change in aspect ratio, 50% variation in wing area, 5° degree variation in wing twist and close to 20° change in wing sweep angle.

Morphing wings with radical wing change can be classified in different categories depending in which plan the deformation or wing variation takes place. The deformation can therefore be 'in-plane morphing' and 'out-of-plane morphing.

2.3.1   Out-of-plane morphing

(Abdulrahim and Lind 2004) got inspiration from the nature to design and manufacture a morphing wing vehicle with wings similar to gull's seabird wing to better understand the effect of this kind of wing configuration on the flight characteristics of a reduced scale aircraft, and to investigate its aerodynamic benefits. To imitate the roll control implemented in the Active Aeroelastic Wing (AAW) Flight Research Program by (Pendleton, Bessette et al. 2000), the demonstrator was equipped with an articulated wing-tip mechanism that modified the outboard area of the twisting wing, and further maintained the flexibility of the structure, while maintaining roll control. The authors only used a linear actuator fixed on the fuselage, and a jointed spar system to realize all the desired wing configurations typically observed on seagulls.

Between 2003 and 2006, Lockheed Martin Aeronautics Company developed an advanced morphing program with the DARPA with the objective of performing a morphing technology maturation activity (Bye and McClure, 2007). A number of different entities (DARPA, Lockheed Martin, Air Force Research Laboratory, and NASA) collaborated in this program to realize the common vision of developing and testing Morphing Aircrafts Structure (MAS) in a wind tunnel environment. A Z-wing morphing unmanned aerial vehicle was developed and manufactured as a result of this program. The drastic change of the wing configuration and the morphing system operation, including actuators, was validated using a large-scale half span wind tunnel model.

Studies were conducted by (Sridhar, Osborn et al. 2006) at the Air Force Research Laboratory to analyze the behaviour of a variable camber trailing edge in a Natural Laminar Flow (NLF) for a High-Altitude and Long-Endurance (HALE) aircraft. The use of a compliant mechanism in conjunction with a low-power active system contributed to extend the laminar boundary layer over a wide range of lift coefficient. It was observed from wind tunnel test flight data that laminar flow extension was visualized over about 60% of the airfoil chord, so that the endurance airplane expanded its flight envelope by at least 15% by permanently optimizing the wing aspect ratio.

(Powers, Webb et al. 1992) at the NASA Dryden Flight Research Center have changed the baseline wings of the F-111 aircraft with the aim to be used in advanced fighter technology integration (AFTI). In fact, they have replaced the variable sweep wings with smooth variable camber in order to improve the flight envelope margins of the aircraft. Both the leading and the trailing edges were able to be modified smoothly to obtain the best suitable camber shape for any flight condition. Leading and trailing edge motion was accomplished in a controlled manner via instrumentation for wing pressure measurement, accelerometers, position and strain gauges, and transducers. A flight deflection measurement system and a boundary-layer rake were also employed. Experimental investigations revealed that the modified version of the F-111 (AFTI/F-111) gave a higher improved flight performance compared to that of its baseline version (F-111A).

A belt rib concept was proposed by (Campanile and Sachau 2000) to realize a camber change to accomplish wing morphing. The new concept permitted a camber change within given limits by keeping unchanged the stiffness properties of the section. Experimental tests were conducted on a fabricated model to verify the adaptability and the overall stiffness properties of the system's shape. (Strelec, Lagoudas et al. 2003) conducted a feasibility study to integrate SMA actuators within a morphing airfoil. Optimal SMA placement inside the reconfigurable airfoil was based on a developed optimization technique. To have the maximum lift to drag ratio for a new generated airfoil at subsonic flow conditions, (Strelec, Lagoudas et al. 2003) used a cost function which take into account the aerodynamic properties of the airfoil. Wind tunnel tests revealed an improvement in lift for different angles of attack when SMAs were powered on or actuated and a good match between measured and numerical pressure data was observed.

(Stanford, Abdulrahim et al. 2007) achieved also a roll control on a small UAV by applying wing twisting. Actuators were linked to the wing, to enable it to perform free motion. The actuation mechanism consisted mainly of torque rods installed along the wing span, and embedded within the wing membrane. When they were actuated, the wing tip was twisted to form an L-shaped rod. This system achieved a good correlation between the wind tunnel test data and the numerical results.

Another morphing concept to control transonic flow, and to reduce total drag was proposed by (Lee, Srinivas et al. 2012). Natural Laminar Airfoil (RAE 5243) was used as baseline airfoil. Its conventional trailing and leading edges were replaced by edges that could be morphed. Two approaches were developed. One approach was to morph either the trailing edge, or the leading edge, while the second approach consisted in morphing both the leading and trailing edges. Numerical simulations predicted a better drag reduction for the second morphing approach design compared to the baseline design.

(Zingg, Diosady et al. 2006) conducted a study for drag reduction at transonic speeds at the Institute of Aerospace Studies at the University of Toronto. They proposed an optimization algorithm to determine the percentage of drag reduction that could be achieved, as well as the

values of displacements needed to change or to modify the airfoil shape. Two studies were conducted on a baseline airfoil. In an initial study, the results (drag reductions) for a baseline airfoil were compared successively with results obtained on nine different airfoils optimized at a single operating point; drag reductions of 4-6% for shape changes were obtained. In the second approach, an optimized airfoil was obtained through a multi-point optimization over eighteen optimizations points.

Flying at transonic speeds means that shock waves are occurring. The shock waves can have a negative influence on the flow over the wing, as they increase the drag. To deal with this issue, (Sommerer, et al. 2000) proposed a controlled bump able to have different configurations. Using this principle, the Mach number can be decreased locally in front of the shock wave, so that the supersonic flow would decelerated due to subsonic flow, and would allow the wing to be shock free. In this case, the local sink of the flow was implemented by induced isentropic compression waves that created a pre-shock compression.

Optimization study has been realized by (Martins and Catalano 1998) aiming to estimate the potential advantage by using an adaptive variable camber morphing wing concept in a jet transport airplane. For this optimization, they have tested two camber variations: camber changing around the trailing edge, and around the leading and trailing edges. The results obtained showed a fuel efficiency increase up to 7.03% for the first camber variation case, that increased up to 24.6% in the second camber variation case. The optimized camber profile was given by a direct function optimization program linked to a viscous-inviscid airfoil analysis routine.

Many authors proposed carrying out plan-form morphing. The plan-form includes the span, chord length and sweep angle of the wing. The next paragraph describes some of these studies of plan-form morphing concepts.

2.3.2   Planform morphing

Many different techniques involving mechanical systems could be used to resize the wing span, including mechanical systems with telescopic actuators and scissor mechanisms. (Neal,

Good et al. 2004) proposed a span-wise segmented wing using a mechanism based on telescopic pneumatic cylinder actuators to achieve two different configurations: 1. a fully retracted, and 2. a fully extended wing. Wing compression and extension were realized in the span-wise direction, so that the wing's cross sectional area was reduced from the wing root toward the wing tip. One segment has slided into an adjacent segment, thus it changed the span length. Their experiments realized with a wing model revealed a span variation of about 38%. This work used a direct current (DC) motor as an actuator to perform planform morphing. The proposed morphed concept was designed to change the span and sweep angles, and the experiments revealed that a wing span geometry has also changed significantly.

The Bell X-5 was the first aircraft equipped with a system allowing the wing to change its sweep angle in-flight. It was inspired from the FP.1101 developed by the Germans after the Second World War. Three static sweep angles of 20, 40 and 60 degrees could be accomplished during flight. The Bell X-5 was able to go from its maximum to its minimum sweep angle within 30 seconds (Wikipedia, 2016).

The F-14 fighter jet was a bioreactor developed in 1970 for the United States Navy. The pilot was able to change the wing sweep angle to improve the control manoeuvrability of the fighter for supersonic and transonic speeds. In 2006, the US Navy decided to renew its fleet and retired this fighter from the market (Wikipedia, 2016).

The main problem in morphing technology is to have a structure that is capable of resisting aerodynamic and structural loads, while is also being flexible enough to achieve the desired configuration or shape. Following developments in smart materials, active materials (actuation systems) were embedded in the structure, or composite materials. Composite materials are often used not only for wing shape changing concepts, but also for other components of the aircraft (in the fuselage, stabilizer, etc...), and other purposes. The composite material covers the surface to morph. Under the surface, an array of actuators and actuation mechanism were installed to push or pull the wing flexible skin (made of composite materials).

2.4 Actuator type and actuation mechanism for the wing shape change concept

Actuation mechanisms and morphing concepts are often linked. This means that to realize a deformation on compliant materials (a morphed skin) which covers a wing section, an actuation mechanism, in conjunction with actuators, should be used to push or pull the compliant structure.

Any type of aircraft or UAV can be a potential candidate for implementing the morphing technology; for exemple AMADOR (2003) developed a morphing-compliant mechanism system for its UAV vehicle. It was a three degree of freedom mechanism based on the Stewart Platform Parallel Manipulator. Two adjacent ribs were linked by a linear hydraulic actuator, and a middle spar was introduced between ribs to increase the stiffness of the structure. Numerical studies of the system revealed that a maximum force of 60 N could produce a 20 mm maximum actuator displacement. It was also observed that with such a configuration, a maximum morphing of 21 degrees in pitch, 20 degrees in yaw and 6 degrees of roll could be achieved.

(Munday and Jacob 2002) used piezoelectric actuators integrated inside a structure to control the boundary layer over the upper surface of a wing. The idea was to maximize the lift-to-drag ratio to enhance the wing efficiency. Their experiments revealed that for the non-morphed case, flow separation occurred at 8 degrees of angle of attack, and for the morphed case, the flow separation occurred at 14 degrees with the actuator located between 55% and 75% of the chord length.

Another study was conducted by (LeBeau, Karam et al. 2010). A modified THUNDER (Thin Layer Composite Uni-Morph Ferroelectric Driver and Sensor) actuator initially fabricated by the NASA Langley Research Center was used to change the shape of a profile based on the NACA 4415. In order to obtain a flexible and smooth wing surface, a latex membrane covered it. By exciting the actuators with a voltage of about 300 V, a wing upper surface deflection was detected via the instrumentation. The authors observed promising results in a

wind tunnel with this type of actuation system. The higher the oscillation frequencies were, the later the flow separation appeared.

The morphing wing benefits were observed by altering both its upper and lower surface. This study, carried out in Singapore by (Debiasi, Bouremel et al. 2013), used Macro Fiber Composite actuators to alter the upper and lower surface of a NACA 0014 airfoil. These MFC actuators were incorporated inside the skin of the upper and lower surface of the airfoil. Then, wind tunnel experiments were conducted. From the experimental results, it was concluded that the aerodynamic performance of the symmetric constructed airfoil was enhanced by changing the shape of its upper and lower surfaces.

(Vos, Barrett et al. 2007) realized a feasibility study to evaluate the use of a Post-Buckled Pre-compressed (PBP) piezoelectric actuator to change the camber line of a wing, and improve roll control. The ability of the bimorph actuator to change significantly the wing camber, was proven by developing a Newtonian deflection model. A demonstrator with two sets of actuators covered with a flexible latex skin was fabricated. Flight test results showed a 38% increase in roll control. It was concluded that the utilization of PBP was promising, as, in addition to the increased roll control, the actuator weight and its power consumption were both less than those of conventional actuators for ailerons used for the roll control.

From the multidisciplinary project CRIAQ 7.1 initiated in 2006 to advance morphing wing technology, a new approach for the design methodology to finalize the geometry and the design of the actuator (Shape Memory Alloy) used in the project was proposed by (Georges, Brailovski et al. 2009). The novel design approach was based on the constrained recovery tests of the actuator. The design was followed by an experimental validation on a bench test with a demonstrator equipped with a flexible extrados made of laminated composite and Shape Memory alloy actuator.

An array of piezoelectric fiber composite (MFC) actuators bonded on a wing surface was utilized to perform a control platform for active wing shape morphing. More than one objective was targeted: to increase lift, reduce induced drag, improve roll maneuver and wing

root moment. (Li, Yuan et al. 2011) concluded that their proposed approach presented more advantages over a conventional wing mainly due to the torsional properties of MFC.

In contrast to (Li, Yuan et al. 2011), where a non-bimorph MFC was used, a new approach was proposed by (Bilgen, Kochersberger et al. 2009) with a bimorph MFC. The active surfaces were constructed with eight MFCs in a bimorph configuration. The expected goals were to obtain a bi-directional camber change of the airfoil, and to improve aerodynamic wing performance by controlling the flow over the wing upper surface. The manufactured airfoil had a chord of 127 mm, and a 133 mm span. Wind tunnel test instrumentation was used to measure the displacements of the skin active surfaces using MFCs. A lightweight amplifier controlled by a National Instrument DAQ (Data Acquisition) card powered the corresponding actuators. The voltage at the output of the amplifier was verified by two digital multimeters, and the skin displacement was measured with a laser sensor. Due to the high force provided by the actuation mechanism, a 72% increase in the slope of the lift curve was observed.

(Barbarino, et al. 2010) suggested a novel flap configuration to realize a variable camber trailing edge morphing. The flap was considered as an integral part of the rib structure. The proposed compliant mechanism was a truss-like structure with active rods made of SMA as active materials. The system configuration was derived from preliminary optimization studies, and the stiffness of the structure was evaluated using the FEM (Finite Element Method) coupled with a Vortez Lattice Method (VLM) in Matlab. The desired optimal shapes were created by a genetic algorithm, accordingly to its optimization variables and constraints. The numerical results showed an improvement of the lift coefficients.

In the same perspective, (Strelec, Lagoudas et al. 2003) carried out a study to determine a suitable location of the SMA within the wing. They used a global optimization method based on a genetic algorithm to determine an efficient solution for the actuator location. Their proposed genetic algorithm combined two different methods: a global, and a local search method. To verify the structural and aerodynamic behaviour of the wing, a demonstrator was manufactured based on the design optimization, and evaluated in a wind tunnel. The

experimental tests revealed an increase in lift for each flight condition tested, and further, a good match (validation) of the measured pressure with the predicted numerical pressure was observed.

(Bilgen, Friswell et al. 2011) presented a new design of a variable-camber morphing airfoil with the particularity to use an actuator made of Macro-fiber composite material. The optimized airfoil was able to move smoothly in both direction by using active surfaces and pinned boundary conditions. For the new approach the airfoil surface was wrapped with a single substrate, which was used as host material for the bimorph actuators. For flow control a technique using surface-induced deformations to reshape the wing configuration has been designed. The research objective consisted in understanding the effects of four structural parameters (leading edge thickness, substrate's thickness under the morphing section, and two pins locations) on the lift coefficient and the lift-to-drag ratio. Numerical results showed a highest lift coefficient (1.79) one pin location at 10% of the chord and the second one at 55 % of the chord while the maximum lift-to-drag ratio (40.3) was observed for the first pin located at 10 % of the chord, the second pin at 55 % of the chord.

The fact that the wing alternation was not fixed, but changed with the flight conditions, was due mainly to a smart system integrated inside the wing. The smart system consisted of a set of actuators, electronic devices and sensors which communicated between each other in real time to accomplish an instantaneous task, such as 'morphing'. Mostly, the electronic system integrates the control unit. The control unit is an entity that could be found either directly on the market, or it could be developed by a research team. Some authors chose the second alternative, to develop, test and apply a different control technique for the actuators used to change the wing configuration. This thesis follows the second approach.

2.5   Control technique developed for the morphing wing actuator

One motivation for developing specific control logics is to have full control over the controller parameters, and thus to have the ability to test different kinds of logic (linear and non-linear). The type of actuator used for the morphing wing would need an appropriate design of a controller model for it.

A morphing wing project developed at the University of Sydney in Australia tested three different kinds of controllers, all of which used actuators incorporating Shape Memory Alloys SMA (Abdullah et al. 2011). In the first part of their project, (Abdullah, Bil et al. 2009) used a Finite Element Method to predict the optimized airfoil shape, and the effectiveness of the SMA to control it. The wing camber change was considered because of the fact that the trailing edge could be morphed. In (Abdullah, Bil et al. 2010), a real model of an adaptive wing was proposed based on the Finite Element Method results. SMAs installed underneath the wing were used as actuators, and Acrylonitrile butadiene styrene (ABS) material was used as the wing manufacturing material. Wind tunnel experiments revealed an increase of lift coefficient when the wing was morphed. SMAs actuators were fixed at the leading edge of the wing. The goal of the project was to morph the wing trailing edge shape, while keeping the leading edge fixed, and thus to reduce the drag, and consequently, the fuel consumption throughout the flight envelope. The controllers were essentially linear: PID, PID-compensated and PID compensated with Anti-Wind-up. The PID coefficients were obtained with the Ziegler-Nichols technique. The PID-compensated improved the PID in terms of *response time* and *static error*. Because the actuators had a physical limitation expressed in the sense that the electrical current flowing in the actuator could not be indefinitely high (as needed by the SMAs), a *non-linear element* was incorporated into the model. The role of the non-linear element was to maintain the control signal of the actuator between its maximum and minimum values. The *saturation element* served to protect the actuator against any kind of electrical warming. With the saturation element added to their models, two of the designed controllers (PID and PID-compensated) were not more able to fulfill their requirements. To overcome this situation, a PID Anti-windup controller version was designed. The latter was faster in term of rise time, and its final static error was less than 5%. The PID compensated with Anti-windup was tested in a subsonic wind tunnel. The aerodynamic coefficients revealed a decrease of the drag for small angles of attack. For an angle of attack of 0 degree, the drag reduction observed was about 20%.

In the Consortium for Research and Innovation in Aerospace in Quebec project (CRIAQ 7.1) realized at the Laboratory of Applied Research in Active Control, Avionics and

Aeroservoelasticity (LARCASE) in collaboration with Bombardier, Thales, and Ecole Polytechnique, which was briefly summarized in (Botez, Molaret et al. 2007) the performance of a WTEA-TE1 wing airfoil equipped with a morphing skin between 7% and 65% of the airfoil chord was evaluated in the IARC-NRC subsonic wind tunnel between 2006-2009. The rest of the wing model was rigid, made in aluminium. A number of 49 flight cases with Mach numbers $M = 0.1$ and $M = 0.3$ and angle of attack between $\alpha = $ -2 degrees and $\alpha = 3$ degrees were tested in a wind tunnel. The flexible skin was a 4-ply composite overlaid shell that was equipped with two actuation lines. The first line of actuators was located at 25% of the chord, and their second line was located at 48% of the airfoil chord. The optimization structural procedure of the flexible upper surface for the WTEA-TE1 airfoil was explained by (Coutu, Brailovski et al. 2010). Different possible targeted structure configurations were obtained by using the Finite Element Method, while the laminar flow improvement was evaluated with the 2D aerodynamic solver XFoil. The purpose of the project was to delay the transition on the upper wing by controlling the flow. The flexible skin was driven with an actuation cam mechanism coupled to a spring. The mechanical system was based on a cam principle, and the maximum deflection of the skin was of +/- 8 mm. To reproduce a smooth shape closer to its numerical aerodynamically equivalent shape, it was decided to allow one side of the skin slide freely, as illustrated by (Coutu, Brailovski *et al.*, 2011).

By controlling the actuators, the skin could change the wing airfoil shape to its desired shape. Different control techniques were tested and validated in the IAR-NRC wind tunnel. For the SMA used in the CRIAQ 7.1 project, the steps used to obtain the non-linear and linear models were explained in (Grigorie, Popov et al. 2011). The non-linear model utilized a numerical Finite Element Method (FE) using Lickhatchev's theoretical approach, while the linear model was obtained using Matlab's System Identification Toolbox.

Different controller methodologies were performed in the CRIAQ 7.1 project. One of them developed by (Grigorie, et al., 2011) included the design of an ON-OFF controller, where in the ON (heating phase of the SMA) phase, a Proportional Integral law performed the control

action, and in the OFF phase (cooling phase of the SMA) the control action was forced to zero (the controller was de-activated).

After developing the final control architecture, the next step was to physically integrate, and validate the developed controller in the experimental wind tunnel testing. The numerical simulations and experimental tests were described by (Grigorie, *et al.*, 2012). They concluded that the SMAs were able to reach the desired displacements for different aerodynamic loads. During experimental tests in the IAR-NRC wind tunnel, the transition point visualization was carried out using the infrared technology, and showed the temperature gradient obtained between the laminar and turbulent flows.

Kulite sensors were installed on the flexible skin upper surface of the wing, that was used in the CRIAQ 7.1 project; these sensors have captured (measured) the pressures characteristics from the flow over the wing. The post processing methods and results of the raw Kulite data were described by (Popov, Grigorie et al. 2010). Applying the Fast Fourier Transformation on the raw Kulite data allowed obtaining the spectral distribution of the waves contained in the flow, while applying the Root Mean Square (RMS) to detect the highest amplitude variation of the pressure signals that characterized the laminar to turbulent flow transition.

(Grigorie, Botez et al. 2012) suggested a Bi-Positional On-Off, and a Proportional Integral Derivative (PID) Fuzzy Logic Controller as a variant to the Proportional Integral Derivative (PID) proposed by (Grigorie, Popov et al. 2012). Three membership functions were used for each input signal. For the command signal (controller output), a total of five membership functions were chosen. The shapes of the membership functions were not the same. A total of nine rules were designed to achieve the desired control objective. Two switches introduced in the controller scheme were controlled through the error signal. Therefore, the first switch was turned ON for positive error signal, and the second switch was turned ON when the SMA temperature became higher than the temperature limit.

The numerical evaluation of the controller designed by (Grigorie, Botez et al. 2012) indicated promising results for both SMA phases (cooling and heating phase). The correlation between the controller parameters, and the system variables (temperature and force) were verified and

followed by experimental bench tests at the LARCASE. Two programmable switching power supplies were used to control in Matlab/Simulink the electrical current flowing through the actuator. For the 35 optimized flight cases tested, a maximal static error of 0.05 mm was observed. Suitable controller behaviour was observed for the unloaded wing, and for a preloaded gas spring force of 1000 N (Newton).

Two different closed loop control strategies to directly control the shape were designed and validated during the wind tunnel tests that took place at the IAR-NRC. The principle was to directly control the shape based on the information from pressure sensors. This control strategy was labelled "closed loop", while the control strategy based on the information from position sensors was called "open loop" because the shape was not directly controlled. (Grigorie, Popov et al. 2012) proposed a summary of the control methods employed to obtain a closed loop for the transition flow controller in the CRIAQ 7.1 project. More details about the functionality and the experimental results obtained during the LARCASE bench tests and NRC wind tunnel tests are provided in (Grigorie, Popov et al. 2014), (Grigorie, Popov et al. 2011) and (Grigorie, Popov et al.). An optimized airfoil corresponding to each flight condition was loaded from a predefined database.

The pressure coefficient distribution of the optimized airfoil from the previous study was found through the 2D solver Xfoil implemented by (Drela et al. 1989). The pressure sensors selected to use for feedback controller information were those located closer on the actuation lines. The set points for this morphing architecture or configuration were the pressure coefficients calculated by XFoil. Therefore, once the controller was activated, the skin was morphed until the measured pressure coefficient values of the selected feedback sensors matched the desired pressure coefficient values. The closed loop controller was designed by multiplying the open loop controller's error by 10.

For the optimized closed loop control, the optimized airfoils database was not taken into account. The morphing shape airfoils were computed in real time through an optimization function. Three optimization methods (gradient ascent, hill climbing, and simulated annealing) were combined to achieve the control objective. An optimization subroutine was

used to compute iteratively, a set of eight transition locations and to generate the displacement of the actuation line. The maximum value of the transition was saved for the next iteration, where it was used as the starting transition point value. Experimental results revealed that the open loop control strategy, which was considered as the first control method, was better for airfoil shape reproduction and aerodynamics than the closed loop control method. The advantage of this closed loop control method was the 'direct control of the skin through the pressure coefficient', and the main disadvantage of the"optimizer closed control" was its long convergence time with respect to the other methods, and its dependency on its starting point.

CHAPTER 3

DESIGN AND WIND TUNNEL EXPERIMENTAL VALIDATION OF A CONTROLLED NEW ROTARY ACTUATION SYSTEM FOR A MORPHING WING APPLICATION

Michel Joël Tchatchueng Kammegne[1], Lucian Teodor Grigorie[2], Ruxandra Mihaela Botez[3], Andreea Koreanschi[4]

[1,3,4]Départment de Génie de la production automatisée, LARCASE Laboratory of Applied Reasearch in Active Controls, Avionics and Aeroservoelasticity, École de Technologie Supérieure, 1100 rue Notre Dame Ouest, Montréal, H3C1K3, Québec, Canada
[2]Université de Craiova, Strada Alexandru Ioan Cuza 13, Craiova 200585, Roumanie

Résumé

Cet article présente la conception et la validation expérimentale d'un régulateur de position pour une aile déformable. Le mécanisme d'actionnement utilise deux moteurs à courant continu pour faire tourner deux arbres excentriques qui déforment une peau flexible de deux lignes parallèles d'actionnement. L'objectif de la commande développée est de contrôler le profil d'une aile pour différentes conditions de vol. Le type de correcteur pour satisfaire cet objectif utilise un algorithme de type Proportionnel-Dérivé. Outre la description du correcteur, cet article met également en évidence une description détaillée du système, de la structure du système d'actionnement ainsi que la validation expérimentale de la loi de commande conçue. Afin de valider les résultats numériques aérodynamiques obtenus en simulation, une comparaison a été effectuée entre les coefficients de pression obtenus numériquement et ceux obtenus suite aux mesures en soufflerie pour différentes conditions de vol. Une autre comparaison a été réalisée entre les positions mesurées et les positions simulées de la peau flexible de l'aile.

44

Abstract

The paper presents the design and the experimental validation of a position controller for a morphing wing application. The actuation mechanism uses two DC motors to rotate two eccentric shafts which morph a flexible skin along two parallel actuation lines. In this way, the developed controller aim is to control the shape of a wing airfoil under different flow conditions. In order to control the actuators positions, a Proportional-Derivative control algorithm is used. The morphing wing system description, its actuation system structure, the control design and its validation are highlighted in this paper. The results, obtained both by numerical simulation and experimental validation, are obtained following the control design and its validation. An analysis of the wind flow characteristics is included as a supplementary validation; the pressure coefficients obtained through numerical simulation for several desired airfoil shapes are compared with those obtained through measurements for the experimentally obtained airfoil shapes under different flow conditions.

3.1   Introduction

Technology progress enables human kind to improve his environment. Obviously, the aeronautical industry benefits from this continuous engineering evolution. Innovative solutions such as soundless propulsion systems will be embedded in future aircraft. In addition, the composite materials used in aircraft manufacturing will be more needed. These needs are essential for aircraft design. Another main need is the reduction of airplane fuel consumption. This need is seen in green technology development that has the aim to improve the aircraft performance while reducing fuel consumption. Morphing wing technology is a solution to reach this target. A lot of research studies are being carried out to reduce the fuel consumption by reducing drag, which is directly related to the airflow type around the aerodynamic aircraft body design. The drag reduction concept is connected to the laminar flow improvement and to the displacement of the transition point between laminar and turbulent flows towards the trailing edge. According to IATA technology roadmap report, it is predicted a fuel burn reduction from 5% to 10% thanks to morphing aircraft technologies.

As numerous studies proved the transition between laminar and turbulent flows on an aircraft wing, it is clear that the flow transition is strongly influenced by the shape of the wing airfoil. Also, it is very well known that, due to the air viscosity, for a flight condition characterized by a given Mach number and Reynolds number, the airflow is laminar starting from the leading edge of a wing airfoil and becomes turbulent at a certain point on the wing airfoil chord. Such turbulent flow is not desired, because of its negative effect in terms of drag increase, which, over time, leads to high fuel consumption, reflected directly in the operating costs levels. Following these research findings, during the last years a strong research trend was developed in this area, having as target the study of the possibilities to modify the shapes of the wings airfoils in order to promote large laminar regions on the wing surface, over an operating range of flow conditions characterized by Mach numbers, airspeeds, and incidence angles; the generated concept was called 'morphing wing'. These research studies were developed around the world, both at industry and university levels. The obtaining of such active systems supposes a high number of aerodynamic optimization studies combined with mechanical structural flexible skin materials design, actuation system and automatic real time control design, implementation and instrumentation. For this reason, the involved work teams are multidisciplinary in order to ensure the needed complementarities of such projects. A short review of the literature shows a lot of morphing architectures conceived for this kind of studies, developed at low or high scale, with different actuation and control principles, and optimized by using different cost parameters and functions.

The optimization of a morphing wing based on coupled aerodynamic and structural constraints was performed by researchers at Universidade da Beira Interior, Portugal. (Gamboa, Vale et al. 2009) designed a morphing wing for a small experimental unmanned aerial vehicle (UAV) in order to improve its performance over its intended speed range. The wing was designed with a multidisciplinary design optimization tool, in which an aerodynamic shape optimization code coupled with a structural morphing model was used to obtain a set of optimal wing shapes for minimum drag at different flight speeds.

With the target to be used on small-sized and medium-sized unmanned air vehicles in order to increase range or endurance for a given fuel load through improved lift-to-drag ratio, a

morphing wing project was developed at the School of Aerospace, Mechanical and Manufacturing Engineering, RMIT University, Melbourne, VIC, Australia by (Bil, Massey et al. 2013). The camber line of an airfoil section, that is the predominant parameter affecting lift and drag, was changed by resistive heating of a shape memory alloy actuator, and cooling in the surrounding air. Experiments were conducted under wind tunnel conditions to verify the analysis results and to investigate their effects on the aerodynamic behavior of the wing.

To vary the geometry of a wing to adapt to different flight conditions, (Moosavian, Xi et al. 2013) specialists from Ryerson University, Toronto, Canada designed a novel under-actuated parallel mechanism. It can be set up in a modular fashion with the aim to offer controlled motion in all six spatial degrees of freedom, while providing multiple degrees of fault tolerance with only four actuators. The main feature of the design consisted in the use of active and passive linearly adjustable members to replace the structure of a conventional wing box. Also, an optimal motion control algorithm for minimum energy actuation was developed based on the kinematics and statics of the mechanism.

At University of Southampton, UK, the design of spinal structures for the control of morphing airfoils was realized by (Ursache, Keane et al. 2006). The aim was to find structures that, when suitably loaded, can alter the aerodynamic shape of a cladding that forms the airfoil. Morphing through different cambered airfoils to achieve aerodynamic properties for different manoeuvres was then possible by exploiting a range of incremental non-linear structural solutions.

(Majji, Rediniotis et al. 2007) developed another morphing wing project at Texas A&M University, where the wing consisted of an elastic structure (ABS plastic material) covered with an elastomeric skin. The aerodynamic models of the wing were developed using Prandtl's Lifting Line Theory, and were validated using wind tunnel tests. It was found that the operating envelope of the angle of attack of the wing was enhanced by the twistable wing sections.

A collaborative research between the specialists of the School of Aerospace Engineering, Beijing Institute of Technology, and the Department of Aerospace Engineering, School of

Engineering, Cranfield University, designed and tested a morphing wing integrated with a trailing edge control actuation system. To achieve a desirable flexible trailing edge deflection for optimal aerodynamic performance of the wing, (He and Guo 2012) developed an actuation mechanism that was integrated in a section of the morphing wing. The mechanism was made of a curved torque tube connected between an actuator and the trailing edge skin structure through discs. The research results demonstrated that the morphing wing integrated with the flexible trailing edge control surface can improve aerodynamic characteristics.

An approach for optimal airfoil-morphing design based on a compact approach to describe the airfoil geometry coupled to a two-level optimization procedure was developed by (De Gaspari and Ricci 2011) at Dipartimento di Ingegneria Aerospaziale, Politecnico di Milano. In the first optimization level, the requested energy to deform the airfoil skin was used as cost parameter to obtain the best configuration of the morphed airfoil shape. The second optimization level used an ad hoc developed topology optimization tool based on genetic algorithms. The tool synthesized a compliant structure able to adapt itself in order to match the optimal shape obtained at the first level.

The use of a new class of flight control actuators employing Post-Buckled Pre-compressed (PBP) piezoelectric elements in morphing wing of Uninhabited Aerial Vehicles was demonstrated by a collaborative research team from Faculty of Aerospace Engineering, Delft University of Technology, and from the Department of Aerospace Engineering, University of Kansas. (Vos, Barrett et al. 2007) implemented the actuation concept that relies on axial compression to amplify deflections and control forces simultaneously. The concept was tested on two different structures; then, both bench test and wind tunnel test results provided significant benefits of the using of this kind of actuators to induce aircraft control.

The 3D aerodynamic performance (roll moment) of morphing wing based on the compliant belt-rib concept was evaluated by (Previtali and Ermanni 2012), researchers of the Swiss Federal Institute of Technology Zurich, Composite Materials and Adaptive Structures Lab. New methods for optimal placing of the actuation and for the quantification of the morphing were used on the in house designed compliant morphing wing made of composite materials.

The results have shown coupling effects between wing twist and section shape change, having as a consequence the obtaining of a lower performance for 3D than the expected one from the 2D calculations. However, the 3D wing aerodynamic efficiency was improved with 10%.

In a study performed by a multidisciplinary research team from National University of Singapore and from School of Mechanical & Aerospace Engineering, Nanyang Technological University in Singapore, macro fiber composite actuators were used to change the shape of an airfoil wing model. The piezoelectric actuators were bonded to the inside and became an integral part of the airfoil flexible skin. This study was performed in two phases, the first one (Debiasi, Bouremel et al. 2012) assumed the actuation of the upper surface of the airfoil, while the second one (Debiasi, Bouremel et al. 2013) assumed the actuation of both upper and lower surfaces of the airfoil. The results from wind tunnel tests concluded that this kind of morphing wings may be used successfully for maneuvering the wings without ailerons, and/or for active control of the flow over the wing in order to have an aerodynamic efficiency improvement. Similar studies, based on macro fiber composite actuators, were realized by (Bilgen, Kochersberger et al. 2013) researchers of Mechanical and Aerospace Department at the Old Dominion University, USA.

In other morphing wing projects, initiated by (Zhao, Schmiedeler et al. 2012), from the Department of Aerospace and Mechanical Engineering, University of Notre Dame, IN, USA and from the Department of Mechanical and Aerospace Engineering, University of Dayton, OH, USA, designed a planar rigid-body mechanism, containing both prismatic and revolute joints, able of approximating a shape change defined by a set of morphing curves in different positions. The design procedure was demonstrated with a synthesis example of a 1-DOF mechanism approximating eight closed-curve wing profiles.

3.2   Our morphing wing experience

Having in mind the previous shortly presented research context, in a previous research project called CRIAQ 7.1, our laboratory research team (Research Laboratory in Active Controls, Avionics and Aeroservoelasticity (LARCASE) - ETS in Montreal, Canada)

coordinated the design, manufacturing and wind tunnel experimental testing of a morphing wing equipped with Smart Material actuators. Bombardier Aerospace, Thales Canada, École de Polytechnique and the Institute for Aerospace Research at the National Research Council Canada have collaborated in this project in which the laminarity of an airfoil was extended by delaying the transition point according to the report proposed by (Botez, Molaret et al. 2007). The experimental wing model was a rectangular one (0.5 m x 0.9 m), having two parts: 1) a metal fixed one, designed to sustain the wing loads; and 2) a morphing part, consisting of a flexible skin installed on the upper surface of the wing. The morphing part was actuated by two shape memory alloys actuators (SMA) (Figure.3.1) to realize the desired optimized airfoil shapes obtained in a preliminary aerodynamic study for thirty-five airflow conditions as combinations of seven angles of attack (between -1˚ and 2˚) and five Mach numbers (between 0.2 and 0.3) ((Grigorie, Botez et al. 2012),(Sainmont, Paraschivoiu et al. 2009)). (Coutu, Brailovski et al. 2007), (Popov, Grigorie et al. 2010) manufactured the flexible skin. It was made of a 4 plies laminate structure in a polymer matrix, with two unidirectional carbon fiber inner plies and two hybrid Kevlar®/carbon fiber outer plies. At the same time, in the final configuration, 12 Kulite pressure sensors were disposed on the flexible skin in different positions along of the chord as illustred by (Grigorie, Botez et al. 2012).

(Grigorie, Popov et al. 2010, Popov, Grigorie et al. 2010, Popov, Grigorie et al. 2010, Grigorie, Botez et al. 2012) designed three control methods to obtain and maintain the optimized airfoils during the experimental tests performed in the wind tunnel: 1) The first method used a database stored in the computer memory, database which contains all the 35 optimized airfoils correlated with the 35 airflow cases. In this way, the method was based on a controller that took as reference value the necessary displacement of the actuators from the database in order to obtain the morphing wing optimized airfoil shape. As feed-back signals were used the position signals from some LVDT sensors connected to each actuator. Because with this kind of control, the information from the pressure sensors installed on the upper surface of the wing was not used in the control loops, this method was associated with an "open loop control" method. To achieve the desired skin displacement, different control algorithms were used with the smart actuation system for this method. 2) The second method

used a similar controller as the first method, but the control loop was built around the changes of the pressure coefficients values calculated by XFoil in two fixed positions along the chord of the wing. The fixed positions were associated to two Kulite sensors linked through aerodynamic interdependence with the actuators positions. Therefore, as feedback signals for the control loop, were used the pressure signals coming from two Kulite sensors linked to the actuators. The control loop commanded the actuators by using the power supplies until the differences between the theoretical pressure coefficients C_p values and the measured C_p values were zero. Because this method used the pressure information from the Kulite sensors in the control strategy, it was called "closed loop control". 3) The third control method was based on the pressure information received from the sensors and on the transition point position estimation. It included, as inner loop, the first control method of the actuation lines. Thus, the previously calculated optimized airfoils database was by-passed in this control strategy. The method used an optimizer code which has found the best actuators configuration in order to maximize the position of the transition, i.e. at the end of optimization sequence, the transition should be founded nearest possible to the trailing edge. For this purpose, the entire array of Kulite sensors was used to give feed-back about the transition position. This method was called "optimized closed loop control".

Figure 3.1 Morphing wing model in CRIAQ 7.1 research project

For all experimentally tested control strategies and control algorithms, the bench tests and wind tunnel tests have shown that the morphing wing controller worked very well in real time. During wind tunnel tests, a drag reduction up to 22% and a transition point delay by up to 30 % of the chord were observed, while lift was kept constant as illustrated in (Sainmont, Paraschivoiuvet al. 2009). The proposed and tested control algorithms were based on various control techniques, classical or unconventional. (Grigorie and Botez 2009) proposed a control algorithm technique based on adaptive neuro-fuzzy inference system that was designed to obtain the actuator position set-point from the difference between the pressure coefficients of the optimized airfoils and the pressure coefficients of the original airfoil. An On-Off and proportional-integral controller to morph the flexible skin was designed and experimented by our team, and then disseminated in (Grigorie, Popov et al. 2011) and (Grigorie, Popov et al. 2012). (Grigorie, Popov et al. 2012) made a numerical analysis and experimental validation of a hybrid controller based on fuzzy logic and Proportional-Integral-Derivative (PID) algorithm to ensure proper SMA actuator displacements. In (Popov,

Grigorie et al. 2010), (Popov, Grigorie et al. 2010), (Grigorie, Popov et al. 2014), the results of different control algorithms recorded during wind tunnel tests were presented and discussed.

As general conclusions regarding the actuation mechanism and control methods over all experimental tests performed during the previous CRIAQ 7.1 project, we can mention:

- the SMA proved a strongly non-linear behavior with a slow dynamics;

- the SMA has responded only to heating or cooling, i.e. pass electrical current or no electrical current: fast response in heating (~10 sec) and slow response in cooling (~1-2 min);

- to energize the SMA, high electrical power was needed (10A/15V DC);

- the SMA working temperatures for necessary actuation forces were higher than 70 Celsius degrees;

- the wind tunnel test revealed that the first control method ("open loop control" method) results were better from the point of view of the desired airfoils shape reproduction in front of the second control method ("closed loop control"). Also, this method proved more accurate from the point of view of aerodynamic results ahead of the second method;

- regarding the third control method ("optimized closed loop control"), the experimental tests showed a convergence time higher than 10 minutes due to the slow response of the SMA actuators especially in the cooling phase of the cycle.

3.3 Our new morphing wing application in this paper

Usually, in aircraft systems, to actuate control surfaces such as slats, flaps, ailerons, elevators and landing gear, hydraulic systems are used. This category of actuators has the big disadvantage to increase the aircraft weight. The actual trend in field is to use linear or rotary electrical actuation systems instead of the hydraulic ones, as they have the advantage to be lighter. For this reason, in our first morphing wing project we tried to use this new actuation concept, based on smart material actuators, which uses electrical power to be activated, supplied and controlled. Although the project was a real success, proving a significant progress vis-à-vis of all integrated technologies, but also vis-à-vis of the aerodynamic efficiency gain through the controlled morphing of the wing, some limitations were found in

using SMA actuators in a morphing wing on a real aircraft: high operating temperatures, slow response and high need in electrical power to obtain the desired actuation forces. On the other way, with theirs small sizes and higher efficiency, the electrical linear or rotary actuators proved an easier integration in aircraft systems relative to other types of actuators. Equipped with electrical motors, which are usually combined with various mechanical components such as a ball screw, belt and pulley, and rack and pinion to convert the motor rotation to a different type of motion needed, such actuators are also characterized by a higher stability in operation, offering accurate controlled displacements of the actuated devices. According to (Janocha 2013), (Gomis-Bellmunt and Campanile 2009) another advantage of linear and rotary actuators over the hydraulic and pneumatic actuators is the providing of smooth acceleration and deceleration operations.

For this application, the control method used in this work is the first one described in Section 2. In this article, the control loop uses the position of the electric actuator measured with the encoder instead with a Linear Variable Differential Transducer (LVDT). Pressure taps are combined to an acquisition device described in Section 3 to acquire manually the pressure. The acquired pressures were processed to obtain pressure coefficients. The calculated pressure coefficients from the acquired pressures were compared with the predicted pressure coefficients by XFoil code to validate the aerodynamic predictions.

The here presented work describes a new morphing wing application developed by using an actuation mechanism based on some electrical rotary actuators. Shown are: the actuation mechanism architecture, the actuator modeling, the actuator control system design (the current controller and the position controller), and the controlled morphing wing experimental testing in wind tunnel. The morphed wing airfoil was an ATR-42 one and its experimental tests were performed in the Price-Païdoussis wind tunnel at LARCASE Laboratory - ÉTS in Montreal, Canada.

3.4 Actuation mechanism architecture

In this study, the wing upper surface is modified by an electro-mechanical system, as shown in figure 3.2. This structure of the actuation mechanism system has been chosen because the

volume of the available space (about 4549 cm^3) was not enough to place directly a commercial actuator inside the wing. The mechanical system consists of two eccentric shafts coupled to two DC motors used as actuators. The first actuation line is located at 30% of the chord and the second at 50% of the chord. The main role of the eccentric shafts is to transform the rotational motion of the actuator into vertical displacement to modify the shape of the flexible skin. The ATR-42 wing has an airfoil chord of 24.9 cm and a span of 60.9 cm. The flexible skin equipping the wing can be morphed between 10% and 70% of the chord, and is made of composite materials. As detailed in (Michaud, Joncas et al. 2013), the upper and lower surfaces of the wing are made of glass/epoxy composite. The used fibers were JB Martin's UD TG-9U fibers. A total of 8 plies were used for the flexible part of the upper surface. To connect the lower and upper surface together, a structural compound was used. The skin was optimized to support the maximal actuator loads. The methodology to improve the structure and functionality of the skin was based on finite element modeling.

Figure 3.2 The actuation mechanism

In order to obtain an optimized reference for the morphed airfoil, some numerical optimizations were performed by our team for several flight conditions as combinations of Mach numbers (*M*) and angles of attack (α). For each flight condition, the numerical

simulation software provided a 2D optimized shape for the airfoil, and, in this way, a pair of vertical displacements associated to the horizontal positions of the two actuation lines (figure 3.3). As a consequence, our team proceeded to the design of the eccentric shafts according to the resulted database of vertical displacement pairs covering all the simulated flight conditions. The literature review had shown us that it is the first time when an electrical rotary actuator is used directly to control the shape of an airfoil under different flow conditions.

Figure 3.3 ATR 42 morphing airfoil coordinates (chord in millimeters)

3.5   Actuator modeling

As we already mentioned, to move the two eccentric shafts, two DC motors were used as actuators. The use of this type of actuators (electrical) was more beneficial for the aircrafts in terms of weight. Usually electrical actuators weights are smaller than the weights of the hydraulic actuators. The weight of the electric actuators used in this research was 1.8 kg. As a preliminary step in the design of the control system for our morphing wing, we need to have a mathematical model for the actuators. This model should be further software implemented, integrated and numerically tested together with the rest of the morphing system components. Having in mind the characteristics of this kind of actuators, their behavior can be described by the next equations

$$V = L \frac{\mathrm{d} i_M}{\mathrm{d} t} + R i_M + k_e w_m,$$

(3.1)

And

$$T_e = k_f w_m + J \frac{d w_m}{d t} + T_L, \tag{3.2}$$

where V is the motor voltage [V], R - motor resistance [Ω], L - motor inductance [H], i_M - motor current [A], W_m - motor angular speed [rad/s], k_e - angular speed constant [revolution/min/V], T_e - motor torque [N·m], k_f - friction coefficient [N·m/(rad/s)], T_L - load torque [N·m], J – inertia [Kg·m^2]. The electromechanical model of the two actuators can be seen in Figure 3.4.

Laplace transform of equations (3.1) and (3.2) give

$$V(s) = LsI_M(s) + RI_M(s) + k_e W_m(s), \tag{3.3}$$

respectively,

$$T_e(s) = k_f W_m(s) + Js W_m(s) + T_L(s), \tag{3.4}$$

where s is the Laplace operator.

In the absence of loads (for $T_L = 0$), and by considering $T_e(s) = k_t I_M(s)$, equation (3.4) becomes

$$k_t I_M(s) = k_f W_m(s) + Js W_m(s), \tag{3.5}$$

from where, the current in the armature of the actuator is written under the form

$$I_M(s) = \frac{Js + k_f}{k_t} W_m(s); \tag{3.6}$$

k_t is the torque constant [Nm/A]. Therefore, the equation (3.3) of the motor voltage can be rewritten as follows

$$V(s) = (Ls + R)I_M(s) + k_e W_m(s) = (Ls + R)\frac{Js + k_f}{k_t} W_m(s) + k_e W_m(s), \tag{3.7}$$

Finally, the angular speed over voltage transfer function is written as follows:

$$G(s) = \frac{W_m(s)}{V(s)} = \frac{k_t}{JL \cdot s^2 + (RJ + k_f L)s + k_f R + k_e k_t}. \tag{3.8}$$

Figure 3.4 Electromechanical model of the actuator

The parameters provided by the manufacturer in the product datasheet were: terminal resistance R =11.4 Ω, terminal inductance L=0.0316 H, torque constant k_t =0.119 N·m·A^{-1}, inertia J_{eq}=65.9e-7 Kg·m^2, and friction coefficient k_f =1.01738·10^{-5} Pas. A validation step of the actuator simulation model was based on the comparison of the datasheet values for the motor electrical current (i_M) and for the motor speed (W_m) with the values obtained from numerical simulation. The obtained values confirmed the validity of the model, the datasheet and simulation values being the same: i_M=34.2mA and W_m=3820 rpm.

3.6   Control system design and analysis

The study is focused on the development of the position control. Although position control is desired, it is needed to integrate a torque control to guarantee that the right torque is always supplied to the load by the motor. Torque control is realized with a current controller. Therefore, the architecture of the whole control system (position control, current control and load) can be organized as in figure 3.5. The figure shows that the inner loop is realized by the

current controller, while the external loop is realized by the position controller. The actuator voltage is provided by a programmable source voltage. Unit feedbacks are used to determine the errors for both controllers. The current set-point or reference is provided by the position controller. Overvoltage protection is integrated inside the current controller in order to protect the actuator.

Having in mind equation (3.5), the motor speed can be calculated as

$$W_m(s) = \frac{k_t}{Js + k_f} I_M(s). \tag{3.9}$$

Therefore, based on the transfer function in equation (3.8), the dependence between the current and voltage is given under the following form:

$$G_i(s) = \frac{I_M(s)}{V(s)} = \frac{Js + k_f}{JLs^2 + (RJ + k_f L)s + k_f R + k_e k_t}, \tag{3.10}$$

i.e.

$$G_i(s) = \frac{I_M(s)}{V(s)} = \frac{4.616 \cdot 10^{-4} s + 7.12 \cdot 10^{-4}}{1.459 \cdot 10^{-5} s^2 + 5.264 \cdot 10^{-3} s + 1}. \tag{3.11}$$

Figure 3.5 Control architecture

The system being stable (poles of the system are located in the left half plane), a Proportional-Integral (PI) methodology is used to control the current. The equation of the controller is assumed to be

$$C_i(s) = K_p\left(1 + \frac{1}{sT_i}\right),$$

(3.12)

where K_p is the proportional gain and T_i the integral time constant. The controller is designed in the frequency domain. The principle of this design is to change the frequency response of the system in open loop in order to fulfill some desired specifications. Many authors (Franklin, Powell et al. 1994), (Ogata et al. 2001), (Dorf and Bishop 1998), (Phillips and Habor 1995), describe with practical examples the way to design a control algorithm in frequency domain. Often, in order to obtain better performance in closed loop, the phase margin in open loop is chosen between 30-70 degrees. Therefore, with a phase margin fixed at 60 degrees for the open loop system and by solving equation (3.13), the total phase of the system in open loop is determined, as follows:

$$180^\circ - \left|\varphi_{C_iG_i}\right| = \theta, \tag{3.13}$$

$$\varphi_{C_iG_i} = \varphi_{C_{i0}} + \varphi_{G_{i0}}. \tag{3.14}$$

θ, $\varphi_{C_{i0}}$ and $\varphi_{G_{i0}}$ are the phase margin of the system, phase margin of current controller and phase margin of the system described by equation (3.11). Figure 3.6 shows the loop scheme of the current controller, while figure 3.7 depicts the system response for a step current value of 0.928 A.

Figure 3.6 Closed loop current control

Figure 3.7 Step response of the actuator current

Regarding the position control loop, it can be added to the current control loop, the full architecture of the control resulting has the form presented in figure 3.8.

Figure 3.8 Closed loop position control

The angular position considered as output value of the controlled system supposes the presence of an integral term in the plant transfer function converting the angular speed. Therefore, the actuator transfer function (3.8) can be rewritten in the next form

$$H(s) = \frac{\phi(s)}{V(s)} = \frac{W_m(s)}{V(s)} \cdot \frac{1}{s} = G(s) \cdot \frac{1}{s} = \frac{k_t}{JL \cdot s^2 + (RJ + k_f L)s + k_f R + k_e k_t}. \qquad (3.15)$$

The open loop transfer function of the system controlled in current can be expressed as follows

$$G_{po}(s) = C_i(s) \cdot H(s) = C_i(s) \cdot G(s) \cdot \frac{1}{s}, \qquad (3.16)$$

Because of the integral term in equation (16), a PD controller is designed to control the position

$$P_d(s) = K_{pd} \frac{1 + T_d s}{1 + 0.001s}. \qquad (3.17)$$

The method proposed by (Ziegler and Nichols 1942) was utilized to determine the coefficients of the position controller K_{pd} and T_d, defined by equation (3.17).

The actuator position control tuning results are presented in figure 3.9. In fact, the airfoil shape is not maintained at the high amplitude shown in figure 3.9. This figure shows ZN's results obtained in the simulation with Simulink, and the way in which the value of the oscillation period is measured. The measured value of T_u in figure 3.9 is 0.07 s, while the system instability characterized by the oscillations (green curve) is obtained by setting the value of K_u to 0.45. Using the values of T_u and K_u, the next parameters of the position controller are obtained: K_{pd}=0.27 and T_d=8.4·10⁻³.

$K_{pd}=0.27$ and $T_d=8.4\cdot10^{-3}$.

controller are obtained: $K_{pd}=0.27$ and $T_d=8.4\cdot10^{-3}$.

Figure 3.9 Actuator position obtained using Ziegler-Nichols
(Blue: position set-point, Green: position simulated response)

3.7 Wind tunnel experimental testing

The low speed, Price-Païdoussis subsonic wind tunnel located at the LARCASE laboratory was used for the experimental testing a nd validation of the integrated morphing wing system. This wind tunnel was calibrated with a new methodology using the combination of neural networks and Extended Great Deluge (EGD). In (Mosbah, Salinas et al. 2013) are given more details about the structure of this wind tunnel and the calibration methodology. Fig. 10 shows the subsonic Price-Païdoussis wind tunnel with the smaller test chamber and the vertical positioning of the morphing wing in the wind tunnel test chamber.

The goals of the wind tunnel experiments were to test the designed control system of the actuators, and at the same time to validate the results of the aerodynamic prediction. Because the programmable electrical power source used to control the actuator was only compatible with the LabView software, it was used as software application, and the designed controllers with Matlab/Simulink were reprogrammed in LabView. Figure 3.11 shows a comparison between the experimentally measured (under aerodynamic load), simulated and set-point position for a repeated step input in degrees. It can be seen that the desired positions are reached without overshoot and at about 1 second. Also, the experimental results confirmed the validity of the designed control, being closer to the numerical simulations results.

Figure 3.10 LARCASE Price- Païdoussis subsonic blow
down wind tunnel and the morphing wing positioning in the test chamber

Figure 3.11 Actuator position in degrees

For the aerodynamic validation, the pressure coefficient was measured at different percentages of the chord on the wing upper surface. A Kinetic pressure set as shown in figure 3.12 was used to measure the static pressure. This pressure set is a portable system that is able to measure and display measured pressure as well as measured temperature, humidity and speed of the wind flow in wind tunnel. A Pitot tube was used for the total pressure measurement. Pressure coefficient curves obtained with XFoil software (Drela 1989) for different flight conditions were compared with those measured during wind tunnel tests. With the XFoil solver, it is possible to estimate aerodynamics coefficients such as drag and lift coefficients as well as transition point locations ((Drela 2003), (Popov, Botez et al. 2008)). Data from XFoil were chosen as reference because of short convergent time, and it works absolutely in two dimensional (2D). This solver distinguishes two types of calculations (inviscid and viscous) and uses the e^N method as transition criterion.

Figure 3.12 Kinetic pressure set

Numerically, these results were predicted on the ATR-42 as seen in (Gabor, Koreanschi et al. 2012). Figures 3.13 to 3.15 show the results obtained for three different flight conditions. The angle of attack varies from -1 deg to 1 deg and the wind speed in wind tunnel is kept constant. Sensor number 6 gave a wrong value because the pressure taps was damaged during assembly of the mechanical system. It could be observed that the predicted aerodynamic results with XFoil agreed with the wind tunnel aerodynamic results. It will be interesting to study also frequency and time domain coupling methods for aeroservoelasticity studies as proposed by (Tran and Liauzun 2006).

Figure 3.13 Pressure coefficient (Blue: Simulation, Red: Measured)
for M=0.2 and α=-1 degree

Figure 3.14 Pressure coefficient (Blue: Simulation, Red: Measured)
for M=0.2 and α=1 degree

Figure 3.15 Pressure coefficient (Blue: Simulation, Red: Measured)
for M=0.2 and α=0 degree

3.8   Conclusions

In this paper, the design and manufacturing of an electrical rotary in-house actuation system, its control methodologies, and their combination to realize the ATR-42 morphing wing was investigated. The goals of the wind tunnel experiments were to test the designed control system of the actuators, and in the same time to validate the results of the aerodynamic prediction in the controlled flight cases.

From an aerodynamic point of view, the optimized shapes improved the laminar flow from 2% to 18% displacement of the transition point position versus the chord on its upper surface, depending on the flight case (the range of improvements applies to all of the 5 cases performed in the wind tunnel). The improvement of the laminar flow gave a reduction of the drag coefficient within 3% to 10.5 % from its original calculated value.

During experimental wind tunnel tests, LabView software was used as software application, while the designed controllers were numerical simulated with Matlab/Simulink program. The control experimental results confirm the validity of the designed control, being closer to the numerical simulations results. The aerodynamic studies were realized using XFoil in order to predict numerically the pressure coefficient distributions for different flight conditions. Experimental validation of the controlled morphing wing was validated in Figures 13 to 15 by comparing the XFoil prediction with the measured coefficients during wind tunnel tests for all tested flight cases. The pressure coefficients were measured at 14 points on the upper surface. The experimental results have shown that the approach used to design the numerical model of the system and of the controller was valid. With a much greater available space inside the wing this new concept could be implemented and integrated on a real aircraft.

CHAPTER 4

DESIGN, NUMERICAL SIMULATION AND EXPERIMENTAL TESTING OF A CONTROLLED ELECTRICAL ACTUATION SYSTEM IN A REAL AIRCRAFT MORPHING WING MODEL

Michel Joël Tchatchueng Kammegne[1], Lucian Teodor Grigorie[2], Ruxandra Mihaela Botez[3],

[1,3]Départment de Génie de la production automatisée, LARCASE Laboratory of Applied Reasearch in Active Controls, Avionics and Aeroservoelasticity, École de Technologie Supérieure, 1100 rue Notre Dame Ouest, Montréal, H3C1K3, Québec, Canada
[2]Université de Craiova, Strada Alexandru Ioan Cuza 13, Craiova 200585, Roumanie

Résumé

Cet article met l'accent sur la modélisation, la simulation et le contrôle d'un actionneur électrique miniaturisé intégré dans le mécanisme d'actionnement d'une nouvelle application d'aile déformable. L'aile déformable est une partie d'une aile d'avion dont son intérieur est constitué de longerons, nervures, et ayant une rigidité structurelle similaire à la rigidité d'un avion réel. La surface supérieure de l'aile est une peau flexible, fabriquée en matériaux composites, et optimisée afin de satisfaire aux exigences du projet. En outre, un aileron rigide contrôlable est fixé sur l'aile. L'architecture établie du mécanisme d'actionnement utilise quatre actionneurs miniatures identiques fixés à l'intérieur de l'aile et qui actionnent directement sur la surface supérieure flexible de l'aile. L'actionneur a été conçu dans notre laboratoire, car aucun actionneur pouvant entrer directement à l'intérieur de l'aile pour satisfaire les conditions imposées pour le rapport désiré entre les forces et les déplacements n'ont pas été trouvés sur le marché. L'actionneur se compose d'un moteur à courant continu sans balais avec une boîte d'engrenages et une vis de poussée et de traction de la surface

70

supérieure de l'aile flexible. Le moteur électrique et la vis sont couplés par un système d'engrenage. Avant de procéder à la modélisation, l'actionneur a été testé expérimentalement pour veiller à ce que l'ensemble des exigences (Couple nominal, courant nominal, vitesse nominale, la force statique) soit rempli. Afin de valider la configuration théorique, la simulation et la configuration autonome, des études expérimentales sur un banc d'essai de quatre actionneurs identiques intégrés sur le modèle de l'aile réelle de l'aile déformable sont effectuées.

Abstract

The paper focuses on the modeling, simulation and control of an electrical miniature actuator integrated in the actuation mechanism of a new morphing wing application. The morphed wing is a portion of an existing regional aircraft wing, its interior consisting of spars, stringers, and ribs, and having a structural rigidity similar to the rigidity of a real aircraft. The upper surface of the wing is a flexible skin, made of composite materials, and optimized in order to fulfill the morphing wing project requirements. In addition, a controllable rigid aileron is attached on the wing. The established architecture of the actuation mechanism uses four similar miniature actuators fixed inside the wing and actuating directly the flexible upper surface of the wing. The actuator was designed in-house, as there is no actuator on the market that could fit directly inside our morphing wing model. It consists of a brushless direct current (BLDC) motor with a gearbox and a screw for pushing and pulling the flexible upper surface of the wing. The electrical motor and the screw are coupled through a gearing system. Before proceeding with the modeling, the actuator is tested experimentally (standalone configuration) to ensure that the entire range of the requirements (rated or nominal torque, nominal current, nominal speed, static force, size) would be fulfilled. In order to validate the theoretical, simulation and standalone configuration experimental studies, a bench testing and a wind tunnel testing of four similar actuators integrated on the real morphing wing model are performed.

4.1   Introduction

The idea of changing the wing shape configuration or geometry has been studied since the 19th century. The Wright brother's airplane was able to do roll control by changing the twist of its wing using cables actuated directly by the pilot as mentioned by (Barbarino, Bilgen et al. 2011). Currently, there are a lot of morphing aircraft studies, developed by industrial entities or by different universities in their research labs.

According to (Xia 2012) green aviation policies have driven the trend to replace air-driven and hydraulic-type transmission devices by motor-driven equipment. Employing a miniature electrical actuator with an integrated BLDC motor makes it possible to control the shape of an aircraft wing in real time with the morphing wing technique. Thanks to morphing technology, it is possible to optimize wing performance at all flight conditions and for each flight segment.

A brushless direct current (BLDC) motor is a synchronous rotary machine controlled by electronic commutation. Its rotor is a permanent magnet with an integrated position sensor that senses the rotor position. The induced voltage in the motor winding (back EMF) has a trapezoidal waveform. According to (Xia 2012) a BLDC motor with its trapezoidal induced voltage waveform has the starting characteristics of a direct current rotary machine. BLDC motors are widely used in aerospace, household appliances, automation and industrial process control. The use of this type of electrical rotary machine is extensive and is growing due to its small size, high efficiency, large torque, long lifetime and low noise, and because it performs commutation electronically. This last feature is particularly interesting for aerospace industries because commutation does not cause any chance of sparks occurrence. BLDCs therefore offer a high level of safety and reliability in addition to their other advantages.

In 2000, researchers at the University of Stuttgart proposed a new method to develop the morphing concept. The approach of (Sommerer, Lutz et al. 2000) consisted on using of a shock control bump inflated with air, while the objective was to minimize the negative effects of shockwaves in transonic flow. The numerical results showed a 70% decrease in the wave drag and a 15% decrease in the wing total drag. A comparative study between the drag

reduction obtained with the developed approach and with the approach using a higher polynomial contour bump was performed. Considering aerodynamics and structural requirements, researchers from Institute for Control Engineering and from Institute for Aerodynamics and Gas Dynamics in Stuttgart, Germany, used a new approach to design an adaptive shock control bump. In this way, (Wadehn, Sommerer et al. 2002) proposed an optimization method to generate optimal shock control bump contour for a given height and position was developed. The proposed concepts were validated by using a small scale demonstrator.

(Sobieczky and Geissler 1999) realized a 10% drag reduction for Mach numbers between 0.72 and 0.77 in similar studies developed by the researchers of DLR German Aerospace Research Establishment. A shape modification concept for transonic wing sections using both MSES (Euler + boundary layer) code and Navier/Stokes code developed by (Sobieczky, Geissler et al. 1999) showed an improvement of the lift-to-drag ratio. For the MSES code 15% of the lift-to-drag ratio and 8.3% for the Navier/Stokes improvement was observed.

(McGowan, Wilkie et al. 1998) discussed in an overview of the research at NASA Langley research center, analytical and experimental results, plans, potential technology pay-offs, and challenges in order to develop the enabling technologies to actively and passively control aircraft and rotorcraft vibration and loads using smart devices. Also, in another overview in which NASA morphing program is focusing on multiple disciplinary research for the development of the smart technologies so as to use them for the improvement of the state of the art aircraft systems, research and development pertinent to self-adapting airframe systems, advanced piezoelectric materials, advanced fiber optic sensing techniques have been exposed. The overview details are explained by (RW, GC et al. 1998)

In 2001 (Stanewsky 2001) presented a summary of flow control methodology and adaptive wing technology, along with a discussion of the aerodynamic contributions to adaptive wing concepts of varying complexity. In 2007, (Gomez and Garcia 2011) presented a new principle of morphing based on a dielectric electroactive polymer (EAP) skin using micro fiber composite actuators. Because the EAP skin could not be sufficiently pre-loaded, a

rubber skin was used in the experimental testing. In another study developed at University of Virginia in 2003 by (Elzey, Sofla et al. 2003), a cellular metal vertebrate structure which relies on the SMA to achieve fully reversing shape change, when these are combined with flexible face sheets a load bearing morphing panel was developed. In 2006, (Weisshaar 2006) a researcher from Aeronautics and Astronautics Department, Purdue University, USA, contributed a review of fixed wing aircraft implementing morphing techniques. Various alternatives of morphing aircraft were exposed and discussed, as well as the associated design techniques and fabrication technologies. Also, an analyze of the four basic elements used in a morphing wing structure has been performed: sensors to measure positions, control systems to convert the measurements into an activation signal, actuation mechanisms to provide mechanical motion and precise positioning, and efficient power sources to drive actuation. Recent work in smart materials and adaptive structures is providing researchers the opportunity to investigate how this adaptive structure can be used to morph the airfoil shape. The most common characteristics of some smart materials used in adaptive structures are listed in Table 4.1 : the maximum strain (Max. strain) - allowable normalized deformation expressed in percent; the maximum stress (Max. stress) – allowable stress expressed in MPa; the elastic energy density (the potential energy stored in a small volume element upon deformation) expressed in J/g; maximum efficiency (Max. effic.), representing the maximum value of efficiency (determined for specific smart materials as a function of the ratio of recovery stress to yield stress), and expressed in percent; the relative response speed (is the speed reaction of the material when submitted to an external disturbance).

Table 4.1 Smart materials and their characteristics
(taken from (Abdullah, Bil et al. 2010))

Material	Max. strain (%)	Max. stress (MPa)	Elastic energy density (J/g)	Max. effic. (%)	Relative speed
Electrostrictor Polymer P(VDF-TrFE)	4	15	0.17	-	Fast
Piezoelectric Ceramic (PZT)	0.2	110	0.013	>90	Fast
Single Crystal (PZN-PT)	1.7	131	0.13	>90	Fast
Polymer (PVDF)	0.1	4.8	0.0013	n/a	Fast
SMA (TiNi)	>5	>200	>15	<10	Slow

Among the materials compared in Table 4.1, shape memory alloy (SMA) appears to be a good candidate to use for flexible skin morphing. Among smart materials, SMAs can produce rather large plastic deformations.

The design of a new flap architecture using compliant (SMA) ribs for a variable-camber trailing edge was assessed. Upon activation of the SMA, the ribs were able to change the camber's morphology. In addition, (Pecora, Barbarino et al. 2011), (Barbarino, Dettmer et al. 2010) performed a numerical optimization process, incorporating practical constraints and finite element (FE) analysis in order to evaluate the structural design and the aero-structural performance. (Song and Ma 2007) realized another study where SMAs were used in morphing flap actuation, controlled by robust non-linear controllers. These flaps were fabricated in ultra-light scaled models made of balsa wood and nylon sticks, utilizing their high strength and low weight characteristics. The use of SMA wires as actuators for wing flaps was submitted to wind tunnel testing. The trailing edge was morphed by means of six SMA wires that could pull the flap assembly upon electrical activation, while ten springs acted to regain the initial wing configuration when the SMA wires cooled down (Benavides, Correa et al. 2004). (Seow, Liu et al. 2008) manufactured and tested a wing prototype with flexible skin made of fiberglass composite and a rubber sheet. SMA was used to change the shape of the flexible skin. (Mason, Robertshaw et al. 2004) have tested torsion bars and SMA wires to control the roll of a morphing wing model aircraft in both a wind tunnel and during flight.

Also, the SMA behavior has been modeled according to the model proposed by (Li and Harada 2013) model, simulation results being presented in terms of output displacements and morphed shape. Linear actuators incorporated in statically determinate structure around which a prototype airfoil has been built, were used for morphing, finally the prototype airfoil was tested in the wind tunnel to analyze drag reduction.

In 2009, a study investigated by (Abdullah, Bil et al. 2009) presented an overview of smart material application. The investigation focused essentially on shape memory alloy as actuator in order to change the camber of the airfoil. Subsequently, an adaptive airfoil was designed

with the aim of changing the camber of the airfoil during cruise conditions as shown in (Abdullah, Bil et al. 2010); different airfoils shape was predicted with the help of finite element analysis.

Based on results provided by a finite element method developed by (Seow, Liu et al. 2008), a wing prototype was manufactured by (Abdullah, Bil et al. 2011) with a specially-designed position control for wing trailing edge deflection. This control system produced a minimum of 5 mm trailing edge deflection. Experimental wind tunnel tests showed that the lift-to-drag ratio was improved at a very low angle of attack variation (cruise conditions) and decreased by increasing the angle of attack.

(Hutapea, Kim et al. 2008) researchers from the Department of Mechanical Engineering, Temple University, Philadelphia, used smart materials to control the flap setting of a given aircraft. One end of the actuator was attached to the wing box and the other was attached tangentially to a rotating cylinder fixed to the flap. The deflection of the flaps was achieved by arranging the SMA springs in an upper and lower layer. A three-way switch was utilized to apply current to the springs. Depending on how and where the current was applied, the flap's deflection was either upward or downward. Wind tunnels tests were carried out at the tunnel outlet in order to demonstrate the feasibility of the design concept.

Another project initiated by (Botez, Molaret et al. 2007) used a camber change to modify the airfoil shape, based on SMA as actuator. A design optimization method was used to generate different airfoil design solutions. The optimization method utilized the aerodynamic properties of the airfoil to optimize the design problem and to maximize the lift-to-drag ratio for the airfoil shape.

The chord wise air collection method was used by (Allison and Dagenhart 1978) to implement a laminar flow control over the upper surface of a wing. That method was used to change the transition location moved to a desired location, which was then maintained with the help of a numerical algorithm developed by (Tutty, Hackenberg et al. 2000). In a study presented by (Pralits 2003), three tasks are involved in moving and maintaining the transition location: keeping the lift and the pitch moment coefficients constant, and wing optimization

by reducing the kinetic energy and drag coefficient.

Morphing wing realization based on maintaining the desired turbulence level over a flat plate equipped with a suction porous panel, was done at Southampton University by (Rioual, Nelson et al. 1994). The degree of turbulence was evaluated by computing the Root Mean Square (RMS) of the pressure signals. (Dimino, Flauto et al. 2014), (Pecora, Magnifico et al. 2014) designed and tested an actuation mechanism to control the wing shape by modifying its trailing edge. The goal of the actuation mechanism was to transmit its rotary motion to the rib aiming to realize the target optimized shape. A control system with the aim to control the shape of a camber trailing edge was proposed in (Pecora, Amoroso et al. 2014). A servo motor integrated inside the wing was installed in order to modify the shape changing of the trailing edge when it was actuated. The optimized trailing edge shape was stored into a database. Through strain sensors installed on the trailing edge the measured shape was reconstructed and compared with the optimized airfoil shape stored in the database. (Popov, Grigorie et al. 2010) investigated two control strategies (open and closed loop). An SMA model has been developed in Matlab and simulation has been carried out to control the laminar to turbulent flow transition point towards the trailing edge of the aircraft.

A closed loop control based on the Fuzzy technique was developed to control the transition point during real time testing in a Canadian project presented in (Grigorie, Popov et al. 2011) Also, in the same project, (Grigorie, Popov et al. 2012), (Grigorie, Popov et al. 2012) designed and tested an On-Off and proportional-integral controller to morph a flexible skin, and a numerical analysis and the experimental validation of a hybrid controller based on fuzzy logic and a Proportional-Integral-Derivative (PID) algorithm to ensure SMA actuator displacements were performed by (Grigorie, Botez et al. 2012), (Grigorie, Botez et al. 2012). PID controller has been used to control the SMA based actuator (see figure 4.1) in order to control the laminar to turbulent transition point for drag reduction. Transfer function was developed in Simulink and used to approximate the PID gains using Zeigler Nichols method. (Grigorie and Botez 2009), (Grigorie and Botez 2010) developed also some adaptive neuro-fuzzy inference system-based controllers for smart material actuator modelling. The

controllers were designed to correlate each set of forces and electrical currents applied to the actuators.

(Neal, Akle et al. 2003) used a LQR control to calculate the optimal aerodynamic forces and the command forces were fed into the fuzzy logic controller that produces required control surface deflection under the preset rules defined by the morphing deflection controller, this work showed a successful tracking of an arbitrary flight path using a hybrid LQR-Neuro fuzzy control scheme.

Despite the progress in smart materials technology, their high power consumption, requiring a heavy power system, has limited their utilization in aerospace ((Grigorie, Popov et al. 2011), (Grigorie, Popov et al. 2011), (Grigorie, Botez et al. 2012), (Grigorie, Botez et al. 2012)). To address this issue, a new airfoil shape-changing concept utilizing an electrical actuator was proposed in 2014 by (Kammegne, Grigorie et al. 2014). The electrical actuator is a direct current motor. Lightweight actuators are part of the trend in green aviation. Maximizing the integration of electrical systems in future aircraft will reduce their weight. Using electrical actuators, such as DC motors, will bring multiple benefits in addition to those gained by morphing, because such actuators are lightweight, can be easily integrated into a system, and need less power than smart materials.

Figure 4.1 Actuation mechanism concept
in CRIAQ 7.1 research project

A wing prototype with an integrated actuation mechanism was fabricated and tested at Ecole de Technologie Superieure in Montreal. The actuator position was controlled using a cascade control algorithm. Wind tunnel tests were carried out to verify the predicted aerodynamic response. Figure 4.2a shows a complete view of the Price-Païdoussis wind tunnel used for those tests, while Figure 4.2b showed that the measured pressure coefficient curve (red) is very close to the curve of the predicted coefficients (blue). The wind tunnel calibration procedure was explained in details in (Mosbah, Salinas et al. 2013).

Figure 4.2 (a): Price- Païdoussis subsonic wind tunnel; (b): Comparison between theory and wind tunnel experiments for a morphing wing

The work presented here describes a new morphing wing application developed by using an actuation mechanism based on some miniature high-force in-house developed electrical actuators. In the following sections the paper exposes: i) the morphing wing project background, including the architecture of the proposed actuation system, ii) the theoretical analysis of the BLDC motor and its gearbox, contained in the developed electrical actuator; iii) the actuator control system design (the current controller and the position controller); iv) experimental results obtained in the morphing wing bench test and wind tunnel test actuation.

4.2 Morphing project background

In this research project, realized at Ecole de Technologie Supérieure in Montréal, Canada in collaboration with Thales, Bombardier Aerospace, École Polytechnique, National Research Council Canada (IAR-NRC), and also with italian researchers from University of Naples Frederico II, CIRA and Alenia, a wing-aileron prototype is designed, tested and validated

using win tunnel tests at National Research Council Canada (IAR-NRC). The project is a multidisciplinary one, the involved entities working together; the research team is divided into three sub-teams covering aerodynamic, structural, and control fields. The project aims to reduce the operating costs for the new generation of aircraft through in-flight fuel economy, and also to improve aircraft performances, expand its flight envelope, replace conventional control surfaces, reduce drag to improve range and reduce vibrations and flutter risk. To achieve these purposes, two particular objectives for our team (Research Laboratory in Active Controls, Avionics and Aeroservoelasticity (LARCASE) of the Ecole de Technologie Supérieure in Montréal, Canada) were established in this project: 1) to detect and visualize airflow characteristics using pressure sensors installed on the upper surface of the morphing wing; and 2) to develop a system for active control of the morphing wing during flight to move the transition point from laminar to turbulent flow closer to the trailing edge, thereby promoting large laminar regions on the wing surface, and thus reducing drag over an operating range of flow conditions univocally defined by mean of Mach numbers, airspeeds, and angles of attack.

To be more specific to a real morphing application, the wing used in this project is a full-scaled portion of the wing of a regional aircraft (Figure 4.3a), having maximum chord of 1.5 m, and a minimum one of 1.08 m. It consists of wing spars, ribs and an aileron (Figure 4.3b).

Figure 4.3 Used wing as a full-scale portion of regional aircraft wing

In a preliminary aerodynamic study, seventy-four optimized airfoils were calculated by modifying the reference airfoil for each airflow condition as some combinations between

fifteen angles of attack (-3˚, -2.5˚, -2˚, -1.5˚, -1˚, -0.5˚, -0.25˚, 0˚, 0.25˚, 0.5˚, 0.75˚, 1˚, 1.25˚, 1.5˚, 2˚), two Mach numbers (0.15, 0.25) and fourteen aileron deflection angles (between -7˚ and 7˚, due to the constraints imposed by the wind tunnel aerodynamic balance). The optimized airfoils were found through numerical simulations by the aerodynamic team, using some Computer Flight Dynamic (CFD) software and optimization algorithms.

The experimental wing model has three parts: 1) a metal part coming from the original aircraft wing, with unmodified structure, able to sustain the wing loads; 2) a morphing part, consisting of a flexible skin installed on the upper surface of the wing; and 3) an actuated aileron, designed starting from the original one on the aircraft (Figure 4.4). The metal part structure contains four ribs, two at the ends (Rib 1 and Rib 4), and two inside (Rib 2 and Rib 3) having also the role to support the actuators. The morphing part is actuated by four similar electric actuators, placed on two actuation lines at 32% (Act. #1 and Act. #3), respectively 48% (Act. #2 and Act. #4) from chord (Figure 4.4). For each of the seventy-four optimized airfoils resulted four vertical displacements corresponding to the positions of the four actuators (Figure 4.5), stored in a database in order to be used as reference vertical displacements for the control system. Therefore, the morphing shape control is achieved by controlling the actuators' positions.

Figure 4.4 Wing structure and actuations lines positions

Two control architectures are planned to be developed: 1) an open loop architecture, controlling the morphing wing system and the aileron deflection angle, and 2) a closed loop architecture, which includes the open loop architecture as an internal loop and controls the transition point position based on the information from the pressure sensors installed on the flexible skin and on the aileron upper surface. A grid of the theoretical (optimized) displacements for all four actuators, for Mach =0.15 and Mach = 0.25, is shown in Figure 4.5.

The project actual status refers only to the open loop control architecture at the level of the morphing system actuation: design, numerical simulations and experimental testing. In the open loop architecture the pressure sensors are used just to visualize the transition point position in the wind tunnel tests, and validate in this way the theoretical aerodynamic

optimization process for all seventy-four optimized airfoils; 32 Kulite pressure sensors are planned to be installed on the flexible skin, while other 8 are planned to be installed on the upper surface of the aileron.

The current paper extends the studies realized by (Kammegne, Grigorie et al. 2014) at École de technologie supérieure in Montreal, but instead of using a mechanical system to convert the rotary motion of the actuator into a vertical displacement, the miniature actuators are fixed directly inside the wing and directly actuate the flexible upper surface of the wing.

Figure 4. 5 Actuators displacements for Mach=0.15 and Mach=0.25

The direct actuation architecture, with estimated forces of over 1300 N per actuator, correlated with the small space inside the morphed wing (the wing thickness varies between 10 cm and 20 cm), and with small maximum displacement (maximum 5 mm) imposed serious size/power constraints to the actuators. As there was no actuator on the market that could fit directly inside the morphing wing model and provide the right forces, the project structural team resorted to the manufacture of a dedicated actuator that fulfils these specific requirements. Therefore, the complete electromechanical miniature actuator was designed in-

house, by using some components acquired on the market such as the miniature brushless direct current (BLDC) motor.

This approach will be very advantageous for aviation because the developed actuators, presented in this paper, are lightweight and have low power consumption (only 15 watts). Because of its small size, this actuator belongs to the category of miniature actuators.
The studies presented in the paper refers to the open loop architecture of the morphing wing, focusing on the modeling, simulation and control of the actuator used in this project to control the wing shape.

4.3   Actuator modeling and simulation

4.3.1   Actuator modeling

An actuator can be defined as a system capable of changing the configuration of another system when it receives a command. The design and simulation are focused on the following parts: the electrical motor, the gearbox, the gearing and the trapezoidal screw. The gearing and the trapezoidal screw are inside the actuator. The electrical motor used by the actuator is a miniature brushless direct current (BLDC) motor. This type of motor is known for its numerous advantages, including small size and high torque. Today, the tendency is to replace brush direct current motors with this type of motor. Much research and several studies have been done on BLDC theory (see, (Krishnan 2001), (Mohan 2012), (Irwin, Kazmierkowski et al. 2002), (Leonhard 2001), (Dorf and Bishop 1998), (Krishnan 2009), (Baldursson 2005)).

The equivalent circuit of a BLDC motor is illustrated in Figure 4.6, while the associated equations are:

$$V_1 = R_1 i_1 + L_1 \frac{\mathrm{d}i_1}{\mathrm{d}t} + E_1,$$
(4.1)

$$V_2 = R_2 i_2 + L_2 \frac{\mathrm{d}i_2}{\mathrm{d}t} + E_2,$$
(4.2)

$$V_3 = R_3 i_3 + L_3 \frac{\mathrm{d}i_3}{\mathrm{d}t} + E_3, \qquad (4.3)$$

where R_1, R_2, R_3 are the windings resistances, L_1, L_2, L_3 are the windings inductances, E_1, E_2, E_3 are the induced voltages (back EMF).

Figure 4. 6 Motor equivalent circuit

The stator windings of the BLDC motor used in this application are star connected. The motor's neutral point is not accessible; therefore, the phase-to-neutral voltage cannot be measured. The mathematical model proposed in this paper uses line-to-line voltage, defined as the voltage differences between two phase-to-neutral voltages.

Subtracting equation (4.1) and (4.2) yields:

$$V_{12} = R_1 (i_1 - i_2) + L_1 \frac{\mathrm{d}(i_1 - i_2)}{\mathrm{d}t} + E_1 - E_2, \qquad (4.4)$$

where $V_{12} = V_1 - V_2$, $R_1 = R_2$, and $L_1 = L_2$. Similarly, it results:

$$V_{23} = R_2 (i_2 - i_3) + L_2 \frac{\mathrm{d}(i_2 - i_3)}{\mathrm{d}t} + E_2 - E_3. \qquad (4.5)$$

For equations (4.4) and (4.5), it is assumed that the BLDC motor is a balanced system, which means that the BLDC motor is a symmetrical system ($R_1 = R_2 = R_3$ and $L_1 = L_2 = L_3$). In a symmetrical system with a neutral point, such as the BLDC motor, the phase currents must satisfy the next equation

$$i_1 + i_2 + i_3 = 0. \tag{4.6}$$

From equation (4.6), the current of phase 3 (i_3) is computed as:

$$i_3 = -i_1 - i_2. \tag{4.7}$$

By replacing i_3 given by equation (4.7) in equation (4.5) we obtain:

$$V_{23} = R_2(i_1 + 2i_2) + L_2\frac{\mathrm{d}(i_1 + 2i_2)}{\mathrm{d}t} + E_2 - E_3, \tag{4.8}$$

which can further be written as:

$$V_{23} = R_2 i_1 + 2R_2 i_2 + 2L_2\frac{\mathrm{d}i_2}{\mathrm{d}t} + L_2\frac{\mathrm{d}i_1}{\mathrm{d}t} + E_2 - E_3. \tag{4.9}$$

From equations (4.4) and (4.9), the motor phase currents i_1 and i_2 equations are obtained, as follows:

$$\frac{\mathrm{d}i_1}{\mathrm{d}t} = \frac{1}{3L}(2U_{12} + U_{23} - 3Ri_1 - E_{23} - 2E_{12}), \tag{4.10}$$

$$\frac{\mathrm{d}i_2}{\mathrm{d}t} = \frac{1}{3L}(-U_{12} + U_{23} - 3Ri_2 - E_{23} + E_{12}) \tag{4.11}$$

while the current in phase 3 is calculated using equation (4.7).

When the BLDC motor is operating, the electromagnetic torque on the motor shaft is constant. To keep the torque permanently constant on the shaft, at each phase the electromotive force (back EMF) needs to be synchronized with its counterpart phase current, as indicated on the graph in Figure 4.7. The induced voltage in the winding increases when the mechanical speed becomes higher. The next equation shows how the back EMF (E_1) and speed (ω) are related, and is valid for each motor phase:

$$E_1 = k_e \cdot \omega \cdot F(\theta), \tag{4.12}$$

where k_e is the back EMF constant, ω is the mechanical motor speed in radians per second, and θ is the electrical rotor position. The function $F(\theta)$ in equation (4.12) has a trapezoidal waveform as shown in Figure.4.7, with a maximum amplitude of +1 and a minimum amplitude of -1.

The electrical power absorbed by the motor is transferred to the rotor via the air gap. This transferred power equals the sum of the products of each current and back-EMF of the three phases and is given by equation:

$$P_e = E_1 i_1 + E_2 i_2 + E_3 i_3. \tag{4.13}$$

On the other way, the electromagnetic power is given by equation:

$$P_e = T_e \cdot \omega \tag{4.14}$$

Figure 4.7 Phase current and back EMFs values

From equations (4.13) and (4.14), it results:

$$T_e \cdot \omega = E_1 i_1 + E_2 i_2 + E_3 i_3. \qquad (4.15)$$

The electromagnetic torque equals the product of the torque constant and the phase current, and is written as:

$$T_e = k_t i, \qquad (4.16)$$

where k_t is the motor torque constant. The characteristics of the BLDC motor chosen in this application are shown in Table 4.2.

Table 4.2 Characteristics of the BLDC motor

Values at nominal voltage	
Nominal voltage	12 Volts
No load speed	4610 rpm
No load current	75.7 mA
Nominal speed	2810 rpm
Nominal torque (maximum continuous torque)	25.1 mNm
Nominal current (maximum continuous torque)	1 A
Stall torque	84.1 mNm
Starting current	3.49 A
Electrical characteristics	
Terminal resistance	3.43 Ω
Terminal inductance	1.87 mH
Torque constant	24.1 mNm/A
Speed constant	397 rpm/V
Mechanical time constant	20.7 ms
Rotor inertia	35 cm^2

4.3.2   Actuator simulation

The equations developed above ((4.1) to (4.16)) were used with Matlab/Simulink to implement the BLDC model. Figure 4.8 shows the BLDC motor model with its power stage

(Inverter). The Matlab/Simulink implementation of equations (4.10) and (4.11) is presented in Figure 4.9. This represents what occurs in the main part of the second block on the right side of Figure 4.8. The power stage applies voltage to the motor's winding based on the rotor position, which is detected by a low-cost hall sensor integrated in the motor. The commutation sequence used by the power electronics to switch the power device ON and OFF (MOSFET) is presented in Figure 4.10.

Figure 4.8 BLDC motor and its power stage

Figure 4.9 Simulink calculation of the phase current

Figure 4.11 shows the speed and torque waveforms, captured when a nominal load of $24.1 \cdot 10^{-3}$ N·m is applied at 0.5 seconds. Figure 4.12 shows the phase current and the back EMF waveforms from the simulated motor model captured when the same load is applied. It is clear that the back EMF and the phase current are well-synchronized.

According to the data from Table 2, the stall torque, no load speed, nominal speed, no load current, and nominal current parameters at nominal voltage are also achieved with the designed simulation model, thus validating the proposed actuator motor simulation model.

After the numerical validation of the actuator's motor, which is the main part of the actuation system, its model (proposed in Figure 4.8) is extended to obtain a complete model of the actuator. In order to model the mechanical part of the actuator, consisting of a gearbox, gearing, screw and nut, the motor's gearbox and the gearing ratio need to be assessed. From the design structural constraints, it was assumed that for a 2 mm linear displacement of the nut, the screw makes one complete mechanical revolution. A complete mechanical revolution of the screw corresponds to two revolutions of the motor's gearbox shaft.

Figure 4.10 Commutation sequence

Figure 4.11 Speed and torque waveforms

Figure 4.12 Current and back EMF for phase 1

Obviously, the actuator is modeled as an open-loop model. Open-loop (in this case) means that the actuator is powered and its output (position in millimeters) is observed without any control. The next chapter will focus on the actuator's current control as well as its position control.

4.4 Actuator control design and numerical simulation

4.4.1 Actuator's current control

The implementation of a current loop is useful to protect the actuator's motor against overcurrent. This loop ensures that the electromagnetic torque on the motor shaft is controlled independently of the load. The schematic of the proposed current control loop is shown in Figure 4.13.

Figure 4.13 Actuator's current control scheme

The reference current generator block generates three reference currents based on the position information from the hall sensor. Depending on the error signal between the reference and the measured current, a pulse with a modulation (PWM) signal is generated. The PWM signal is used as a firing signal for the inverter power devices. The actuator's motor is taken into account because its current is defined by the current in the motor's winding.

The power stage or inverter illustrated in Figure 4.8 is extended with the current controller. The hysteresis control law for the current is implemented here because of its simplicity and accuracy. The drawback of this method is the variable switching frequency. The principle of this type of control is illustrated in Figure 4.14. Figure 4.15 shows the simulation result obtained using this control technique. The current ripples visible in Figure 4.15 can be reduced using a combination of a proportional-integral (PI) controller with a saw tooth signal.

4.4.2   Actuator's position control

A BLDC motor can be approximated as a direct current motor with brush when two phases are conducted or excited. This approximation is used to design the actuator's position control. The structure of a BLDC motor is shown in Figure 4.16.

Figure 4.14 Illustration of the hysteresis control ([49])

Figure 4.15 Simulation results with current control

Figure 4.16 Structure of the BLDC motor

To design the position control, the transfer function $\theta(s)/U(s)$ is used. This transfer function is derived from Figure 4.16 as follows

$$I = \frac{U - k_e w}{L \cdot s + R} \tag{4.17}$$

and,

$$w = \frac{k_t I}{Js + B}. \tag{4.18}$$

From equation (4.18) the motor's current yields:

$$I = \frac{w(Js + B)}{k_t}, \tag{4.19}$$

By equalizing equation (4.19) with equation (4.17) it results:

$$\frac{U - k_e w}{Ls + R} = \frac{w(Js + B)}{k_t}. \tag{4.20}$$

Re-arranging equation (4.20) we have:

$$\frac{w}{U} = \frac{k_t}{LJs^2 + RJs + k_e k_t}, \tag{4.21}$$

which, by considering the motor speed in revolution per minute (rpm), can be rewritten as:

$$\frac{w}{U} = \frac{30}{\pi} \cdot \frac{k_t}{LJs^2 + RJs + k_e k_t} \tag{4.22}$$

From Figure 4.16, we can write:

$$w = s \cdot \theta \tag{4.23}$$

Therefore, the transfer function (4.22) becomes:

$$\frac{\theta}{U} = \frac{30}{\pi} \cdot \frac{k_t}{LJ_{eq}s^2 + RJs + k_e k_t} \frac{1}{s} \tag{4.24}$$

The structure of the position control closed-loop architecture is presented in Figure 4.17.

Figure 4.17 Structure of position control

The controller used for position tracking is a proportional-derivative (PD) one because the existing integral term (I of the PID) in equation (4.24) eliminates the steady state error. Among the different available tuning methods ((Ogata 2001), (Ogata 2008), (Paraskevopoulos 2001)), the Ziegler-Nichols method was selected, being simple and easy to implement. The root locus (zoomed view around the imaginary axis) of the system defined by equation (24) is shown in Figure 4.18.

From Figure 4.18, the critical gain (K_c) is found to be about 4 and the oscillation period (T_c) of the system output is found to be the inverse of the frequency. Following the tuning rules proposed by Ziegler-Nichols, the coefficients of the PD controller (K_p and T_d), defined by the next equation, can be determined:

$$E(s) = K_p(1 + T_d s) \tag{4.25}$$

Figure 4.18 Zoomed view of the system's root locus

Figure 4.19 shows the simulation results obtained with the position controller designed with the Ziegler-Nichols technique. The controller parameters were tuned so that no overshoot occurred.

Figure 4.19 Simulation results obtained
with the position controller

4.5   Morphing wing experimental test

To develop the open loop architecture of the morphing wing system, the database of the seventy-four optimized airfoils is used. Four vertical deflections $(dY_{1opt}, dY_{2opt}, dY_{3opt}, dY_{4opt})$ are given for each optimized airfoil. The four displacements characterize the differences between the optimized airfoil and the reference airfoil in the four actuation points. In this way, the actuator designed controller should be used to control the actuators linear positions until the real vertical displacements $(dY_{1real}, dY_{2real}, dY_{3real}, dY_{4real})$ of the morphing skin in the four actuation points equal the desired vertical displacements of the optimized airfoil $(dY_{1opt}, dY_{2opt}, dY_{3opt}, dY_{4opt})$ corresponding to a flow condition.

The firsts experimental tests were performed at Ecole de Technologie Supérieure in the LARCASE facility with the physical wing model installed on the bench (Figure 4.20). The architecture of the interface system between the remote computer and experimental model in

the morphing wing open-loop control system is shown in Figure 4.21, being made by using a National Instruments Real Time (RT) Target. The control feedback for the morphing actuators is provided by four LVDT sensors having axes parallel to the actuators axes.

Figure 4.20 Bench test at LARCASE

The experimental instrumentation includes: **1)** a NI PXIe-1078, 9-Slot 3U PXI Express Chassis; **2)** a NI PXIe-8135 embedded controller, Intel Core i7-3610QE quad-core processor (2.3 GHz (base), 3.3 (single-core Turbo Boost)), up to 8 GB/s system, up to 4 GB/s slot bandwidth, 4 GB (1 x 4 GB DIMM) dual-channel 1600 MHz DDR3 standard, 16 GB (2 x 8 GB DIMM) maximum; **3)** four NI PXIe-4330 Data Acquisition Cards with Integrated Signal Conditioning for Bridge-Based Measurements, with 8 simultaneously sampled analog input channels each, 25 kS/s/ch sampling rate, 24-bit ADC per channel; **4)** a NI PXI-8531, 1-Port CANopen Interface (up to 1 Mbit/s) for PXI; **5)** a NI PXIe-6356 Simultaneous X Series Data Acquisition Card, 8 simultaneous analog inputs at 1.25 MS/s/ch with 16-bit resolution, 10 MS/s total AI throughput, two analog outputs, 3.33 MS/s, 16-bit resolution, ±10 V, 24 digital I/O lines (8 hardware-timed up to 10 MHz), Four 32-bit counter/timers for PWM, encoder, frequency, event counting, and more; **6)** a SCXI-1000 rugged, low-noise chassis that can hold up to four SCXI modules; **7)** a NI SCXI-1540 8-Channel LVDT Input Module,

programmable 1 or 3 Vrms excitation per channel at 2.5, 3.3, 5, or 10 kHz, programmable input range per channel (0.05 to 6 Vrms), 333 kS/s maximum sampling rate (250 Hz output bandwidth); **8)** a NI SCXI-1315, 8-channel, front-mounting terminal block for the NI SCXI-1540 LVDT input module; **9)** two Programmable power supplies Aim-TTi CPX400DP, dual, 420 watt, 60 V max, 20 A max.

Figure 4.21 National Instruments RT target and remote computer configurations

The bench testing was a first experimental validation for the designed controller and its hardware integration architecture, and it simultaneously provided a means to observe the quality of the experimental reproducibility of the theoretical reference and optimized airfoils. On the other way, the bench testing offers the opportunity to make some adjustments in the mechanical part of the model and some adjustments regarding the LVDT transducers zero positions. When the controller was tested on the bench two steps were performed: 1) Independent testing of the actuators - here was observed if each actuator acting independently can successfully manage the high level forces appearing under the skin morphing; 2) Simultaneous testing of the actuators. For both of these steps in bench test, was asked to the actuators to perform vertical displacements corresponding to the values (dY_{1opt}, dY_{2opt}, dY_{3opt}, dY_{4opt}) obtained for each of the seventy-four optimized airfoils.

All of the bench test results were very good and proved the proper functioning of the designed control system. For example, view the results obtained for the simultaneous control of the morphing skin actuators in the Mach=0.15, and attack angle = -1 deg airflow case

(dY_{1opt}=-2.86 mm, dY_{2opt}=4 mm, dY_{3opt}=-2.53 mm, dY_{4opt}=3.53 mm, aileron deflection = 5 deg) presented in Figure 4.22. The desired values for the actuators vertical displacements (dY_{1opt}, dY_{2opt}, dY_{3opt}, dY_{4opt}) were provided by the aerodynamic team of the project as results of the aerodynamic numerical optimization. These values are used as reference values in the control strategy of this airflow case. The real vertical displacements of the actuators ((dY_{1real}, dY_{2real}, dY_{3real}, dY_{4real}) are measured by using the LVDT position sensors equipping each actuator. The wing is considered to be optimally morphed in a flow case when the real vertical displacement equal the desired vertical displacements. The four actuators are placed on two actuation lines, at 32% (Act. #1 and Act. #3), respectively 48% (Act. #2 and Act. #4) from chord as was presented in Figure 4.4

Figure 4.22 Bench test results for Mach = 0.15
and attack angle = -1 deg

Figure 4.23 confirms also the good functioning of the control system, presenting the responses of the actuation system for various repeated step signals applied as inputs for the actuators. The desired values (dY_{1req}, dY_{2req}, dY_{3req}, dY_{4req}) were taken in order to have repeated step signals on all actuators, with positive and negative vertical displacements.

From the numerical values obtained for all seventy-four optimized airfoil cases, it was observed that the position control absolute error due to plays in actuators mechanical systems, when the actuators maintain a desired position, was less than 0.1 mm. These plays were fully agreed by booth structural and aerodynamic teams. From the first team point of view, the plays are important to protect the actuators in the wing bending situations, while, from the point of view of the aerodynamic team it is a safe variation because the simulation results for this wing revealed that the airflow transition point position is insensitive at deflections between -0.1mm and 0.1mm around the optimized vertical deflections of the actuators. A static loading test of the fully equipped wing, developed by the structural team, proved that the actuators were not jammed and worked properly.

The next experimental tests of the morphing wing system were realized at the IAR-NRC wind tunnel by using the same instrumentation. In this first wind tunnel test the open loop architecture of the morphing wing control system was evaluated. At this step were tested the control system of the actuators morphing the wing upper surface and the control system for the aileron deflection angle, while the pressure sensors were used just to visualize the transition point position. During this first wind tunnel test were evaluated all optimized airflows stored in the database. The obtained results confirm the good functioning of the designed control system. Figure 4.24 presents the wind tunnel test results for Mach=0.15, and attack angle = -0.5 deg airflow case, while Figure 4.25 describes the tracking error for all four actuators integrated in the morphing wing actuation mechanism.

Figure 4.23 Bench test results for repeated step signals

Figure 4. 24 Wind tunnel test results for Mach = 0.15
and attack angle = -0.5 deg

Figure 4. 25 Displacement error (zoom) for Mach = 0.15
and attack angle = -0.5 deg

Evaluating the obtained tracking errors due to the plays in mechanical parts of the actuators for this flow case resulted absolute values lower than 0.02 mm. On the other way, the absolute maximal values of these kinds of errors observed during all wind tunnel tested flow cases sustain the conclusion drawn during the bench tests, being smaller than 0.1 mm. Another pertinent observation is that the actuator response was not drastically affected by the aerodynamic loads produced by the airflow in the wind tunnel tests.

4.6   Conclusions

The work presented here described a part of a new morphing wing application developed by using an actuation mechanism based on some miniature high-force in-house developed electrical actuators. This paper illustrated the design, simulation, and control of the miniature linear actuator used in the actuation mechanism of the morphing wing. Designed and manufactured by the structural team of the morphing wing project, the actuator consists of a miniature BLDC motor, a gearing system and a trapezoidal screw.

In order to design a control system for the actuator a preliminary modeling step is needed. Therefore, to obtain the overall model of the actuator, a model for the used BLDC motor was first designed. Its numerical validation was conducted by comparing the simulation results with the values from the motor's technical datasheet presented in Table 2. During the simulations, all parameters were achieved with the designed simulation model, thus validating the model. Further, the model was extended by adding the mechanical components. Once finalized the actuator's model, a hysteresis current controller and a position controller were developed, to control the current in the actuator and to maintain the actuator at a desired position. The controller used for position tracking was a proportional-derivative (PD) one because the existing integral term in the system mathematical model eliminated the steady state error. As tuning method, the Ziegler-Nichols method was selected, and the controller parameters were tuned so that no overshoot occurred.

At the next step four similar actuators were integrated in the actuation mechanism of the morphing wing and experimentally tested. First experimental validation for the designed controller and its hardware integration architecture was performed through bench testing at École de Technologie Supérieure in the LARCASE facility, without wind blowing. Two bench testing steps were performed: 1) Independent testing of the actuators - here was observed if each actuator acting independently can successfully manage the high level forces appearing under the skin morphing; 2) Simultaneous testing of the actuators. For both of these steps in bench test, was asked to the actuators to perform vertical displacements corresponding to the optimized values obtained by the project aerodynamic team for each of the seventy-four optimized airfoils.

The final experimental test of the open loop controlled morphing wing system was realized at the IAR-NRC wind tunnel. During this wind tunnel test were evaluated all optimized airflows stored in the database, being tested the control system of the actuators morphing the wing upper surface and the control system for the aileron deflection angle. At this stage, the pressure sensors were used just for aerodynamic reasons, i.e. to visualize the transition point position on the wing.

Both experimental tests revealed a very good behavior of the actuation mechanism. I was observed, also, that the actuators responses were not drastically affected by the aerodynamic loads produced by the airflow in the wind tunnel tests. From the numerical values obtained in both experimental tests for all tested optimized airfoil cases, it was observed that the position control absolute error due to plays in actuators mechanical systems, when the actuators maintain a desired position, was less than 0.1 mm. These plays were fully agreed by booth structural and aerodynamic teams implied in the morphing wing project. From the first team point of view, the plays are important to protect the actuators in the wing bending situations, while, from the point of view of the aerodynamic team it is a safe variation because the simulation results for this wing revealed that the airflow transition point position is insensitive at deflections between -0.1mm and 0.1mm around the optimized vertical deflections of the actuators. A static loading test of the fully equipped wing, developed by the structural team, proved that the actuators were not jammed and worked properly.

Acknowledgments

CHAPTER 5

PROPORTIONAL FUZZY FEED-FORWARD ARCHITECTURE CONTROL VALIDATION BY WIND TUNNEL TESTS OF A MORPHING WING

Michel Joël Tchatchueng Kammegne[1], Ruxandra Mihaela Botez[2], Lucian Teodor Grigorie[3] Mahmoud Mamou[4] and Youssef Mébarki[5]

[1,2]Départment de Génie de la production automatisée, LARCASE Laboratory of Applied Reasearch in Active Controls, Avionics and Aeroservoelasticity,
École de Technologie Supérieure, 1100 rue Notre Dame Ouest,
Montréal, H3C1K3, Québec, Canada
[3]Université de Craiova, Strada Alexandru Ioan Cuza 13,
Craiova 200585, Roumanie
[4,5] Aerodynamics Laboratory, NRC Aerospace, National Research Council Canada, Ottawa,
Ontario, Canada, K1A0R6

Résumé

Dans la conception de l'aile d'avion, les ingénieurs visent à fournir la meilleure performance aérodynamique possible à des conditions de vol de croisière, en termes de rapport portance entre la portance et la traînée. Les surfaces de contrôle classiques tels que les volets, les ailerons, les ailes avec de flèche variable et les aérofreins sont utilisés pour manœuvrer l'avion pour les autres conditions de vol. L'apparition du concept de l'aile déformable a lancé un nouveau défi dans le domaine de l'amélioration de la performance globale des ailes pendant différents segments de vol en modifiant localement l'écoulement sur les ailes de l'avion. Cet article décrit le développement et l'application d'un système de commande pour un mécanisme d'actionnement intégré dans une nouvelle structure d'aile déformable. Le système d'actionnement comporte quatre actionneurs électromécaniques miniatures similaires, disposés selon deux lignes parallèles d'actionnement. Le modèle expérimental de l'aile déformable reproduit à l'échelle 1:1 est équipé d'un aileron (rigide et flexible). Les quatre actionneurs sont commandés au même moment afin de déformer la surface supérieure flexible pour améliorer la qualité de l'écoulement au dessus de l'aile, en retardant ou en

avançant le point de transition de laminaire vers turbulent. Les actionneurs transforment le couple moteur en forces verticales poussant ou tirant ainsi la structure en composite. Leurs bases sont fixées sur les nervures de l'aile, et leurs bras de liaison supérieurs sont fixés à des plaques de support se trouvant sur la peau flexible et liés avec des vis. Les actionneurs poussent ou tirent la peau flexible en utilisant le couple nécessaire jusqu'à ce que le déplacement vertical désiré de chacun soit atteint. Les quatre déplacements verticaux des actionneurs sont fournis par une base de données obtenue à travers une optimisation aérodynamique préliminaire pour des conditions de vol spécifiques. Le système de contrôle est conçu pour commander les positions des actionneurs en temps réel afin d'obtenir et de maintenir la forme désirée de l'aile pour une condition de vol spécifique. La faisabilité et l'efficacité du système de contrôle mis au point par l'utilisation d'une méthodologie basée sur la connaissance du système combinée à une action anticipatrice (en anglais *Proportional Fuzzy Feed-Forward*) sont démontrées expérimentalement sur un banc d'essai en absence des forces aérodynamiques et puis par des essais en soufflerie.

Abstract

In aircraft wing design, engineers aim to provide the best possible aerodynamic performance at cruise flight conditions, in terms of the lift to drag ratio. Conventional control surfaces such as flaps, ailerons, variable wing sweep and spoilers are used to trim the aircraft for other flight conditions. The appearance of the morphing wing concept launched a new challenge in the area of overall wing and aircraft performance improvement during different flight segments by altering locally the flow over the aircraft's wings. This paper describes the development and application of a control system for an actuation mechanism integrated in a new morphing wing structure. The controlled actuation system includes four similar miniature electromechanical actuators, disposed in two parallel actuation lines. The experimental model of the morphing wing is based on a full-scaled portion of an aircraft wing, equipped with an aileron. The upper surface of the wing is a flexible one, being closed to the wing tip; the flexible skin is made of light composite materials. The four actuators are controlled in unison to deform the flexible upper surface to improve the flow quality on the upper surface by delaying or advancing the transition point from laminar to turbulence. The

actuators transform the torque into vertical forces. Their bases are fixed on the wing ribs and their top link arms are attached to supporting plates fixed onto the flexible skin with screws. The actuators push or pull the flexible skin using the necessary torque until the desired vertical displacement of each actuator is achieved. The four vertical displacements of the actuators, correlated with the new shape of the wing, are provided by a database obtained through a preliminary aerodynamic optimization for specific flight conditions. The control system is designed to control the positions of the actuators in real time in order to obtain and to maintain the desired shape of the wing for a specified flight condition. The feasibility and the effectiveness of the developed control system by use of a Proportional Fuzzy Feed-Forward methodology are demonstrated experimentally through bench and wind tunnel testing of the morphing wing model.

5.1   Introduction

In today's world, fuel burn reduction is a serious concern of all of the players in the aerospace industry, not only because of the environmental impacts but also due to the economic aspects. The aerodynamic force component most responsible for fuel burn is the drag (weight also affects drag and thus fuel burn). Therefore, reducing drag through the advanced design of aircraft wings is where aerodynamicists can develop advanced technologies towards green aviation. Among the recent (feasible) technologies used to reduce aerodynamic drag, (Sofla, Meguid et al. 2010) have evaluated the effectiveness of aircraft wing morphing. Aiming at the improvement of the aerodynamic performance by increasing the lift-to-drag ratio, various scenarios to change the wing shape were tested: morphing of the wing upper surface or morphing its trailing or leading edges. From the morphing upper surface point of view, the target is to increase the laminar flow region over the aircraft wing by moving the laminar-to-turbulent transition point close to the wing airfoil trailing edge to obtain in this way a lower drag force as reported by (Zingg, Diosady et al. 2006). Also, the inclusion of the morphing wing technology in the aircraft conception brings another advantages related to the possibilities to fly multiple types of missions as a multi-role aircraft and to create superior system capabilities, performing radically new maneuvers not possible with conventional control surfaces as specified in (Friswell 2009).

(Weisshaar 2006, Rodriguez 2007, Sofla, Meguid et al. 2010, Barbarino, Bilgen et al. 2011) have described the technologies to enable the morphing concept in the aircraft industry that have been tested to date. The literature also revealed that numerous studies and research projects have been developed in the field by various entities such as universities, research institutes and industry. (Prock, Weisshaar et al. 2002) in a collaborative research study explored a process to link analytical models and optimization tools with design methods to create energy efficient, lightweight wing/structure/actuator combinations for morphing aircraft wings. (Pern and Jacob 1999) from the University of Kentucky an adaptive circular arc airfoil was used to control the aerodynamic flow, while (Suzuki, Rinoie et al. 2010) from the University of Tokyo realized a cross-sectional deformation of a laminar airfoil in order to obtain a drag reduction at the off-design angles of attack. In Germany, at the Aerodynamics Institute, RWTH Aachen, an experimental model of an adaptive wing with an adjustable upper side over the entire chord has been proposed by (Schroder, Meijering et al. 2005). The model was used in wind tunnel tests to show the possible improvement of the aerodynamic performance of wings at transonic speeds. (Munday, Jacob et al. 2001) used an adaptive actuator integrated in the wing structure. Experimental results showed an expansion of the laminar flow when the actuator was activated. (Munday and Jacob 2001) extended the previous research work with a conformal camber and with an oscillating camber as stated by (Munday and Jacob 2002). A similar experiment, with an oscillating camber, was performed by (LeBeau, Karam et al. 2010) that investigated the low Reynolds number flow over an adaptive wing assembly. They used a NACA 4415 airfoil for their reference profile; the experimental model was equipped with piezoelectric actuators and a latex membrane to provide a flexible and smooth upper surface. Some adaptive structure concepts for aeroelastic drag reduction and load alleviation were investigated by (Miller 2011) in his PhD thesis at the University of Manchester, UK, wherein a rotating spars concept enabling the adaptive aeroelastic shape control of aircraft wings to reduce drag was developed. That work also showed the application of an all-moving wing tip device with an adaptive torsional stiffness attachment as a passive loads alleviation system. Another method to change the camber line was introduced by (Monner, Hanselka et al. 1998) at the DLR, Germany, designing flexible Fowler flaps for an adaptive wing that allows both a chordwise as well as spanwise

differential camber variation during flight. Some active ribs flex both upper and lower skins. The same concept, but with segmented ribs, was studied by (Poonsong 2004) in his master's thesis at the University of Maryland. His model used the ribs divided into six sections, each section being able to rotate approximately five degrees without causing significant discontinuity on the wing surface. The morphing wing actuation mechanism included two pneumatic actuators. A different approach to adapt the structure shapes in wing morphing applications is based on the compliant mechanisms powered by a single input actuator. Such a system was built at the University of Michigan by (Saggere and Kota 1999) to control a wing section. The mechanism, in which the leading and trailing edges were reshaped by means of actuators, allowed the airfoil camber to change. A similar mechanism was designed, fabricated and in flight tested by a collaborative research team conducted by (Kota, Osborn et al. 2009) from FlexSys Inc., MI, USA and from Air Force Research Laboratory, Dayton, OH, USA, for a Mission Adaptive Wing. (Baker and Friswell 2008) from the University of Bristol, UK, presented another morphing design for airfoils using compliant mechanisms. Their design includes an early skeletal frame-type ground structure, in which the actuators were substituted to obtain a preset surface deflection. Another method to adapt the structure's shapes, instead of using a mechatronic solution with hinges or linear bearings, is the "belt-rib" solution", presented by (Campanile and Sachau 2000) from the DLR, Germany. The new "belt-rib" replaces the classical rib and allows camber changes within prescribed limits, while keeping the remaining parts' stiffness properties unaffected. In addition to changes in the internal mechanism, various actuation mechanisms have been investigated. One of these methods is based on piezoelectric actuation. (Wang, Bartley-Cho et al. 2001) in the Smart Wing 2 program of DARPA, developed a high-rate, large deflection, hinge-less trailing edge control surface for a smart wing model. The model consists of distributed piezoelectric stack actuators with and without hydraulic amplifiers and pumps, as well as aggressive tendon actuation. (Vos, Barrett et al. 2007) from the University of Kansas, USA, and from Delft University of Technology, Netherlands, presented a morphing wing model for UAVs using post buckled pre-compressed (PBP) piezoelectric bender actuators. Flight testing showed that the roll control authority was increased by 38%, and that the control derivatives were more than 3.7 times larger than conventional variants. Using PBP

actuators also increased the actuation frequency, and did so by an order of magnitude. Another morphing application, developed by (Lim, Lee et al. 2005) from Konkuk University, South Korea, used lightweight piezo-composite actuators (LIPCA) to actuate the trailing edges of a biomimetic wing sections. At the same university, (Heryawan, Park et al. 2005) developed another morphing wing application for a small-scale expandable wing, which was separated into inner and outer wings as in a typical bird wing. Under the inner wing section, two LIPCA actuators were attached and activated in the expanded wing state to modify the camber of the wing. Wind tunnel tests showed that the actuators' activation created significant additional lift. (Ray, Singler et al. 2010, Ray, Batten et al. 2011) at Oregon State University, USA, investigated the use of piezoceramic actuators to control bio-inspired flexible wings.

Two approaches for creating control surfaces with the support of microfiber composite actuators (MFCs) were tested at California State University, USA by (Usher, Ulibarri et al. 2013). In the first, flap-like structures were formed by bonding MFCs to each side of a metal substrate, while in the second, MFCs were bonded directly to the wing. Another actuation concept based on piezo-ceramic composite, and known as Macro-fiber composite actuators, was used by (Bilgen, Kochersberger et al. 2009, Bilgen, Kochersberger et al. 2010, Bilgen, Friswell et al. 2011). for adjusting the camber of wings in a series of studies. Similar actuators were also used by (Na, Kim et al. 2006) at Seoul National University, South Korea, in a study related to the nonlinear static analysis of smart wings that aimed to determine the most efficient location for these actuators on smart wings.

An Italian collaborative research project conducted by (Barbarino, Pecora et al. 2009), with researchers from the University of Naples "Federico II", CIRA and Alenia Aeronautica, studied a morphing wing trailing edge concept by replacing the conventional flap device with a compliant rib structure actuated with Shape Memory Alloy (SMA) wires. A feasibility study to deflect a wing flap using SMAs as actuators was undertaken by (Seow, Liu et al. 2008) at Nanyang Technological University, Singapore, in collaboration with DSO National Laboratories, Singapore. They designed and manufactured a wing prototype, and the entire system, consisting of a rib, SMA wires and the flap, was experimentally tested. At the

University of Catania, Italy, (Mirone 2007) realized a study with SMA as actuators which were used to test the ability of a wing to modify its cross section by assuming the shape of two different airfoils, and to test the possibility of deflecting the profiles near the trailing edge in order to obtain hinge-less control surfaces; two prototypes were realized, incorporating the variable airfoil and the hinge-less aileron features respectively. (Abdullah, Bil et al. 2009) in his thesis analyzed the application of smart materials for adaptive airfoils control. Further, the researchers designed, developed and tested a deformable wing model using ABS material for the skin. The deflection of the 8 variable cambered wings was controlled by means of SMA actuators fixed underneath the wing skin, near the leading edge as presented by (Abdullah, Bil et al. 2010).

With the final aim to obtain real-time optimized airfoils, our research team from the ETS in Montreal, Canada, used the laminar-to-turbulent flow transition point as control variable in a morphing wing project financed by Consortium for Research and Innovation in Aerospace in Quebec (CRIAQ). Called CRIAQ 7.1, the project was developed in collaboration with Thales, Bombardier Aerospace, Ecole Polytechnique, and IAR-CNRC. The team conducted by (Popov, Botez et al. 2008) developed a possibility to detect the transition point starting from the surface pressure distribution, the precision of the method being dictated by the density of the pressure sensors distributed along the airfoil chord. The morphing wing experimental model was equipped with SMA actuators, actuating on two parallel lines. Two adaptive neuro-fuzzy controllers were designed by (Grigorie, Botez et al. 2009) in order to correlate each set of pressure differences, calculated between the optimized and the reference airfoils, with each of the airfoil deformations produced by the two actuation lines. (Grigorie, Popov et al. 2011) described the procedure to obtain a linear model of the heating and cooling phase from an SMA actuator in order to be used in the design of its controllers. Subsequently, With the linear model, (Grigorie, Popov et al. 2012) designed an on–off combined with a proportional–integral controller and experimentally tested in the wind tunnel. Due to the strong nonlinear behavior of the SMA actuators, (Grigorie, Botez et al. 2012, Grigorie, Botez et al. 2012) developed and experimentally evaluated a hybrid control system combining a fuzzy logic proportional-integral-derivative controller and a conventional on-off controller. The final wind tunnel testing of the morphing wing model

performed by (Popov, Grigorie et al. 2010, Popov, Grigorie et al. 2010) by using a real time optimizer to close the control loop confirmed the project formulated hypothesis, proving the drag reduction as a consequence of the laminar flow expansion on the upper surface of the wing.

In another small-scale morphing wing model developed in our research team by (Kammegne, Grigorie et al. 2014), the actuation mechanism was based on some DC motors which rotated two eccentric shafts and morphed a flexible skin along two parallel actuation lines. A position controller aiming to control the shape of the wing airfoil under different flow conditions was designed and tested in the Price-Païdoussis Wind Tunnel at the ETS in Montreal, Canada. As a supplementary validation, an analysis of the wind flow characteristics was performed; the pressure coefficients predicted by the numerical simulations evaluated by (Koreanschi, Sugar-Gabor et al. , Gabor, Koreanschi et al. 2012) and (Hassih, Brossard et al. 2013) were compared with those obtained from the experimental testing.

In this context, a new morphing wing international collaborative research project was initiated by industrial entities, research institutes and universities from Canada and Italy, project developed on a full-scaled portion of the wing of an aircraft, fully actuated by using electrical actuators. The work disseminated here is a part of this project and describes the numerical and experimental results obtained with a variant of the control system developed to be used in the actuation of the flexible skin on the upper surface of the wing.

5.2   Morphing Wing Project Specific Issues

The present morphing wing research project may be considered as a continuation of the CRIAQ 7.1 project developed by our research team in the Research Laboratory in Active Controls, Avionics and Aeroservoelasticity (LARCASE) of the ETS in Montreal, Canada, in which Shape Memory Alloy (SMA) wires were used as actuators to morph the upper surface of a WTEA-TE1 wing profile. The multitude of specific issues solved in the previous project, came from the multidisciplinary integration in the same experimental demonstrator model of strongly nonlinear actuators (SMA actuators) with optical and Kulite pressure sensors, real

time control 10 algorithms for actuators positions, and real time estimators and optimization algorithms for the laminar to turbulent transition point position. In the new multidisciplinary project, specialists participate by working from aerodynamics, aeroservoelasticity, mechanics, control and electrical engineering. Called "Multi-Disciplinary Optimization" 505 (MDO 505), this new CRIAQ funded project seeks to realize fuel consumption optimization by applying morphing wing technology to an aircraft wing equipped with a morphing aileron. In this project, realized at the ETS in Montreal, Canada in collaboration with Thales, Bombardier Aerospace, Ecole Polytechnique, the Institute for Aerospace Research - National Research Council Canada (IAR-NRC), and with Italian researchers from Frederico II Naples University, CIRA and Alenia, a wing-aileron prototype (Figure 5.1) is designed, tested and validated using wind tunnel tests at IAR-NRC. Unlike the previous morphing project (CRIAQ 7.1) of our research team, this project uses miniature electromechanical actuators instead of smart material actuators. The special challenges of the MDO 505 are four-fold: 1) to aerodynamically optimize a non-symmetrical wing by using numerical simulations; 2) to adapt the actuation mechanism of the flexible skin and its control system to fit into the very small space inside the wing; 3) to obtain a good reproducibility of the numerically optimized shape of the upper surface of the wing with the experimental one by using a minimum number of actuation points; and 4) to attach the flexible skin on all four sides of the wing, which hampers the achievement of the upper surface reproducibility (experimental versus numerical). Moreover, all of these challenges need to be overcome by keeping the resistance structure of the wing segment in its original form. Our research team first aim was to design and to integrate in the experimental model a control system able to morph the wing according to the requirements imposed by the aerodynamic optimization results obtained for different flow cases given by various Mach numbers (M), wing angles of attack (α) and aileron deflection angles (δ). On the other way, to evaluate the aerodynamic gains of the morphing wing model during the wind tunnel tests, the team had the task to develop a mechanism able to detect and visualize the airflow characteristics based on the data obtained from the pressure sensors installed on the upper surface of the morphing wing.

Figure 5.1 Schematic structure of the morphing wing

The wing model was based on the dimensions of a full scale wing tip structure, the span and chord of the model matching the dimensions found on a real aircraft wing tip, 1.5 m span and 1.5 m root chord with a taper ratio of 0.72. An optimization procedure was run by the aerodynamic team aiming to find the optimum airfoils shapes through local thickness modifications to improve the upper surface flow. The optimization was applied for several flight cases as combinations of Mach numbers (M), angles of attack (α) and aileron deflection angles (δ). The adaptive upper surface is a flexible skin made from carbon fiber composite materials, which was positioned between 20% and 65% of the wing chord. The rigid structure, as well as, the flexible skin was specifically designed to meet aeronautical industry requirements. On the other way, in the flexible skin design and optimization procedures the match with the aerodynamically optimized upper surface shapes was considered as a determinant objective. Once established the structural constraints of the flexible skin and chosen the flight cases, the team resorted to the design of the actuation system, including here the actuation mechanism and the actuators. It resulted that the actuation mechanism should include four actuators disposed on two actuation lines, the first

one placed at 32% of the chord, and the second one at 48% of the chord. The low space inside the wing required a direct actuation of the flexible skin, the in-house manufactured actuators being fixed with the lover part on the wing ribs and with the top on the flexible skin. To solidify the entire structure the high grade industry steel and aluminum alloy material were used for the manufacturing of different internal structure elements.

The aerodynamic optimization procedure correlated with the actuators positions on the wing structure generated a database relating the actuators displacements and the optimized airfoils for different flight cases. Therefore, the actuators need to morph the upper surface of the wing until the desired displacements are achieved and an experimental airfoil approximating the optimized airfoil for a specified flight case is obtained. In order to achieve and maintain this airfoil shape even under the influence of external perturbations such as structural and aerodynamic loads a robust control system should assist the actuation system. For each of the four actuation points, the actuation mechanism included a brushless direct current motor whose shaft was coupled to a gearing system with the other end attached and linked to a nut. Four Linear Variable Differential Transducer (LVDT) were also used to measure the displacements of the four actuators (Figure 5.2).

Figure 5.2 Experimental model of the morphing wing

In the next sections of the paper are exposed the design and the experimental testing of the system controlling the positions of the four actuators.

5.3   Controller Design and Bench Test Experimental Results

The control system of the experimental model was developed in two successive steps, called generically "open loop" and "closed loop". In the first architecture (open loop) are controlled the wing morphing system, and the aileron deflection angle, while in the second one (closed loop architecture), which includes the open loop architecture as an internal loop, is controlled the transition point position based on the information from the pressure sensors installed on the flexible skin and on the aileron upper surface. Therefore, the difference between the two architectures is the use of the information from the pressure sensors as feedback signal in the control algorithm.

The actuation system was equipped with four identical actuators, requiring in this way the same position controllers. In the open loop architecture the control system was experimentally tested in two situations: 1) on the bench, with no aerodynamic load, and 2) in the wind tunnel, with aerodynamic load corresponding to each optimized flight case. The testing of the open loop architecture of the control system in the wind tunnel allows also the validation of the numerically obtained optimized airfoils through the real time visualization of the transition point position based on the pressure sensors data. For each flight case the control system asks to the actuators to morph the skin until the real vertical displacements $(\mathrm{d}Y_{1\mathrm{real}}, \mathrm{d}Y_{2\mathrm{real}}, \mathrm{d}Y_{3\mathrm{real}}, \mathrm{d}Y_{4\mathrm{real}})$ in the actuation points equal the vertical deflections $(\mathrm{d}Y_{1\mathrm{opt}}, \mathrm{d}Y_{2\mathrm{opt}}, \mathrm{d}Y_{3\mathrm{opt}}, \mathrm{d}Y_{4\mathrm{opt}})$ characterizing the differences between the optimized airfoil and the reference airfoil; the real vertical deflections (the control feedback) is measured by using the four LVDT sensors associated with each of the four actuators.

On the other way, the bench testing of the open loop architecture given the opportunity to evaluate of the level of reproducibility of the numerically optimized shape of the upper surface of the wing with the experimental obtained one. To verify this reproducibility, the morphed wing was laser-scanned (Figure 5.3) for each optimized airfoil in the database (for

all optimized flight cases), and software results were compared with the numerical results in terms of skin shapes. To scan the surface, a portable scanner, called the Handy Scan 3D, was used, and targets were added on the skin surface. These targets are the white dots on the surface of the wing shown in Figure 5.3.

Targets were used when the object did not supply enough geometrical information to allow acquisition; thus, approximately 200 targets were used on the surface of the skin and ribs. Because a mirror-like surface (especially aluminum) prevents the laser from detecting the surface, a fine powder was applied on the wing. The targets were also needed to provide a reference for the scanner.

Figure 5.3 Laser scanning of the morphing wing during bench tests

The second testing of the open loop architecture, the wind tunnel test, allowed, on the other way, the validation of the aerodynamic optimization of the system through the visualization of the transition point position for each optimized airfoil in the database (for all optimized flight cases). These visualizations are based on the information provided by the pressure sensors installed on the flexible skin. As a supplementary evaluation method for the transition point position in wind tunnel tests, an infrared visualization of the flow was performed by using the IAR-NRC experimental facility.

The bench testing of the experimental model was performed in the LARCASE laboratory at the ETS in Montréal, Canada; the scheme of the experimental bench test used to validate the

implemented controller in the open loop is presented in Figure 5.4.

Figure 5.4 Open loop control architecture in bench tests

In this control mechanism, the real-time system converts the desired vertical positions in motor rotation units and asks to the actuators to go to this positions (commands represented by the lines in magenta in Figure 5.4), and obtains in the same time the feedback signals related to the real linear positions of the actuators by using the LVDT sensors data (signals represented by the cyan lines in Figure 5.4). The controller's input and output are configured with the physical input/output of the target, so that when it is compiled and downloaded in the real-time target via the Ethernet cable (blue line with double arrows in Figure5.4), the data exchange can flow freely between the target and the hardware.

For the bench tests our team conceived a Graphic User Interface (GUI) (Figure 5.5) which helped the safe testing of various situations, both from the control point of view but also from the flexible skin and actuators integration on the experimental model. Besides the simultaneous actuation, we followed the independent testing of the actuators in custom situations, evaluating in this way their power and in the same time the strength of the flexible skin in limit situations. In the same time, there was set a communication between the GUI and the database relating the actuators displacements and the optimized airfoils for different flight cases, the user being able to command the actuation for all of these cases. In Figure 5.5, depicting the GUI, may be noted the eight distinct areas, numbered in yellow boxes. The

first area is reserved to the displaying of the aerodynamic data associated with each flight case included in aerodynamic database; there was implemented a button allowing the flight case selection for the test. In the second area, reserved to the "Motion control" were implemented two buttons, one for the emergency stop and another one who brings the drives into listen mode. There are also some fields allowing the setting of the actuator speed and the assignation of a node Id to each of the actuators drives. The third area contains four graphical windows plotting the time evolution of the required and of the measured displacements of each of the four actuators. Information in numeric format related to the electrical current used by the actuator and to the actuators positions provided by the encoder and by the LVDT are displayed in the area number four. To switch between the custom actuation mode and actuation of the optimized cases a "Custom" button was added in seventh area of the GUI. Once the custom actuation mode activated the buttons in fifth area can activate each actuator individually, while the button in sixth area can activates all the actuators simultaneously.

The desired numerical values in custom or optimized cases are displayed in the area numbered with eight. The Stop button on the GUI is used to stop the program.

Figure 5.5 The Graphic User Interface (GUI) developed for the bench testing of the model
To develop the control system of the morphing wing actuators, a proportional fuzzy feed-forward architecture was chosen (Kovacic and Bogdan 2005, Hampel, Wagenknecht et al. 2013) for each of the four controllers; its architecture is shown in Figure 5.6, wherein each actuator is coupled to a controller. Fuzzy approach was chosen because no numerical model of the system was developed.

Figure 5. 6 Open loop control architecture
of the morphing wing model

The controller's input is the position error, and its output is the number of pulses required to reach the desired vertical position in millimeters. The controller's output is sent directly to the motor integrated in the actuator.

The developed control system includes four similar controllers, each one associated to an actuator. Both for input and for output we decided to use eleven membership functions (mf). The input mf were distributed in [-10, 10] universe of discourse, having triangular shapes

(Figure 5.7), while the output mf were considered as constants distributed in the same universe of discourse. The designed controllers were tuned based on knowledge obtained from the system behavior, the membership functions parameters being determined by the trial and error method. The rule set in the fuzzification process contained eleven rules as shown in Figure 5.8.

Figure 5.7 The membership functions associated to the input

Figure 5.8 Rules set in the Fuzzification process

In the bench tests the actuators were controlled simultaneous or independently to cover a large spectrum of interactions between them, the flexible skin and the rigid structure of the experimental model. All tests were performed in the laboratory conditions, in the absence of the aerodynamic forces. Figure 5.9 exposes the actuation results obtained in a custom actuation situation when the four actuators where simultaneously triggered and two of them (Act. #1 and Act. #3) morph the flexible skin negatively while the other two (Act. #2 and Act. #4) morph the skin positively. The actuators responses were very good, although it was observed a slight time delay induced by the system inertia both from software processing and mechanical points of view.

Similar results were noticed in all performed bench tests, Figure 5.10 presenting the responses of the actuators triggered independently for various repeated step signals as control inputs. From the Figure 5.9 and 5.10 can be also easily observed the very low level of the noise superposed on the LVDT sensors signals. It is due to the filters integrated in the SCXI-1540 LVDT modules from National Instruments used as signal conditioners for LVDTs.

Figure 5.9 Simultaneous actuation in
the four morphing wing points

Figure 5.10 Repeated step independent actuation
in the four morphing wing points

5.4 Experimental Setup in the Wind Tunnel

The schematic of the instrumented wing configuration for the wind tunnel tests is shown in Figure 5.11. In the wind tunnel tests, under aerodynamic loads for a given optimal case, the miniature electrical actuators would push or pull the flexible skin using the necessary torque until the desired vertical displacement of each actuator is achieved. The skin displacement in each of the four actuation points is sensed by the linear positioning sensor (LVDT) mounted on the corresponding actuator. The acquired raw skin displacement is send to the signal conditioner (SCXI), which supplies and processes the linear positioning sensor; it is indicated in Figure 5.11 by the orange line. The output signal from the signal conditioner (the brown line in Figure 5.11) is the actual skin displacement in millimeters. The encoder position needed to achieve the positioning control of the actuator is processed by the drive and read by the real-time system (PXI express); the encoder position is represented by the blue line.

Figure 5.11 Experimental setup in the wind tunnel

The PXI express is a real-time machine using an integrated real-time operating system. The main advantages of that system are that it can be extended with other real-time systems and it is modular. Modular, in the sense that it is used here, means that different modules or cards can be inserted into the PXI express (PXI-e) chassis. For this project, the PXI-e chassis has been extended by five different modules. The first four modules (from left to right) are used to acquire the pressure sensors' signals, while the last module, which is a CAN open module, is used to communicate with the CAN network defined by the motor drive systems. Each of the pressure sensor signal modules is able to process at most 8 pressure sensors signals, thereby covering all 32 of the used Kulite pressure sensors. The pressure data acquisition was performed at 20k samples/s for each channel. All pressure data were connected directly to the modular cards inserted inside the PXI-e chassis. All raw data for the 32 Kulite sensors were saved into the real time system's hard drive for post-processing. The pressure coefficient curves obtained by calculating the dynamic pressure and by using the pressure Kulite data

were displayed in real time for all the optimized flight cases. Signals from the LVDTs were also displayed for the different optimized flight cases. The end user selects the desired flight case from the Graphical User Interface (GUI) and the desired displacements were automatically loaded.

The data flow between the real-time controller and the computer is indicated by the double arrow line in yellow in Figure 5.11, while the CAN open communication in the network is highlighted by the green arrow.

5.5   Wind Tunnel Test Results

Wind tunnel testing was performed at the IAR-NRC wind tunnel facility in Ottawa. During this first set of wind tunnel tests, 97 flight cases were tested: Nineteen values for the angles of attack, three values for the Mach numbers, and thirteen for the aileron deflection angles. The angles of attack values varied from -3 degree to +3 degree, the Mach number values varied between 0.15 and 0.25, and the aileron deflection angles varied between - 6deg. to +6 deg. The ninety seven desired optimized airfoils were obtained by changing the upper surface of the wing in the vertical direction. The aerodynamic goal was to extend the laminar region by moving the transition point as near as possible to the wing trailing edge with a constant lift (Paraskevopoulos 2001). Other publications regarded adaptive trailing-edge device research has been developed by (Diodati, Ricci et al. 2013, Ameduri and Pecora 2015). Various genetic, neural network new methodologies implemented by (Mosbah, Botez et al. 2016) and (Xu, Shuo et al. 2005, LU, Hu et al. 2006, Yuan and Guangchen 2011, Roudbari and Saghafi 2014)were used for morphing wing control, modeling and identification, as well as for aircraft and helicopters.

Thus, the wing model was tested in open loop architecture; the main signals such as the raw pressure signal data from the Kulite sensors, the skin displacements from linear positioning sensors, actuator current, and actuator speed were recorded. In this configuration, the loop was closed by using the LVDT signal as feedback for the controller. The pressure sensor signals were used to visualize the start of the transition in real time through power spectra analyses, while the calculated pressure coefficients were used to validate the aerodynamic

predicted wing shapes. The real time acquired raw pressure signals were post-processed to obtain the FFT spectral decomposition, the standard deviation (STD) calculation, and the location of the transition. The raw pressure signals were filtered to remove parasitic noise.

The results obtained for an actuation case (Mach=0.25, α=0.5˚, δ=-1˚) are shown in Figure 5.12. For all actuated cases it was found that the controller performed well with the static error consistently less than 0.1 millimeters. The rise times were between 1 and 2 seconds, more than adequate for our morphing application. The measured positions for the four actuators were sensed by the LVDTs, while the desired positions were loaded from the database made from the data predicted by the aerodynamic team.

During the tests, the user's computer was installed in the control room of the wind tunnel facility, linked to the real time system with an Ethernet cable. The four miniature actuators installed inside the wing and the aileron actuator were controlled via a new Graphical User Interface (GUI). The GUI used to control the whole equipment during the wind tunnel tests is shown in Figure 5.13. The graphical characteristics in Figure 5.13 (orange frame) show the plots of the measured skin displacements and the reference skin displacements. The "emergency stop" push button deactivates the entire system and brings it back to its reference.

Figure 5.12 Wind tunnel controller results for flight case 38 (Mach=0.25, α=0.5˚, δ=-1˚)

The "flight case selection" select button loads the flight case number with its flight conditions (Mach number, aileron deflection angle and angle of attack), as it is shown in the blue frame of Figure 5.13. Under "Mode selection", the user is able to select three different modes: Manual, Flight case and Homing. The "Homing" mode sends the system back to its reference state. The "Manual" mode allows the user to give skin position set points that are different than those of the data base. The numerical controls ("Set point act 1", "Set point act 2", "Set point act 3", and "Set point act 4") are used for this purpose. Each actuator can be controlled individually in "Manual" mode by pushing one of the following buttons, "Activate act 1", "Activate act 2", "Activate act 3", "Activate act 4", or they can be moved simultaneously after pushing the "Act_all_manual" button. The numerical values for the skin displacements as well as the real skin displacements are displayed using the numerical indicators shown in Figure 5.13 (white frame).

In "Flight case" mode, when a flight case is selected and the flight conditions have been loaded, the user has to activate the controller by changing the value of the numerical control buttons "Activated act 1 & 3" and "Activated act 2 & 4" to 1.

Kulite pressure sensors are used to capture what happens over the flexible skin when the wind is blowing. They are very sensitive, highly accurate differential sensors, and the pass band of their values are logged for each flight case. The log file is created once the "Logging Enabled" button is pressed, and the logging starts immediately. The logging stops when the button is released. The same procedure is used for the logging of the numerical values of the LVDTs and motor data such as velocity, encoder, and current.

An aileron is attached to the experimental wing; its position is controlled by means of an electromechanical actuator. The red frame in Figure 5.13 indicates how all the information to control the aileron actuator is collected. The aileron drive status is given by the radio button "DRIVSTAT", where the actual aileron actuator position in degrees is displayed on the numerical indicator "Aileron_angle", while the motion task to send to the drive is inputted by selecting "Motion task" from the menu "operation". Each flight case has a corresponding motion task which is programmed directly, according to the manufacturer's recommendations. For instance, to obtain 0 degree aileron deflection, a motion task with the value of 6 deg. is sent, to obtain -6 degree deflection, a motion task with the value of 0 deg., and to obtain 6 degree deflection angle, a motion task with the value of 12 deg. is sent respectively.

The 32 Kulite pressure sensors are installed on the upper surface to sense the static pressure on the wing. They are located between 28% of the chord and 68% of the chord. To understand the physical phenomena that occurs when the wind is blowing, the power spectra and the standard deviation of all their 32 channels are evaluated. The transition region is delimited by two Kulite sensors, where the first indicates the sensor with a higher power spectra value than the previous one, and the second is given by the sensor with the highest standard deviation.

Figure 5.13 Graphical User Interface (GUI) for wind tunnel tests

The power spectra for flight case 70 (Mach=0.2, α=1˚, δ=4˚) for the morphing wing case is depicted in Figure 5.14. The first set of 8 sensors is named "CH 1-8", the second set of 8 sensors is named "CH 9-16", the third set of 8 sensors is named "CH 17-25", and the last set is named "CH 26-32". During wind tunnel testing, it was decided to go back with the system to its reference between two flight cases, and logged the data when the system was morphed or not morphed. From Figure 5.14, it can be observed that for this case, the transition is located between the channel 15 and channel 19.

The standard deviation of the pressure data acquired for flight case 70 is shown in Figure 5.15. Pressure sensor 19 has the highest value. To compute the standard deviation, the noise at 5 kHz has been removed. This noise was due to the electromagnetic field generated by the wind tunnel electrical devices, and was present in the FFTs for all the tested flight cases.

Figure 5.14 The power spectra for the flight case 70 (Mach=0.2, α=1˚, δ=4˚)

Figure 5.15 Standard deviation of the pressure data
acquired for the Mach=0.2, α=1˚, δ=4˚)

The infrared (IR) image of the whole wing during wind tunnel testing for flight case 70 is shown in Figure 5.16: Figure 5.16a – un-morphed/reference airfoil, Figure 5.16b - morphed airfoil. The IR technique makes it possible to visualize and estimate online the transition location on the wing. The red frame indicates the limits of the flexible skin, which is made of composite materials. The line of Kulite sensors and the spots showing the four actuators are visible as well. The black line indicates the estimated transition line, and the white lines indicate the tolerance band. The thermography methodology (Infrared methodology) is based on the temperature gradient in the laminar and turbulent flow. The blue region inside the red frame in Figure 5.16 indicates the laminar region (low temperature region) while the yellow color inside the same frame shows the turbulent region (high temperature region). The wind is blowing from left to right. According to the IR transition images given by Figure 5.16a (un-morphed/reference airfoil) and Figure 5.16b (morphed airfoil) for Mach=0.2, α=1˚, δ=4˚, the transition has been delayed by about 4%. With no actuation, the transition was located at about 48% of the chord (see Figure 5.16a), while for the same flight conditions with the system actuated the transition was moved to 52% of the chord. In addition, a very good match was obtained between the IR imaging and the Kulite sensors in terms of the transition location.

Figure 5.16 Infrared image capture for flight case 70 (Mach=0.2, α=1˚, δ=4˚)

5.6 Conclusions

This paper has presented results obtained in a new morphing wing project, as part of the development and experimental testing of a variant of the control system used in the actuation of the flexible skin on a wing upper surface. In the exposed control architecture (open loop) were controlled the wing morphing system, and the aileron deflection angle. In this first phase of the control development, the designed position controller for the four morphing wing actuators was tested experimentally in bench tests with no aerodynamic load, and then, in wind tunnel tests, with aerodynamic load(s). Proportional Fuzzy Feed forward architecture was chosen for controlling the actuation lines.

The first testing of the open loop architecture, the bench test, allowed also the evaluation of the level of reproducibility of the numerically optimized shape of the upper surface of the wing with the experimental obtained one. The bench testing of the experimental model was performed in the LARCASE laboratory at the ETS in Montréal, Canada. To verify this

reproducibility, the morphed wing was laser-scanned for each optimized airfoil in the database (thus, for all optimized flight cases), and software results were compared with the numerical results. The bench tests results were very good, and prepared us for the next tests with aerodynamic loads, conducted in the IAR-NRC wind tunnel in Ottawa. During all tests performed for each of the optimized flight cases the values of the static errors were under the limit established by the aerodynamics, i.e. 0.1 millimeters; from the numerical simulations the aerodynamic team observed that in a range between -0.1 mm and 0.1 mm around the optimized position the estimated transition point position of the upper surface flow is approximately the same.

The second testing of the open loop architecture, the wind tunnel test, allowed the validation of the aerodynamic optimization of the system, through the visualization of the transition point position for each optimized airfoil in the database (for all optimized flight cases) based on the information provided by the pressure sensors installed on the flexible skin. The IAR-NRC experimental facility allowed for a supplementary evaluation method for the transition point position in wind tunnel tests, the infrared (IR) visualization of the flow. Similar to the bench tests, for all actuated cases it was found that the controller performed well, with static error consistently being less than 0.1 millimeters. The rise times were between 1 and 2 seconds, which is absolutely good enough for our morphing application. To understand the physical phenomena appearing when the wind was blowing, the power spectra and the standard deviation of all 32 used Kulite pressure sensors channels were evaluated. The results obtained for the FFT, STD and IR evaluations, and for the flight case 70 (Mach=0.2, α=1˚, δ=4˚) have shown that the transition was delayed by about 4%, from close to 48% of the chord in the un-morphed situation to 52% of the chord in the morphed situation. In addition, a good match was obtained between the IR and Kulite pressure sensors' results in terms of the transition location.

Acknowledgments

CHAPTER 6

CONTROL OF THE MORPHING ACTUATION MECHANISM INTEGRATED IN A FULL-SCALED PORTION OF AN AIRCRAFT WING

Michel Joël Tchatchueng Kammegne[1], Yvan Tondji[2] Ruxandra Mihaela Botez[3], Lucian Teodor Grigorie[4]
Mahmoud Mamou[5] and Youssef Mébarki[6]

[1,2,3]Départment de Génie de la production automatisée, LARCASE Laboratory of Applied Reasearch in Active Controls, Avionics and Aeroservoelasticity,
École de Technologie Supérieure, 1100 rue Notre Dame Ouest,
Montréal, H3C1K3, Québec, Canada
[4]Université de Craiova, Strada Alexandru Ioan Cuza 13,
Craiova 200585, Roumanie
[5,6] Aerodynamics Laboratory, NRC Aerospace, National Research Council Canada, Ottawa,
Ontario, Canada, K1A0R6

Résumé

Cet article présente quelques résultats obtenus au cours d'un projet de recherche sur une aile déformable réalisée en collaboration avec de nombreux partenaires industriels. Le processus de modélisation de l'actionneur électromécanique miniaturisé utilisé dans l'application de l'aile déformable, la loi de commande développée pour l'actionneur, et la validation expérimentale du système de contrôle conçu sont présentés dans cet article. L'actionneur assemblé est constitué d'un moteur à courant continu sans balais couplé à un système de boîte de vitesses, une vis, un écrou et un système d'engrenage. Un capteur de position linéaire fixé sur l'actionneur mesure la position de l'actionneur en millimètres pour le système de contrôle, tandis que la position de l'arbre du moteur est donnée par un encodeur intégré à l'intérieur du moteur. Deux lignes d'actionnement ayant chacun deux actionneurs sont intégrés à l'intérieur de l'aile pour modifier sa forme. Pour ce projet, un démonstrateur fabriqué à l'échelle 1:1 avec la longueur de corde de 1,5 mètres est utilisé. La peau flexible sur l'extrados de l'aile est réalisée en fibre de carbone. Les bordures de la peau en composite

136

sont fixées à l'aide des vis sur l'intrados de l'aile. Pour agir sur le système d'actionnement le moteur a été relié à un amplificateur capable de l'alimenter via une tension d'alimentation contrôlable. Trois boucles de contrôle en cascade, c'est-à-dire une boucle de commande de couple et deux boucles parallèles de commande de position sont conçues et validées expérimentalement. Les deux boucles de commande de position sont différenciées par les capteurs de rétroaction utilisés; le premier capteur utilise le signal de rétroaction de l'encodeur comme signal de retour pour le premier correcteur de position, tandis que le second capteur utilise le signal du capteur de position linéaire comme signal de retour pour le second correcteur de position. Les paramètres du contrôleur pour la commande du couple et de la première boucle de commande de position sont implémentés à l'intérieur de l'amplificateur de puissance, tandis que la seconde boucle de commande de position est validée expérimentalement en utilisant un système temps réel. La validation expérimentale du système de contrôle développé est réalisée en deux étapes indépendantes en utilisant le banc d'essais sans la présence des forces aérodynamiques, et par des essais en soufflerie. Dans le but de valider l'objectif aérodynamique du projet, les données de pression fournies par certains capteurs de pression Kulite qui sont montés sur la surface supérieure de la peau flexible sont utilisées pour estimer la position du point de transition du régime laminaire au régime turbulent. De la même manière, pour la capture de la zone de transition sur toute la surface du modèle de l'aile, des visualisations à l'aide de caméra infrarouge sont effectuées.

Abstract

The paper presents few results obtained during a morphing wing research project realized with the collaboration of numerous industrial partners. Shown are the modeling of a miniature electromechanical actuator used the morphing wing application, the development of a control concept for this actuator, and the experimental validation of the designed control system integrated in the morphing wing model. The assembled actuator consists of a brushless direct current motor coupled to a gearbox system, a screw, a nut and a gearing system. A Linear Variable Differential Transducer (LVDT) is attached on the actuator giving back the actuator position in millimeter for the control system, while the motor shaft position is given by an encoder integrated inside the motor. Two actuation lines each having two

actuators are integrated inside the wing to change its shape. For this project a full-scaled portion of an aircraft wing with the chord length of 1.5 meters is used, the flexible skin mounted on the extrados being made of composite fibber materials. To bring the actuator system in motion, its motor has been connected to a power amplifier able to energize it via a controllable voltage. Three control loops, a torque control loop and two parallel position control loops are designed and implemented. The two position control loops are differentiated by the feedback sensors used; the first one uses the encoder signal as feedback, while the second uses the LVDT signal as feedback sensor. The controller's parameters for torque control and the first position control are implemented inside the power amplifier while the second position loop are experimentally validated using a real time system. The experimental validation of the developed control system is realized in two independent steps, bench testing with no airflow, and wind tunnel testing. As a way to validate the aerodynamic purpose of the project, the pressure data provided by some Kulite sensors mounted on the upper surface of the flexible skin are used to estimate de laminar-to-turbulent transition point position. Also, for capturing the transition region over the entire wing model surface, infra-red (IR) thermography camera visualizations are performed.

6.1   Introduction

Although widely used in the aviation industry since its beginning, the morphing wing technology successfully generates research subjects of present and future interests, which engages entities that cover the entire spectrum of the field: industry, universities and research laboratories. All these subjects are closely related to the new trends in the aviation industry both in terms of the "green" component in the new technologies, and in terms of the operating costs decrease for the next-generation of aircraft. Both directions of optimization have found in the morphing wing technology a common point related to the fuel consumption reduction. This reduction impacts practically the operating costs and the emissions as well. In aviation aerodynamics, one the mechanisms that allows fuel burn reduction is based on the aircraft aerodynamic performance improvement by morphing their wings.

There are different types of morphing wing applied in aviation: 1) morphing with fixed-wing, where the wing shape is changed using controls such as slats, flats, etc...; 2) morphing wing

by using a flexible skin integrated in the wing structure. The second type of morphing was put aside for a long time because of the technological limitations. For example, to accomplish it an actuation system has to be designed judiciously to best fit inside the aircraft wings structure. On the other way, to maintain a reduced aircraft weight such kind of actuation system need to be light, fast, low energy consumer, and self-locking. Researchers are still dealing with the morphing technology today despite the little impact observed several decades ago. The interest becomes more important and more ambitious as the current technology is more advanced; many new actuators (lightweight), actuation systems, materials (composite materials) and devices have been developed and tested in various morphing wing applications ((Weisshaar 2006, Min, Kien et al. 2010, Sofla, Meguid et al. 2010, Barbarino, Bilgen et al. 2011)).

In the context of SARISTU project realized and conducted by (Diodati, Ricci et al. 2013) at the Italian Aerospace Research Center, aiming to reduce fuel consumption on a regional aircraft using adaptive trailing edge (ATE) device, different actuation mechanisms was proposed. It had been proved that it was possible to have a suitable actuator system concept able to fulfill for an ATE modifying the wing camber and attaining significant fuel savings; ATE architecture allowed the device to morph and reach the desired configuration, but also, it played the role of a load reduction mechanism by transferring only a fraction of the aerodynamic load to the actuator. In the same project, an adaptive control system dedicated to the actuator used for wing trailing edge was implemented by (Dimino, Flauto et al. 2014). A classical PID controller with constant coefficients was used to control the actuator's position. The tuning methodology of the gains was a combination of the Ziegler-Nichols with a trial-and-error method. Via numerical simulation results, it was observed that such kind of control law was as well as suitable for morphing wing application.

Another research project, developed at Konkuk University by a team of (Heryawan, Park et al. 2005), South Korea, concerned the design, manufacturing, and wind tunnel testing of a small-scale expandable morphing wing. The wing was made of carbon composite and balsa strips, along with carbon fiber composite forms mimicking bird wing feathers. Two LIPCAs

(lightweight piezo-composite actuators) were utilized to modify the wing's camber. Wind tunnel tests showed that the LIPCA-activated wing created significant additional lift.

Wing spar variation is one of the techniques used to change the profile of a wing. By applying this technique, a segmented telescopic morphing wing for an unmanned aerial vehicle (UAV) was designed by (Blondeau, Richeson et al. 2003) at the University of Maryland, USA ([8]). In order to minimize the weight of the UAV, pressurized telescopic spars were used. Such kinds of actuators were able to achieve various wingspan configurations withstanding the aerodynamic load. They argued through experimental results that the drag to lift ratio of the wing was about 25% lower than its rigid fixed wing spars counterpart when fully extended.

(Joo, Sanders et al. 2006) from University of Dayton, Air Force Research Laboratory - Wright-Patterson AFB, and Pennsylvania State University in USA proposed and studied another approach to alter the wing span by using scissors-like mechanism. Firstly, the mechanism for a single cell, made of four linkages, a single actuator and the flexible skin, was simulated. Further, results for multiple cells cases were generated. Numerical analysis allowed them to find the suitable locations for the actuators.

Changing the wing span and chord at the same time was made possible according to the research work realized at Instituto Superior Tecnico, Universidade Técnica de Lisboa, Portugal, in collaboration with Universidade da Beira Interior, Portugal, and University of Victoria, Canada by (da Costa Aleixo 2007, Gamboa, Aleixo et al. 2007). Numerical results predicted a significant drag reduction between 14% and 30% for different flight stages.

To realize the desired displacements, the use of some servo actuators was suggested. The main objective of the work was to ascertain the feasibility and functionality of the morphing mechanism and investigate the solutions of some problems encountered during the manufacturing process and the solutions.

(Perkins, Reed Jr et al. 2004) conducted a wing morphing study by changing the chord length in collaboration with the research group at Cornerstone, USA. Shape Memory Polymer (SMP) which is a lightweight flexible foam, was used as actuators. Because of its small

recovery stress, the wing once extended it was not able to regain its original position during the cooling phase.

A complex internal actuation mechanism was designed at German Aerospace Center - DLR by (Monner, Hanselka et al. 1998) to modify the original camber line of an airfoil. The mechanism principle was to break the rib structure like finger (articulation). The ribs consisted of segmented plate connected between each other by revolute joints. Both side of the trailing edge was covered by the flexible skin and were able to move with respect to each other so that important deformation of the trailing edge was achieved.

From the perspective of actuator systems, a surface-induced deformation using a macro fiber composite actuator was tested by a collaborative research team from Swansea University, UK, and Center for Intelligent Material Systems and Structures, Virginia Tech, USA. (Bilgen, Friswell et al. 2011) designed an airfoil which was made of two cascading active surfaces and a pair of optimized pinned boundary conditions. The goal of these studies was to achieve the highest possible lift coefficient and lift-to-drag ratio by identifying the effects of four structural parameters. The camber line of the studied airfoil was varied and the lift-to-drag ratio improved accordingly.

In this context, our team from the Research Laboratory in Active Controls, Avionics and Aeroservoelasticity (LARCASE) of the Ecole de Technologie Supérieure in Montréal, Canada, developed two major morphing wing collaborative research projects financed by the Consortium for Research and Innovation in Aerospace in Quebec (CRIAQ). Also, by using the testing facilities in the Price-Païdoussis wind tunnel at LARCASE laboratory we experienced a lot of morphing wing models, actuated by using different mechanisms, and equipped with various pressure sensors and actuators.

In the first morphing wing project developed at the LARCASE (CRIAQ 7.1), Shape Memory Alloys (SMA) was used as actuators to change the profile of a manufactured wing. These smart actuators deformed the upper wing surface, made of a flexible skin, so that the laminar-to-turbulent transition point could move close to the wing trailing edge. The transition point position was monitored by using the data from a set of pressure sensors fixed on the upper

surface of the wing. The ultimate goal of this research project was to obtain a drag reduction as a function of flow condition by changing the wing shape. The actuation mechanism and its control has been explained in (Grigorie, Popov et al. 2011). The strong nonlinear character of the used actuators generated various studies in order to obtain a good control system. In this way, different kinds of control concepts were developed by (Grigorie, Popov et al. 2010, Grigorie, Popov et al. 2011, Grigorie, Popov et al. 2012) and experimented in a wind tunnel at the National Research Council Canada. An integrated controller was a combination of a bi-positional (on–off) controller and a PI (proportional–integral) controller, tuned by using some linear models of the actuators in the heating and cooling phases obtained with Matlab's System Identification Toolbox. The second control designed by (Grigorie, Botez et al. 2012, Grigorie, Botez et al. 2012) was based on a hybrid fuzzy logic proportional-integral-derivative and conventional on-off controller, tuned by using a non-linear model of the actuators realized with a numerical finite element method and the Lickhatchev's theoretical approach. Other used intelligent controllers implemented by (Grigorie, Botez et al. 2011, Grigorie, Botez et al. 2012, Grigorie, Popov et al. 2012, Grigorie, Botez et al. 2013, Grigorie, Popov et al. 2013) were based on fuzzy logic techniques tuned by using the same non-linear model of the actuators or by using some non-linear models of the actuators realized with adaptive neuro-fuzzy identification methodologies explained in details by (Grigorie and Botez 2010, Grigorie and Botez 2010). Finally, a two stages fuzzy logic control system developed by (Grigorie, Popov et al. 2011) was considered with self-tuning.

All developed controllers were used to control the actuators positions without any information from the pressure sensors in the control law. In this configuration of the morphing wing, called generically "open loop", the controllers used a database that contained some numerically optimized airfoils correlated with the airflow cases as combinations of Mach numbers and angles of attack. The controllers took the necessary displacement of the actuators from the database as reference values in order to obtain the morphing wing optimized airfoil shape. The controllers designed for the open loop were described in (Popov, Grigorie et al. 2010, Grigorie, Popov et al. 2014). The final configuration of the morphing wing used a control method based on the pressure information received from the sensors and on the transition point position estimation. It included, as inner loop, the first control method

of the actuation lines. The method used an optimizer code which finds the best actuators configuration in order to maximize the position of the transition, i.e. at the end of optimization sequence the transition should be found as the nearest possible point to the trailing edge. The final configuration of the closed loop was developed by (Popov, Grigorie et al. 2010, Popov, Grigorie et al. 2010, Grigorie, Popov et al. 2014)

Another actuator and actuation mechanism were designed and tested in the Price-Païdoussis wind tunnel at LARCASE laboratory for another morphing wing project by (Kammegne, Grigorie et al. 2016). For this project a resized wing of the ATR42 aircraft was used with a flexible skin covering the upper surface. Two motors used as actuators were coupled to the actuation mechanism. PID controllers were developed to control the position of the actuators and the obtained experimental results showed a good correlation between the predicted and measured pressure coefficient data. The calibration methodology of the used wind tunnel was proposed by (Mosbah, Salinas et al. 2013).

(Gamboa, Aleixo et al. 2007, do Vale, Leite et al. 2011, Falcão, Gomes et al. 2011) proposed and applied various aero-structural optimization methodologies for morphing wing tip and UAVs.

To bring the morphing technology closer to be integrated on aircrafts, another morphing wing project (MDO505) financed by CRIAQ was undertaken at LARCASE laboratory in collaboration with Thales Avionics, Bombardier Aerospace, École Polytechnique, the National Research Council, Canada (NRC), and with Italian researchers from Frederico II Naples University, CIRA (Italian Aerospace Research Centre) and Alenia Aeronautica. For this project, a full-scaled portion of an aircraft wing with the chord length of 1.5 meters was used, the flexible skin mounted on the extrados being made of composite fibber materials (Kammegne, Botez et al. , KAMMEGNE, BOTEZ et al. , Michaud F et al. 2014) . Spars, ribs, and stringers and aileron are integral parts of the wing model. Contrary to the ATR-42 project, there was no actuation mechanism used between the actuators and the flexible skin; the four used miniature electromechanical actuators were placed directly at the actuation

points on two actuation lines located chord wise at 32% and 48% as illustrated in (Kammegne, Botez et al. , KAMMEGNE, BOTEZ et al.), and (Michaud F et al. 2014).

The used actuators were identical and they were controlled by using a control logic developed in LARCASE laboratory. The first test of the developed control system was realized in LARCASE laboratory on a bench test, with no airflow. To validate the aerodynamic results given and predicted by the aerodynamic team working in the project, wind tunnel tests were performed at NRC. The objective of the aerodynamic optimization was to extend the laminar flow or delay the appearance of flow laminar-to-turbulence transition targeting drag reduction. The wind tunnel considered for the experimental validation is a subsonic wind tunnel used for both academic and industrial purposes.

Figure 6.1 The flexible skin position
on the aircraft wing

The present paper discusses the modeling, the design and the control of the four electromechanical actuators used to morph the flexible skin. In addition, the experimental results obtained during the experimental validation of the control system are shown. A brief description of the hardware used for the experimental validation is presents as well. The particularity of the developed position controller is that it combines the data obtained from an encoder and from a Linear Variable Differential Transducer (LVDT) in order to synchronize the sensors. The loop which uses the LVDT as feedback was developed to compensate the mechanical plays inside the actuators.

Figure 6.2 Structure of the morphing wing model

6.2 Morphing wing control system design

6.2.1 Project motivation

Due to its multidisciplinary character, the project gathered different technical experts from aerodynamics, aeroservoelasticity, mechanics, control and electrical engineering, from both, academic and industrial entities. According with the trend in the field, it aimed to enhance the environmental impact of the aeronautical industry among other industry area such as transport industry, fuel or petroleum facilities. The drag is one of the parameters to be influenced to achieve that goal as its reduction contributing to that purpose. Here, the drag reduction was realized by delaying the transition region or by moving the transition region towards the trailing edge, thus the laminar region was extended on the wing surface for the operating range of flow condition. Therefore, the aerodynamic team of the project developed an optimization algorithm to search for the optimum shapes for the airfoil through local thickness modifications with the aim to improve the upper surface flow and thus the

aerodynamic performances of the airfoil. Therfore, an in-house developed genetic algorithm/Xfoil implemented by (Koreanschi, Sugar-Gabor et al.) coupled software was applied to the problem of airfoil upper-surface morphing. The objective function was constructed based on the desired objective of influencing the upper surface flow of the wing with the purpose of minimizing drag and delaying the transition from laminar to turbulent flow for a more stable boundary layer. The optimization was applied for several combinations of Mach numbers (M), angles of attack (α) and aileron deflection angles (δ). In this way, speed, Reynolds number, angle of attack and aileron deflection angle were some of the parameters that determined the control of the actuators for the skin deformation. More details could be found in (Kammegne, Botez et al. , KAMMEGNE, BOTEZ et al.).

The optimized flexible skin mounted on the wing was deformed by the mean of four miniature electrical actuators, while the up and down deflection of the aileron attached on the wing was realized by an electrical actuator linked to the aileron by using a lever arm. Each of the four morphing actuators had the ability to operate independently from the others. The aerodynamic optimization of the airfoil shape provided the displacement values for a pair of actuators, while the displacements for the second pair of actuators were calculated as a linear dependence. Therefore, the genetic optimization of the wing airfoil described by (Kammegne, Botez et al. , KAMMEGNE, BOTEZ et al.) provided the vertical displacements of the four morphing actuators in each optimized flow case $(\mathrm{d}Y_{1opt}, \mathrm{d}Y_{2opt}, \mathrm{d}Y_{3opt}, \mathrm{d}Y_{4opt})$, generating in this way a database with the needed actuators displacements for different flight conditions. These stored displacements database was used as reference vertical displacements for the morphing wing control system.

6.2.2   Experimental setup of the morphing wing model

Having in mind that all four morphing wing actuators are identical, the designed controller for one of them was used in the same configuration for all four actuators. For a given flow condition, it needed to control the actuators linear positions until the real vertical displacements of the morphing skin in the four actuation points equaled the desired vertical displacements of the optimized airfoil. The feedback signals from the actuators in terms of

linear displacements were provided by the LVDTs attached to each of them, and simultaneously, by the encoders, integrated inside the motors equipping the actuators, in terms of the rotor angular position. As a practice to validate the aerodynamic purpose of the project, the pressure data provided by some Kulite sensors mounted on the upper surface of the flexible skin were used. A National Instruments Real Time (RT) Target technology allowed the development of the system interfacing the remote computer and the morphing wing experimental model as shown in (Kammegne, Botez et al. , Kammegne, Grigorie et al.).

The hardware component of the experimental model included (Figure 6.3): 1) a *PXIe chassis*, which served as support for the PXIe controller and the module; 2) a *PXIe-8135 real time controller*, the embedded controller inserted in the PXIe chassis, with a quad–core processor, a high performance hard drive and an optimal platform for the testing of real time control applications; 3) four *NI PXIe-4330 Data Acquisition Cards*; 4) a *SCXI chassis*, used as signal conditioner for the LVDT sensors connected to the box front via SCXI module; the chassis supplies the connected sensors and post process directly the Wheatstone's bridge signals so that the end user can obtain directly the physically measured signal; 5) a *CANOpen box extension*, with 14 ports and multiple nodes which could be connected at the same time to CAN interfaces; 6) a *Power amplifier*, with one of its controllable outputs connected directly to actuator's motor; its interface consists of one USB port, CAN port, RS232 serial port, analog/digital input/output port, Hall sensor interface, motor supply interface and encoder interface; 7) two *Programmable power supplies* Aim-TTi CPX400DP.

The microcontroller attached to the amplifier had an integrated control loop with tunable gains. All the parameters of the power amplifier were accessible through the object dictionary, bringing more flexibility for the user. The connection diagram of the drive can be schematized as in Figure 6.4. The user was able to validate experimentally any linear control logic for motion control with such a drive by means of the implementation of the obtained numerical controller gain inside the loop; the manufacturer suggested formula to convert numerical obtained coefficients into hardware corresponding coefficients.

Figure 6.3 Hardware component of the experimental model

Figure 6.4 Connection diagram of the drive

6.2.3   Mathematical modeling of the controlled morphing actuators

To design the control system for the morphing wing actuators, a preliminary modeling phase was needed. Each of the four actuators used to morph the flexible skin consisted of a brushless direct current (BLDC) motor produced by Maxon Motor Company, coupled to a gearbox system, a trapezoidal screw, a nut and a gearing system. The four morphing actuators included the same type of motors and the same type of gearbox, being designed and manufactured in our laboratory at ÉTS in Montreal. These types of motors are known for their numerous advantages, including small size and high torque. For an easiest modeling, such kind of motor could be approximated with enough precision by a linear direct motor.

Usually, the power amplifier or electrical drive circuit serves as a converter for the voltage command $u(t)$ into a torque. The equilibrium between the motor torque and the required torque to move the load must be established in order to overcome any friction. Therefore, we can write

$$J\frac{d\omega_m}{dt} + B\omega_m = T_e - T_L, \tag{6.1}$$

where ω_m, is the angular speed of the motor output shaft [rad/s], J - the inertial load of the output motor shaft [Kg·m^2], B - the friction coefficient of the load bearing [N·m/(rad/s)], T_e - the motor torque [N·m], and T_L - the load torque [N·m]. The shaft angular speed is related to its position by equation

$$\omega_m = \frac{d\theta}{dt} \tag{6.2}$$

The desired shaft torque is related to the motor current by the torque constant k_t [N·m/A]:

$$T_e = k_t i_M \tag{6.3}$$

Therefore, from equations (6.1) to (6.3) it can be demonstrated that

$$J\ddot{\theta} + B\dot{\theta} = k_t i_M - T_L. \tag{6.4}$$

In addition, the electric part of the motor is expressed as follows:

$$U = L\frac{di_M}{dy} + Ri_M + e; \tag{6.5}$$

U is the motor voltage [V], R - the motor resistance [Ω], L - the motor inductance [H], and e - the back EMF [V]. Combining previous equations with $e = k_e * \omega_m$; we have

$$\frac{\omega_m}{U} = k_t /(LJs^2 + RJs + k_e k_t); \tag{6.6}$$

k_e - angular speed constant [revolution/min/V]. The servo model driving the morphing wing was developed in Simulink, the continuous model being shown in Figure 6.5; the red block models the electric part while the green part models the mechanical part of the motor.

Figure 6.5 Linear model of the DC motor

6.2.4   Design of the actuation control system

To bring each actuator system in motion, its motor needs to be connected to the power amplifier able to energize it via a controllable voltage. Valid to be used for each of the four actuators due to the fact that the used motors were identical, three control loops (a torque control loop and two position control loops) were designed and implemented by our research team. The two position control loops were differentiated by the feedback sensors used. The first position control loop used the encoder as feedback sensor and the second one used the LVDT as feedback sensor. The controller's parameters for torque control and the first position control were implemented inside the power amplifier, while the second position loop was independently programmed and experimentally validated using the real time system. The final architecture for the control of the morphing is shown in Figure 6.6.

Figure 6.6 Control loops

As we already specified, the actuators were designed and manufactured in LARCASE according to the specificity of our application. Having in mind that the experimental

morphing wing model was based on the dimensions of a full scale wing tip structure, being designed and manufactured to meet aeronautical industry requirements, some mechanical plays were considered inside the actuators to avoid their blockage. Actually, the structural team of the project realized a 1g structural static test to evaluate the integration of the actuators inside the wing structure and its structural integrity (Figure 6.7). Therefore, the reason of using the second position control loop based on the LVDT sensors data as feedback signals was to compensate these mechanical plays inside the actuators from the position control point of view and to do not alter the aerodynamic performance of the morphing wing in various flow conditions.

In the next subsections, the design of the torque control loop will be discussed followed by the design of the position control loops.

Figure 6.7 The wing on the bench test
during 1g structural static test

6.2.5   Design of the torque control loop

The torque loop design considers just the electrical part of the motor, characterized by the following transfer function

$$G_e(s) = \frac{1}{Ls+R} = \frac{1/R}{(L/R)s+1} \tag{6.7}$$

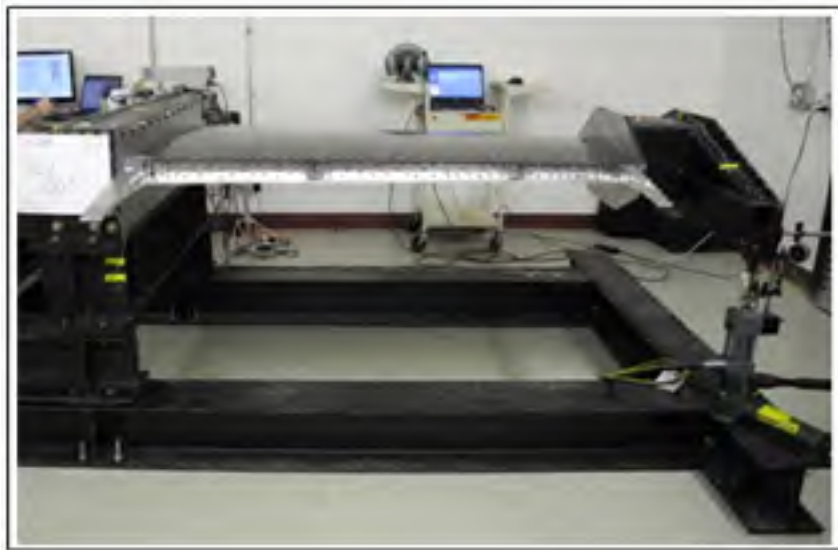If the electrical time constant of the motor is defined by

$$\tau_e = L/R, \tag{6.8}$$

then the equation (6.7) can be rewritten as

$$G_e(s) = \frac{1/R}{\tau_e \cdot s+1} = \frac{1/R}{1+\dfrac{s}{1/\tau_e}}. \tag{6.9}$$

The motor torque and the electrical current are related by a proportional gain, namely the torque constant. Therefore, the current flowing in the motor winding can be considered as the control variable for the torque control. A Proportional Integral (PI) controller was used for the current, which conducted to the Simulink model in Figure 6.8 for the system with controlled torque. Choosing the transfer function of the current controller below

$$G_i(s) = K_{pt} + \frac{K_{it}}{s} = \frac{K_{it}}{s}\left[1+\frac{s}{K_{it}/K_{pt}}\right], \tag{6.10}$$

the open loop transfer function of the controlled system (PI controller and motor) is obtained as follows

$$G_{io}(s) = G_i(s) \cdot G_e(s) = \frac{K_{it}}{s}\left[1+\frac{s}{K_{it}/K_{pt}}\right] \cdot \frac{1/R}{1+\dfrac{s}{1/\tau_e}}; \tag{6.11}$$

where K_{pt} and K_{it} are the proportional and the integral gains in torque controller, respectively.

Figure 6.8 System with torque control

To obtain the coefficients of the torque controller the pole-zero cancellation method was used (Abe, Shoyama et al. 2011). As a consequence, the zero of the current controller was chosen to cancel the pole of the electrical part of the motor transfer function, such that

$$K_{it}/K_{pt} = 1/\tau_e \tag{6.12}$$

Therefore,

$$K_{pt} = \tau_e \cdot K_{it} = \frac{L}{R} \cdot K_{it}, \tag{6.13}$$

and the open loop transfer function of the controlled system becomes

$$G_{io}(s) = (K_{it}/s) \cdot (1/R). \tag{6.14}$$

The module of the open loop transfer function in frequency domain is given by

$$\left| G_{io}(j\omega) \right| = \sqrt{K_{it}^2/[R^2(j\omega)^2]} = K_{it}/(R\omega), \tag{6.15}$$

where ω is the pulsation, $\omega = 2\pi f$ (f is the frequency). Rewriting equation (15) yields

$$\left| G_{io}(j\omega) \right|_{dB} = 20\log_{10}(K_{it}) - 20\log_{10}(\omega R), \tag{6.16}$$

which, at the crossover frequency f_s, is null. Therefore,

$$20\log_{10}(K_{it}) - 20\log_{10}(\omega_s R) = 0, \tag{6.17}$$

and

$$K_{it} = \omega_s R; \tag{6.18}$$

with $\omega_s = 2\pi f_s$. It results,

$$K_{it} = 2\pi 1000\,s^{-1} \cdot 3.43\,\Omega = 21551.33\,\Omega s^{-1}, \tag{6.19}$$

$$K_{pt} = \frac{1.87e - 3\,H}{3.43\,\Omega} \cdot 21551.33\,\Omega s^{-1} = 11.74\,Hs^{-1}.$$

According to the formulas provided by the motor producer, the gains obtained were recalculated (converted) in order to fulfill the manufactured requirements

$$K_{P...SI} = 3.91e - 3K_{P...EPOS2},$$ (6.20)

$$K_{I...SI} = 3.910 \frac{\Omega}{s} K_{I...EPOS2}.$$

Therefore, the current controller parameters to be implemented are

$$K_{P...EPOS2} = \frac{11.74}{3.91e - 3} = 3002.6,$$ (6.21)

$$K_{I...EPOS2} = \frac{21551.33}{3.910} = 5512.$$

6.2.6 Design of the position control system

6.2.6.1 Encoder based position control loop

Because the innermost loop had to be faster than the outer loop the electrical current loop was replaced by one as shown in generated Simulink model from Figure 6.9. According to the actuators mathematical model previously established, the transfer function of the mechanical part is

$$G_m(s) = \frac{1}{Js + B} = \frac{1/B}{(J/B)s + 1},$$ (6.22)

which, rewritten by using the constant $\tau = J/B$, gives

$$G_m(s) = \frac{1/B}{\tau \cdot s + 1} = \frac{1/B}{1 + \frac{s}{1/\tau}}.$$ (6.23)

The transfer function of the PD position controller can be written as

$$G_p(s) = K_{pp} + K_{dp} \cdot s = K_{pp} \cdot \left(1 + \frac{s}{K_{pp}/K_{dp}}\right),$$ (6.24)

while the open loop transfer function of the controlled system from Figure 6.9 is obtained as

$$G_{po}(s) = G_p(s) \cdot G_m(t) \cdot k_t = k_t K_{pp} \cdot \left(1 + \frac{s}{K_{pp}/K_{dp}}\right) \cdot \frac{1/B}{1 + \frac{s}{1/\tau}} \cdot \frac{1}{s}; \tag{6.25}$$

where K_{pp} and K_{dp} are the proportional and the derivative gains in position controller, respectively.

Figure 6.9 Position control with feedback based on encoder

Using the pole-zero cancellation method (Abe, Shoyama et al. 2011), equation (6.25) yields

$$K_{dp} = \tau \cdot K_{pp} = \frac{J}{B} \cdot K_{pp}, \tag{6.26}$$

and the open loop transfer function of the controlled system becomes

$$G_{po}(s) = k_t \cdot \frac{K_{pp}}{s} \cdot \frac{1}{B}. \tag{6.27}$$

The module of the open loop transfer function in frequency domain is given by

$$\left|G_{po}(j\omega)\right| = \sqrt{K_{pp}^2 k_t^2 /[B^2(j\omega)^2]} = K_{pp}k_t /(B\omega), \tag{6.28}$$

where ω is the pulsation, $\omega = 2\pi f$ (f - the frequency). Similar with the previous designed controller, at the crossover frequency f_p, we have

$$\left|G_{po}(j\omega)\right|_{dB} = 0, \tag{6.29}$$

i.e.

$$20\log_{10}(K_{pp}k_t) - 20\log_{10}(\omega_p B) = 0; \tag{6.30}$$

with $\omega_p = 2\pi f_p$. Therefore,

$$K_{pp} = \frac{\omega_p B}{k_t} = \frac{628\,\text{rad/s} \cdot 3.8e-6\,\text{Nm/(rad/s)}}{24.1e-3\,\text{Nm/A}} = 0.099\,\text{A}, \tag{6.31}$$

$$K_{dp} = \frac{J}{B} \cdot K_{pp} = \frac{0.099\,\text{A} \cdot 35.3e-7\,\text{Kg}\cdot\text{m}^2}{3.8e-6\,\text{Nm/(rad/s)}} = 0.0919\,\text{As}.$$

For a repeated step signal as a reference position, the numerical simulation results for the designed position controller based on the encoder signal as feedback are shown in Figure 6.10.

Figure 6.10 Position control simulation based
on encoder signal as feedback

6.2.6.2   LVDT based position control loop

A particular element of this controller would be to have two parallel loops for the same control variable (position). The control loop based on the LVDT feedback was imposed because of the plays inside the actuation mechanism, aiming at the compensation of all the plays inside the actuation mechanism and getting the real vertical displacements of the morphing skin in the actuation points. Instead to have two inputs (position set point and feedback) as the standard controllers, the designed controller had three inputs: one for the position set point, one for LVDT position and the last one for the encoder position. The third input was necessary for the controller in order to synchronize both loops. The Simulink model reflecting the control structure is shown in Figure 6.11.

Figure 6.11 Position control with feedback based on LVDT signal

The LVDT position control was implemented using the Fuzzy logic techniques. It usually offers tools to experts to interpret the human knowledge into real world, which enhances conventional system design with engineering expertise. In many applications it is difficult to obtain a reliable and rigorous mathematical model of systems, in this situation the fuzzy logic technique could be used to overcome this kind of situation. The fuzzy logic is also recommended when a linear controller shows some limitations; fuzzy controllers belong to the category of nonlinear controllers and are based on rules. Mainly, a basic fuzzy logic controller has the structure shown in Figure 6.12: the fuzzifier, the inference engine, the defuzzifier, and a knowledge base.

Figure 6.12 Fuzzy logic controller architecture

The first step is the fuzzification, at this stage the fuzzifier converting, scaling and transforming the crisped input into linguistic variables using the appropriated membership functions. At the second step the control logic used by the controller is required under the form of rules set. The linguistic values for the output linguistic variables are obtained after a

knowledge base call by the interference engine. The last step is the defuzzification, which converts the linguistic output variable from the universe of discourse into a crisp output for the real world using the output membership functions from the knowledge base. More details regarding fuzzy logic could be found in (Zadeh 1978, Mahfouf, Linkens et al. 1999, Kovacic and Bogdan 2005, Grigorie, Popov et al. 2012, Grigorie, Botez et al. 2011).
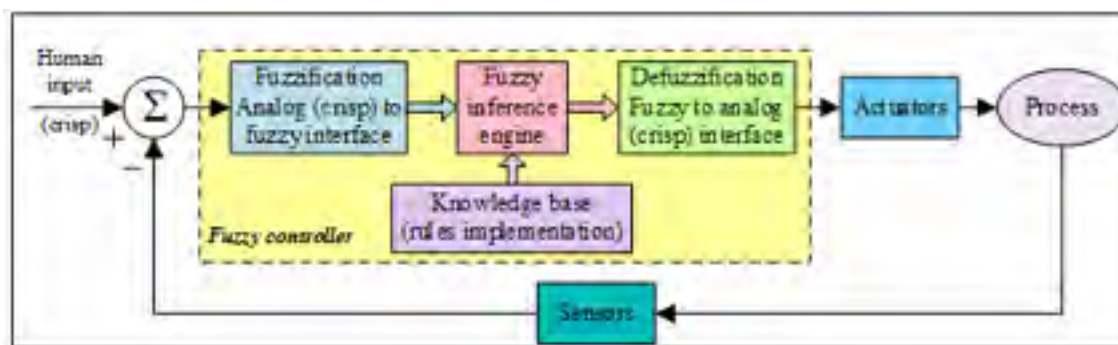
For our application we developed a fuzzy controller with one input and one output, a proportional controller (FP), its input being the actuation error based on the LVDT feedback signal and the output the control signal. The interval of the crisp values (input of the Fuzzy controller) is [-10, 10]. Considering this interval as universe of discourse for the controller input, we choosing eleven membership functions (mf) for the input ($A_1^1 \div A_1^{11}$), and eleven membership functions for the output. The linguistic terms of the input and output are: Zero (Z), Positive Very Small (PVS), Positive Small (PS), Positive Medium (PM), Positive Large (PL), Positive Very Large (PVL), Negative Very Small (NVS), Negative Small (NS), Negative Medium (NM), Negative Large (NL), and Negative Very Large (NL). The shape for the input membership functions was triangular:

$$f_\Delta(x;a,b,c) = \begin{cases} 0, & \text{if } x \le a, \\ \dfrac{x-a}{b-a}, & \text{if } a < x < b, \\ \dfrac{c-x}{c-b}, & \text{if } b \le x < c, \\ 0, & \text{if } c \le x, \end{cases} = \max\left[\min\left(\frac{x-a}{b-a}, \frac{c-x}{c-b} \right), 0 \right], \tag{6.32}$$

where x is the independent variable on the universe, the parameters a and c locate the feet of the triangle and b gives its peak; the parameters characterizing the membership functions of the inputs are given in Table 1, while the allures of the membership functions are shown in Figure 6.13.

Table 6.1 Parameters of the input membership functions

mf parameters	Membership functions (mf)										
	mf1 (Z)	mf2 (PVS)	mf3 (PS)	mf4 (PM)	mf5 (PL)	mf6 (PVL)	mf7 (NVS)	mf8 (NS)	mf9 (NM)	mf10 (NL)	mf11 (NVL)
a	-2	0	2	4	6	8	-4	-6	-8	-10	-10
b	0	2	4	6	8	10	-2	-4	-6	-8	-10
c	2	4	6	8	10	10	0	-2	-4	-6	-8

To define the rules, a Sugeno fuzzy model was chosen, which was proposed by Takagi, Sugeno and Kang as detailed by (Mahfouf, Linkens et al. 1999). A Takagi, Sugeno and Kang fuzzy rule, for a single input - single output system, is written in the following form

$$\text{"if } (x_1 \text{ is } A) \text{ then } y = f(x_1)\text{"},\tag{6.33}$$

where A is fuzzy set in the antecedent, and $y = f(x_1)$ is a crisp function in the consequent; $f(x_1)$ is a polynomial function. If f is a first order polynomial, then the resulting fuzzy inference is called a first-order Sugeno fuzzy model, while if f is a constant then it is a zero-order Sugeno fuzzy model. For a single input- single output system, a first-order Sugeno fuzzy model, with N rules is given by (Mahfouf, Linkens et al. 1999):

$$\text{Rule 1}: \text{ If } x_1 \text{ is } A_1^1, \text{ then } y^1(x_1) = b_0^1 + a_1^1 x_1,\tag{6.34}$$
$$\dots$$
$$\text{Rule } i: \text{ If } x_1 \text{ is } A_1^i, \text{ then } y^i(x_1) = b_0^i + a_1^i x_1,$$
$$\dots$$
$$\text{Rule } N: \text{ If } x_1 \text{ is } A_1^N, \text{ then } y^N(x_1) = b_0^N + a_1^N x_1,$$

where x_1 is the individual input variable, $y^i\ (i = \overline{1, N})$ is the first-order polynomial function in the consequent, and $A_1^i\ (i = \overline{1, N})$ are the associated individual antecedent fuzzy sets of input variable. The coefficients $a_1^i\ (i = \overline{1, N})$ are parameters of the linear function and $b_0^i\ (i = \overline{1, N})$ denote scalar offsets.
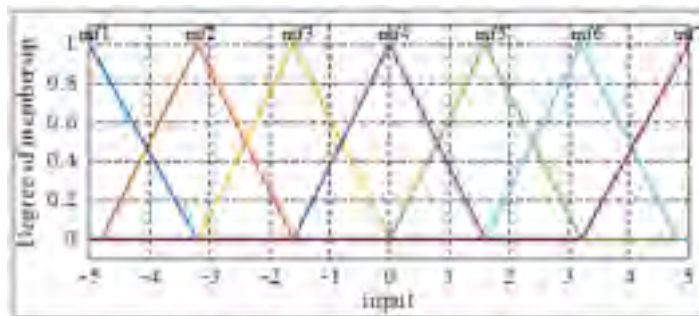

Figure 6.13 Membership functions of the input

For any input x, if the singleton fuzzifier, the product fuzzy inference and the center average defuzzifier are applied (Sugeno type), then the output of the fuzzy model y is inferred as follows (Figure 6.14 a) (weighted average)

$$y = \left(\sum_{i=1}^{N} w^i(x) y^i \right) / \left(\sum_{i=1}^{N} w^i(x) \right), \tag{6.35}$$

$$w^i(x) = A_1^i(x_1),$$

and it represents the degree of fulfillment of the antecedent, i.e., the level of firing of the ith rule.

For the output membership functions constant values were chosen (NVL=-10, NL=-8, NM=-6, NS=-4, NVS=-2, Z=0, PVS=2, PS=4, PM=6, PL=8, PVL=10), so the values of $a_1^i (i = \overline{1,N})$ parameters in equation (6.35) are null. Starting from the inputs' and output's membership functions, a set of 11 inference rules were obtained ($N=11$) (Figure 6.14 b).

a)   b)

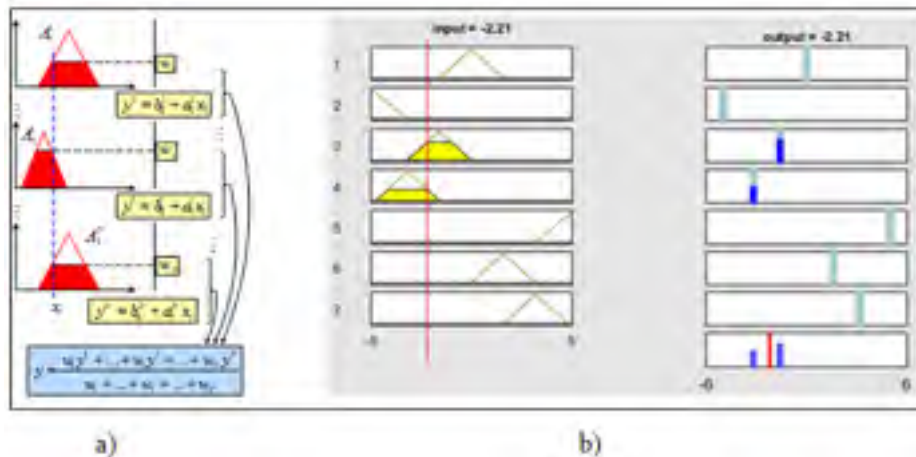Figure 6.14 Output of the fuzzy model and the obtained inference rules

In a first validation test of the controller, some numerical simulations were performed. The LVDT based controller responses, allowing the control of the real morphing skin displacement, are presented in Figure 6.15 for various repeated step signals as reference positions. For all desired displacement, no matter is the direction of rotation of the motor,

there is no overshoot; the rise time is about 1.6 second. Additionally, there is no steady state error, fulfilling in this way the aerodynamic requirements which asked for an absolute maximum value of the error lower than 0.1 mm.

Figure 6.15 Position control simulation with feedback
based on LVDT: negative and positive excitations

6.3 Experimental testing of the morphing wing control system

The experimental validation of the developed control system was performed in two independent steps: 1) bench testing in the LARCASE laboratory, with wind off; 2) wind tunnel testing at NRC. The control was used in the same form for all four morphing actuators placed inside the wing.

6.3.1 Bench test results

The experimental bench test with different components is displayed in Figure 6.16. The controller gains for the innermost controller and the position controller with encoder feedback are implemented directly inside the power drive through the object dictionary, while the position control with LVDT feedback was compiled with Simulink, in order to generate a C code, which has been loaded into the real time system via an Ethernet cable. The LVDT signal conditioner supplies directly the LVDT, which process the output signal

and send it back to the controller as input. The motor position given by the encoder, mounted on the stator, was accessible by the real time controller or real time system through CANopen and sends it back to the position controller with LVDT as feedback signal.

Figure 6.16 Experimental model in bench test
(lower face of the wing is removed)

The bench test validation of the controller was started with the independent control in time for each of the four actuators. In this way, desired displacements by the form of successive steps signals were applied at the input of the actuators as in the numerical simulations. Figure 6.17 shows the experimental results obtained during this test for one of the actuators, under the flexible skin load but with no wind blowing; the graphical characteristics include also the numerical simulation results for the same inputs. Both from the graphical characteristics and from the acquired numerical values we observed that the measured position follow the shape of the simulated position with a slightly difference during the transition phase, which is not a drawback for our application.

Figure 6.17 Bench test experimental
validation of the designed controller

In the next phase of the controller bench test validation, all groups dY_{1opt}, dY_{2opt}, dY_{3opt}, dY_{4opt}, of the desired displacements characterizing the optimized airfoil cases were imposed like input signals on the four actuators. From the numerical values obtained for all optimized airfoil cases, for the real vertical displacements $(dY_{1real}, dY_{2real}, dY_{3real}, dY_{4real})$ of the morphing skin in the actuation points, we observed that the experimental version of the designed controller works well in the laboratory conditions, where no aerodynamic forces are loaded. Therefore, as the aerodynamic loads effect of the flexible skin deformation was expected to be negligible, the experimental model was cleared for testing in the wind tunnel.

6.3.2   Wind tunnel test results

The NRC 2 m × 3 m atmospheric closed circuit subsonic wind tunnel was used. About 97 flight cases were tested based on the combinations between nineteen values for the angles of attack, varied from -3 degree to +3 degree, three values for the Mach numbers (0.15, 0.2 and 0.25), and thirteen values for the aileron deflection angles, between − 6 degrees and +6

degrees. Figure 6.18 presents the MDO 505 morphing wing model installed in the tunnel test section, viewed from both the leading edge (left picture) and the trailing edge (right picture). The experimental model was mounted in a vertical position in the wind tunnel test run, the different incidence angles being obtained by rotating the model around a vertical axe.

Figure 6.18 MDO 505 wing model setup in wind tunnel tests

A typical test for one of the flight conditions consisted in a wind tunnel tare run, followed by a run for the reference (un-morphed) airfoil, and finally by a run for morphed airfoil, reproducing the corresponding optimized airfoil. Our controller morphed the reference airfoil by acting the four actuators inside the wing until the optimized airfoil was achieved. The real positions of the four actuators were provided by the LVDTs, while the required positions were loaded from the database made from the data predicted by the aerodynamic team. During these tests the main signals such as the raw pressure signal data from the 32 Kulite sensors, the skin displacements from linear positioning sensors, actuator current, and actuator speed were recorded. On the other way, the pressure sensor signals were used to real time visualize the transition point position based on the FFT (Fast Fourier Transform) comparative analyze between the detection channels; the calculated pressure coefficients were used to validate the aerodynamic optimized wing shapes for each flow case. For booth runs (un-morphed and morphed airfoils) the transition point real time position detection and visualization demonstrated the validity of the optimized airfoils theoretically obtained. This

mechanism corresponds to the open loop architecture of the morphing wing system, when no feedback for the pressure sensors was used. Subsequently, a data post processing step was performed by using the acquired raw pressure signals in order to obtain the FFT spectral decomposition, the standard deviation (STD) calculation, and the location of the transition.

Figure 19 illustrated the standard deviations of the pressure data acquired for the flow case 43 (Mach=0.15, α=2˚, δ=0˚) for both un-morphed (reference) and morphed airfoils. The Kulite sensors were positioned on the flexible skin between 28% and 68% of the chord. A higher standard deviation picked up by a Kulite among the others suggests that the sensed pressure signal was induced by turbulence, which started somewhere between that Kulite sensor and the previous one. Similar effects can be observed at the level of the FFT evaluated for all pressure sensors. A detached FFT curve indicates that a turbulent flow over the respective pressure sensor occurred. The resolution of the laminar to turbulent transition point position is directly influenced by the density of the pressure sensors evaluating the flow characteristics. Figure 6.20 and Figure 6.21 depict the FFT evaluation results respectively for un-morphed airfoil and morphed airfoil for flow condition case 43 (Mach=0.15, α=2˚, δ=0˚). For a better visualization of the transition location, the 32 Kulite sensors FFTs were represented in four independent windows in groups of eight consecutive sensors starting from the leading edge. Figures provided also a centralized representation of the FFTs for all 32 sensors for an easiest observation of the FFTs curves detachment.

Figure 6.19 Standard deviations of the pressure data acquired for the flow case 43
(Mach=0.15, α=2°, δ=0°, Reynolds number $5.2*10^6$)

The results presented in Figure 6.19 showed that the transition for un-morphed airfoil started on the presure sensor #10 positioned at 42.45% of the chord and has a maximum value on the presure sensor #13 positioned at 45.16% of the chord. The morphed airfoil improves the flow over the wing by moving the transition point on the pressure sensor #16, positioned at 50.79% of the chord.

Figure 6.20 FFT results for the unmorphed airfoil in the flow case 43

(Mach=0.15, $\alpha=2°$, $\delta=0°$, Reynolds number $5.2*10^6$)

From the FFT point of view, the graphical courves in Figure 6.20 for un-morphed airfoil sugested also that the transition started on the presure sensor #10 and the maximum influenced FFT curve was associated to the sensor on the channel #13, confirming in this way the STD results. From the fifth picture of the figure can be easily observed that the first detached FFT curve was associated with the pressure sensor #9.
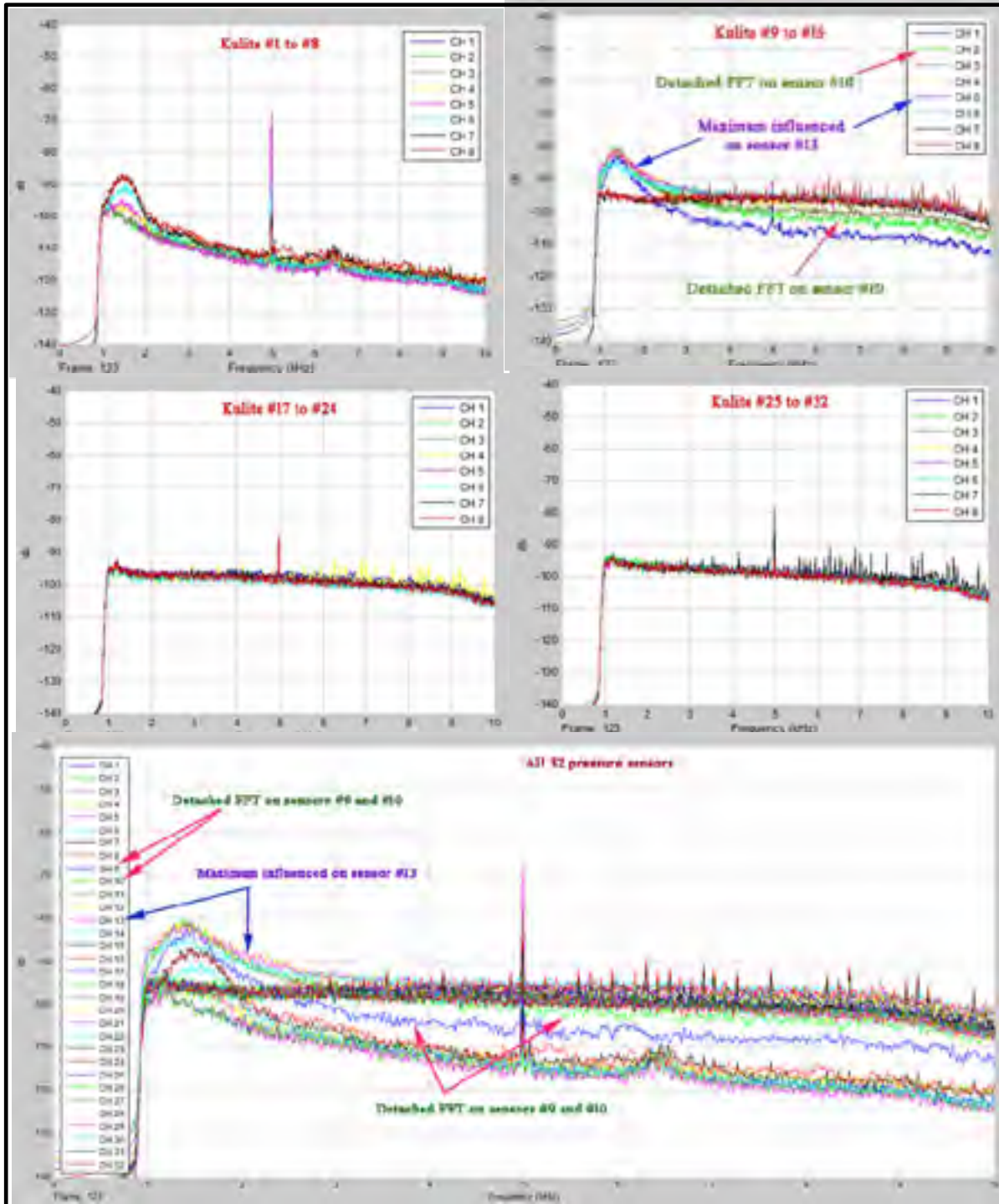
Figure 6.21 FFT results for the morphed airfoil in the flow case 43
(Mach=0.15, $\alpha=2°$, $\delta=0°$, Reynolds number $5.2*10^6$)

From Figure 6.21, coresponding to FFT curves for the morphed airfoil in the flow case 43, we can observe that the turbulence is maximum on the sensor #16, while the FFT curves detachement starting around the sensors on the channels #14 and #15. The conclusion sustained the alure obtained for the STD curve in the second picture of the Figure 6.19.

For capturing the transition region over the entire wing model surface, infra-red (IR) thermography camera visualizations were performed. The wing leading edge, its upper surface flexible skin and the aileron equipping interface were coated with high emissivity black paint to improve the quality of the IR photographs. The span-wise stations, where the two pressure sensors lines were installed were not painted, in order to not influence the pressure reading quality. A Jenoptik Variocam camera utilized by (Gabor, Koreanschi et al. 2016), with a resolution of 640×480 pixels, was used to measure the surface temperatures (Merbarki, Mamou et al. 2009). This camera was equipped with 60° lens in order to capture the flow transition on the entire upper surface of the wing.

Figure 6.22 presents the results of the IR visualization of the wing model upper surface transition, for the flow case 43 (Mach=0.15, α=2°, δ=0°, Reynolds number $5.2*10^{6}$) and for both un-morphed (left figure) and morphed (right figure) skin shapes.
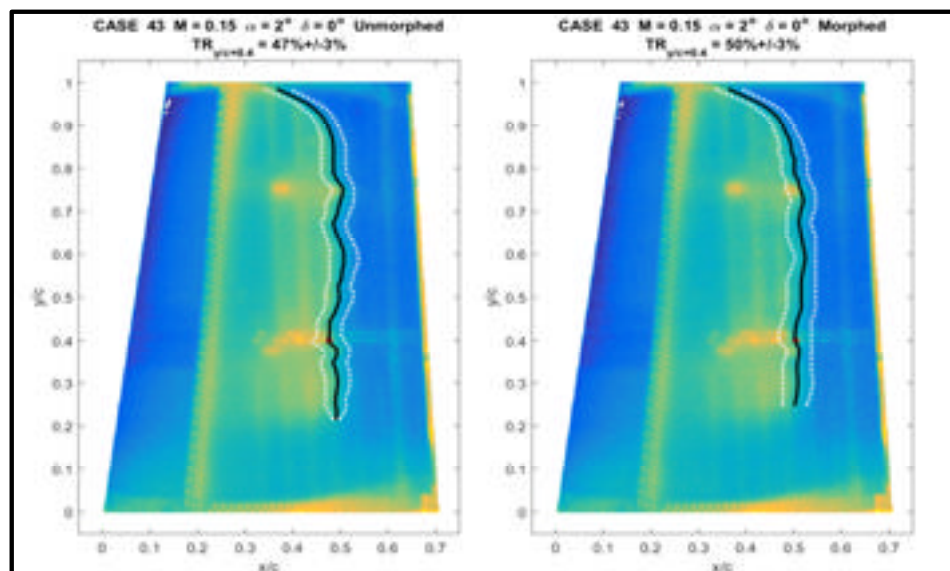

Figure 6.22 IR visualization of the laminar-to-turbulent transition region
for Mach=0.15, α=2°, δ=0°, Reynolds number $5.2*10^{6}$

The black line from Figure 6.22 represented the average transition line on the upper surface being estimated in following steps. At each spanwise station, an automatic detection of the temperature gradients due to the transition was performed. The temperature gradient method allowed to detect the onset of the transition (upstream dotted white line in figures) as well as the established turbulent boundary layer (downstream dotted lines). The mean transition location front is the spanwise average of the upstream and downstream fronts. From the figure, it was observed that the transition location is a function of the chordwise position. The two dashed white lines represent the estimated extent of the transition region, determined as a function of the chord-wise temperature gradient existing between laminar and turbulent regimes. The red dot corresponds to the estimated transition in the half-way between the two Kulite piezoelectric pressure sensors lines, span-wise section which is situated at 0.612 m from the root section (40% of the model span). The accuracy of the transition detection for this section was estimated to ± 3% of the local chord, based on the known Kulite positions and their thermal signatures in the images. We can observe that the infra-red (IR) visualizations validate the STD and FFT estimated positions of the transition points on the Kulite pressure sensors area, for both unmorphed and for morphed airfoils in the exposed flow case; for unmorphed airfoil the transition position was obtained at approximately 47% of the chord, while for for the morphed airfoil it was located at aproximately 50% of the chord. The average transition location for this flow case was 40.58% of the chord for the unmorphed airfoil and 46.62% of the chord for the morphed airfoil.

Therefore, for this flow case the laminar region was extended with an average value of 6.04% of the chord as a result of morphing. A close value for the laminar region extension is also obtained by using the data provided by the pressure sensors STDs and FFTs (50.79% - 45.16% = 5.63% of the chord).

6.4   Conclusions

The paper presented the modeling, the design and the control of the miniaturised electromechanical actuators used to morph the flexible skin in new multidisciplinary morphing wing research project. The results obtained during the experimental validation in bench tests and wind tunnel tests of the control system were analysed and discussed. A full-

scaled portion of an aircraft wing, equipped with an aileron was used as a reference to design and manufacture the experimental model, with its upper surface being a flexible skin made of light composite materials. The actuation system included four similar actuators disposed in two parallel actuation lines, which were designed and manufactured according to the specificity of the developed application. The feedback signals from the actuators in terms of linear displacements are provided by the LVDTs attached to each of them, and simultaneously, by the encoders integrated inside the motors driving the actuators in terms of the rotor angular position. The reason of using the second position control loop based on the LVDT sensors data as feedback signals was to compensate the mechanical plays inside the actuators from the position control point of view and for not altering the aerodynamic performance of the morphing wing in various flow conditions. To validate the aerodynamic purpose of the project, the pressure data provided by a number of Kulite sensors mounted on the upper surface of the flexible skin were used. A National Instruments Real Time (RT) Target technology allowed the development of the system interfacing the remote computer and the morphing wing experimental model.

After the mathematical modeling of the actuators, the architecture of the associated control system was established and the design of the included control loops was performed. The torque control loop and the encoder based position control loop were tuned by using the pole-zero cancellation method, while the LVDT position control was implemented using the Fuzzy logic techniques. In a first validation test of the control system, some numerical simulations were performed. The experimental validation of the developed control system was performed in bench testing in the LARCASE laboratory at ETS, with no airflow. The control was used in the same form for all four morphing actuators placed inside the wing.

The bench test validation of the controller was started with the independent control in time for each of the four actuators, while all groups of the desired displacements characterizing the optimized airfoil cases were imposed later as input signals on the four actuators. For all tested optimized airfoil cases, the experimental version of the designed controller worked well in the laboratory environment and in the wind tunnel flow conditions.

The wind tunnel testing was performed in the NRC subsonic wind tunnel, a typical test for one of the flight conditions consisted in a wind tunnel tare run, followed by a run for the reference (un-morphed) airfoil, and finally by a run for morphed airfoil, reproducing the corresponding optimized airfoil. During these tests the main signals such as the raw pressure signal data from the 32 Kulite sensors, the skin displacements from linear positioning sensors, actuator current, and actuator speed were recorded and further used in a data post processing step. Also, the pressure sensor signals were used to real time visualize the transition point position based on the FFT (Fast Fourier Transform) comparative analyze between the detection channels; the calculated pressure coefficients were used to validate the aerodynamic optimized wing shapes for each flow case. The tests of the un-morphed and morphed airfoils demonstrated the validity of the morphing wing concept in terms of the transition location improvement due to morphing, therefore the functionality of the wing model and the designed control system. To confirm in real time the transition region detection over the entire wing model surface, infra-red (IR) thermography camera visualizations were performed. The infra-red (IR) results served as a tangible reference in validating the STD and FFT estimated positions of the transition points.

Acknowledgments

CHAPTER 7

MORPHING WING DEMONSTRATOR TESTED IN A SUBSONIC WIND TUNNEL IN OPEN LOOP CONFIGURATION

Michel Joël Tchatchueng Kammegne[1], Yvan Tondji[2] Ruxandra Mihaela Botez[3], Lucian Teodor Grigorie[4]
Mahmoud Mamou[5] and Youssef Mébarki[6]

[1,2,3]Départment de Génie de la production automatisée, LARCASE Laboratory of Applied Reasearch in Active Controls, Avionics and Aeroservoelasticity,
École de Technologie Supérieure, 1100 rue Notre Dame Ouest,
Montréal, H3C1K3, Québec, Canada
[4]Université de Craiova, Strada Alexandru Ioan Cuza 13,
Craiova 200585, Roumanie
[5,6]Aerodynamics Laboratory, NRC Aerospace, National Research Council Canada, Ottawa,
Ontario, Canada, K1A0R6

This article was submitted to Aerospace Science and Technology

Résumé

''L'aile déformable'' pourrait améliorer la performance aérodynamique des avions en changeant le profil de l'aile en fonction des conditions de vol. Dans cet article, la modélisation et les essais expérimentaux des performances aérodynamiques d'un prototype d'aile déformable sont présentés. Les actionneurs intégrés à l'intérieur de l'aile sont utilisés pour modifier la structure flexible qui fait partie intégrante de l'aile. Dans ce projet, les actionneurs ont été conçus et fabriqués à l'École de technologie supérieure et, par conséquent, ils sont contrôlés par une logique de commande développée par l'équipe de contrôle du projet. La caractérisation de l'écoulement (laminaire ou turbulent) sur l'aile est donnée en utilisant les capteurs de pression intégrés dans la partie flexible de l'aile. La technique utilisée pour collectionner des données de pression des capteurs piezoélectriques Kulite et la méthodologie de post-traitement sont expliquées. Les données de pression enregistrées sont parfois soumises à des bruits qui sont filtrés avant le traitement de ces données. Les visualisations de l'écart-type et des spectres de puissance des données de

174

pression sont utilisées pour trouver la zone de transition sur l'aile. En outre, la visualisation des résultats obtenus par la thermographie infrarouge est présentée pour observer la zone de transition sur l'extrados de l'aile afin de valider l'analyse des capteurs de pression. Les dimensions du prototype sont données par une corde de 1,5 mètres et une envergure de 1.5 mètres. Quatre actionneurs miniaturisés fixés sur deux lignes d'actionnement sont utilisés pour modifier la partie flexible de l'aile. Un aileron rigide est attaché à l'extrémité de l'aile. Les résultats aérodynamiques obtenus après le post-traitement ont permis de valider l'emplacement de la transition prévue numériquement.

Abstract

Morphing wing could help to improve the aircraft aerodynamic performance by changing the wing airfoil depending of flight conditions. In this paper the modeling and experimental testing of the aerodynamic performances of a morphing wing demonstrator are presented. Actuators integrated inside the wing are used to modify the flexible structure which is an integral part of the wing. In this project the actuators are house made and consequently they are controlled with control logic developed by the project control team. The characterization of the flow (laminar or turbulent) over the wing is given using the pressure sensors incorporated in the flexible part of the wing. The technique used to collect Kulite pressure data and the post processing methodologies are explained. The recorded pressure data are sometimes subjected to noises which are filtered before being processed. The Standard deviation and Power spectrum visualization of the pressure data approaches are used to find the transition area of the wing. In addition, the Infrared thermography visualization is implemented to observe the transition area on the extrados of the wing in order to validate the pressure sensors analysis. The demonstrator measures chordwise 1.5 m and spanwise 1.5 m. Four miniature actuators fixed on two actuation lines are used to morph the wing. At the end of the wing a rigid aileron is attached. The aerodynamic results obtained after post processing validate the numerical predicted transition location.

7.1 Introduction

Aircraft fuel consumption reduction is actually one of the major challenges to be mastered by many aircraft companies. The aim is to reduce until 2020 by half the CO2 rejected by airplanes. Many technologies are proposed to achieve this objective. Among the proposed technologies belong biofuel, utilization of composite materials and morphing wing. To enhance the aerodynamic performance of the aircraft, the morphing wing technology could be used. It increases the aircraft performance by extending the flight range and improving the lift-to-drag ratio as presented in the research work realized by (Zingg, Diosady et al. 2006), and also can reduce flutter as explained by (Rodriguez 2007)).

Numerous morphing wing approaches have been studied in last decade. A small scaled model of a fighter wing with incorporated smart materials was validated experimentally with the purpose of enhancement of the rolling moment. The deformation of the control surface of the model developed by (Coutu, Brailovski et al. 2009) was realized by the actuators (smart materials) and it was found to be appropriate for take-off and landing. The modeling of the wing was performed by using a genetic algorithm described in (Sanders, Eastep et al. 2003).

It is often recommended before testing a demonstrator in wind tunnel to realize aeroservoelasticity studies to consolidate the stiffness of the demonstrator in term of flutter and vibration. Thus, flutter analyze has been realized by (Grigorie, Popov et al. 2011) for a laminar airfoil with an integrated flexible made of carbon Kevlar composite material. Shape memory alloys have been used to change the shape of the manufactured prototype. The results of the studies showed that at a wind speed of Mach = 0.55, the aeroelastic instabilities appeared. It was observed no flutter during wind tunnel testing because the maximum wind speed was fixed at 0.3.

Different optimization techniques are used in the design phase of morphing aircraft. The work presented by (Chowdhary and Pant 2010) investigated the reduction of take-off gross weight W_{t0} of a jet fighter aircraft by morphing the wing aspect ratio and wing area. The proposed method was an extension of the technique proposed by (Roth and Crossley 2003), where only the wing aspect ratio was used as sizing variable. Results showed that by

morphing the wing area and aspect ratio at the same time, 8% reduction in W_{t0} was obtained, while just the change of the aspect ratio allowed 4.7% reduction in W_{t0}.

At the Granfield University, (Perera and Guo 2009) presented and analyzed a new concept for the design of an aerosevoelastic wing structure together with its actuation system. For the actuation system, two different approaches were numerically simulated and tested for a small air vehicle. The required trailing edge deflection was obtained with a minimum control power. To achieve the desired deflection on open trailing edge has been used. To the trailing edge upper and lower surfaces, two metallic sheets were attached. This new configuration allowed the flexible skin to slide to each other during the deflection of the trailing edge. It was observed that the proposed actuation mechanism provided a significant weight reduction.

The design of a valid morphing wing is not an easy work, the complexity of the integrated structure and the unknown design parameter being issues, among others, to be mastered by the designers. With the objective to find some unknown design parameters to improve the finite element (FE) of the morphing wing, a design methodology was proposed by (He and Guo 2012). Additionally, a new concept of a seamless morphing wing that integrated a flexible trailing edge control system has been investigated. The proposed methodology was based essentially on the collection of vibration test data, with the idea to build a FE model starting from these data. To validate the model, the numerical and experimental parameters were finally compared. (Perera, He et al. 2010) studied the dynamic and aeroservoelastic behavior of a Seamless Aeroservoelastic Wing (SAW) structure for a small air vehicle. To cover the whole flight envelope and to fulfill the desired wing performance, two new concepts were integrated in the SAW: 1) a torque tube actuation mechanism (TTAM), and 2) a sliding trailing edge (TE) mechanism. The TTAM system was tested on a bench test and data were logged to identify some parameters such as the stiffness of the actuation system. The dynamic characteristics of the SAW were analyzed based on the experimental flutter data.

During a research project realized at Research Laboratory in Active Controls, Avionics and Aeroservoelasticity (LARCASE) of the Ecole de Technologie Supérieure in Montréal,

Canada, in collaboration with the Ecole Polytechnique in Montréal and the Institute for Aerospace Research at the National Research Council Canada (IAR-NRC), a morphing wing box has been manufactured and tested in a subsonic wind tunnel in Ottawa. The goal of the project was to increase the laminar region or to delay the transition. The transition point was moved towards the trailing edge. The consequence of moving the transition towards the trailing edge was the reduction of the drag induced inside the boundary layer. An actuation mechanism system with an integrated cam system has been mounted inside the wing box with the aim of changing the flexible skin. The role of the integrated cam system was to convert the horizontal motion of the actuator into vertical displacement of the flexible skin. Shape Memory Alloys (SMAs) were used as actuators. SMAs were heated with an electrical current in order to deform the actuator. In the heating phase the SMAs were contracted allowing the flexible skin to move upwards, while in the cooling phase (no electrical current) the skin was pulled downwards. To achieve the desired skin displacement each actuation line was controlled independently. Different control algorithms were developed and validated experimentally in the subsonic wind tunnel. Prior to the controller design, a numerical model of the actuator has been obtained and validated in bench tests by (Georges, Brailovski et al. 2009, Terriault and Brailovski 2011). Due to the required control accuracy, the used actuators model was a non-linear one, based on a numerical finite element method, and was built by using Lickhatchev's theoretical model. During the first phase of the controller design, numerical simulation of the controlled actuation system was performed. Due to the fact that no electrical current was needed during the SMA cooling phase, a combination of a bi-positional (on–off) controller and a PI (proportional–integral) controller was developed by (Grigorie, Popov et al. 2011) and used in one of the developed configurations for the control system; it acted like a switch between the cooling and the heating phases, situations where the output current is $0\,A$, or is controlled by a PI type law. The control experimental validation was performed by (Grigorie, Popov et al. 2012) firstly on bench tests and then in the wind tunnel tests. During the wind tunnel tests, the flexible skin was heated with powerful spot lights to increase the temperature over the wing surface. The temperature rising over the wing surface allowed visualizing very well the separation zone between the laminar and turbulent regions; the images were captured with an infrared camera. Another approach to understand the phenomena which happened during wind blowing on the wing presented by (Popov, Grigorie et al. 2010) was the utilization of the pressure sensors. Because of their frequency range, precision and accuracy, Kulite

pressure sensors have been installed or integrated in the flexible skin, the obtained pressure data being used to evaluate the aerodynamic gains of the project and to validate the results obtained with the infrared technique. The strong nonlinearities of the SMA actuators' characteristics and the system requirements conducted to the development of a nonlinear controller for the same actuator. In this way a hybrid controller architecture as a combination of a fuzzy logic controller and a bi-positional on-off controller was chosen. A bench test and wind tunnel test were performed by (Grigorie, Popov et al. 2012, Grigorie, Botez et al. 2012) to experimentally validate the morphing wing system controlled in this way. For the experimentation, a data acquisition card Quanser Q8 and two programmable switching power supplies (AMREL SPS100-33) were used. The acquisition board's output channels were used to control power supplies in order to obtain the desired skin deflections. Linear Variable Differential Transducer (LVDT) and thermocouples were used to sense the actuator position and its temperature respectively as explained in (Grigorie, Popov et al. 2010, Grigorie, Popov et al. 2011, Grigorie, Popov et al. 2012, Grigorie, Popov et al. 2014).

The configuration tested previously, regarding the morphing wing project developed at LARCASE, was called "open loop" configuration or architecture although the actuator position has been controlled. This convention has been adopted to make the difference between control based on pressure sensor data and control based on LVDT as feedback signal. Control based on pressure sensor as feedback signals was called "closed loop". The "open loop" configuration used a database of some optimized airfoils correlated with the airflow cases as combinations of Mach numbers and angles of attack, and controlled the actuators positions taking as reference value the necessary displacement of the actuators from the database in order to obtain the morphing wing optimized airfoil shape. In a first variant, the "closed loop" method was based on a similar controller as in the actuators position control, but the control loop used the pressure data form the pressure sensors evaluating the changes of the C_p values with the XFoil software in two fixed positions along the chord of the wing; the two positions were associated to two pressure sensors linked through aerodynamic interdependence with the actuators positions. The second closed loop architecture, called suggestive "optimized closed loop", implemented by (Popov, Grigorie et al. 2010, Popov, Grigorie et al. 2010, Grigorie, Popov et al. 2014) was based on the pressure information received from the sensors and on

the transition point position estimation. It included, as inner loop, the "open loop" control method of the actuation lines based on the LVDT feedback. The best wing shape for a flow condition was achieved based on a real time optimizer code which funds the best actuators configuration maximizing the delay of the transition; a mixed optimization method was used, between „the gradient ascent" or „hill climbing" method and the „simulated annealing" method.

(Kammegne, Grigorie et al. 2014, Kammegne, Belhadj et al. 2015, Kammegne, Grigorie et al. 2016) realized also at LARCASE a new actuation mechanism used to change the shape of a wing prototype (ATR-42). It consisted of two electrical machines coupled to two eccentric axes. Numerical model of the system was simulated and subsequently a linear control for the system was designed. It was observed a very low static error that was eliminated later by a nonlinear control based on Fuzzy logic approach. The wing prototype was tested in the Price-Païdoussis wind tunnel at LARCASE laboratory.

The current paper presents the experimental results obtained during the wind tunnel testing of a new morphing wing demonstrator, developed at LARCASE starting from a real wing structure equipped with an aileron and a flexible skin on its upper surface. Shown are the morphing actuators control results in a special configuration based on the two loops controlling the same variable and the aerodynamic gain of the project produced by the controlled morphed shapes of the wing. This control configuration was developed starting from the particular requirements imposed by the wing desired structure, which need to have a behavior similar to a real wing. Therefore, the morphing actuators placed inside the wing need to work properly by avoiding their blockage even at the wing bending.

7.2   A General Description of Morphing Wing Project

In parallel with the ATR-42 morphing wing project, our research team from LARCASE developed a big morphing wing research project under the name CRIAQ MDO 505, called "Morphing architectures and related technologies for wing efficiency improvement". It is funded by CRIAQ (Consortium for Research and Innovation in Aerospace in Québec), NSERC (Natural Sciences and Engineering Research Council of Canada), Thales Canada,

and Bombardier Aerospace, being realized in collaboration with Thales Canada, Bombardier Aerospace, Ecole Polytechnique de Montréal, IAR-NRC (Institute for Aerospace Research - National Research Council) - in Canada and with University of Naples, CIRA (Italian Aerospace Research Centre) and Alenia Aeronautica in Italy. The particularity of this new project is the utilization of a real wing structure having a structural rigidity similar to the rigidity of a real aircraft, with spars, stringers, and ribs in the interior, and equipped with a flexible skin on the upper surface (made of composite materials) which is directly actuated by four similar in house designed and manufactured miniature electrical actuators. More details regarding numerical model of the actuator and aerodynamic results were presented by (KAMMEGNE, BOTEZ et al. , Kammegne, Grigorie et al.).

For this project a wing demonstrator was manufactured. The chord length was 1.5 meters and the span was 1.5 meters. The adaptive upper surface was positioned between 20% and 65% of the wing chord (Figure 7.1), and it was specifically designed and optimized to meet aeronautical industry requirements. Speed, Reynolds number, angle of attack and aileron deflection number were some of the parameters that determined the actuator control of the skin deformation. To morph the upper surface of the wing the team decided to use two actuation lines; each comprised of two electrical actuators. The actuation lines were positioned at 37% and 75% of the wing's span. Chordwise, on each of the actuation lines, the actuators were positioned at 32% and 48% of the local chord as shown in (KAMMEGNE, BOTEZ et al. , Kammegne, Grigorie et al.).

An in-house developed genetic algorithm was used by the aerodynamic team of the project for the optimization of the morphing wing. In this way, starting from a reference airfoil (Figure 7.2), the algorithm searched the optimum shapes for the airfoil through local thickness modifications with the aim to improve   the upper surface flow and thus the aerodynamic performances of the airfoil. The optimization was applied for several combinations of Mach numbers (M), angles of attack (α) and aileron deflection angles (δ), providing in the each optimized flow case the vertical displacements for the two actuators placed on the first actuation line; the displacements for the other two actuators were calculated as a linear dependence. Figure 7.3 presents a Monte Carlo map obtained for

M=0.2, α=2° and δ=4° flow case, with the optimization results plotted on it. The map shows the transition position evaluation for all possible combinations of the two actuators vertical displacements, the plotting of the optimization results on it being used to estimate how accurate the optimization code was developed by (KAMMEGNE, BOTEZ et al. , Koreanschi, Sugar-Gabor et al. , Koreanschi, Gabor et al. 2016). The aerodynamic analysis was done by using the open source XFoil aerodynamic solver developed by (Drela 1989) which allows both inviscid and viscous calculation.
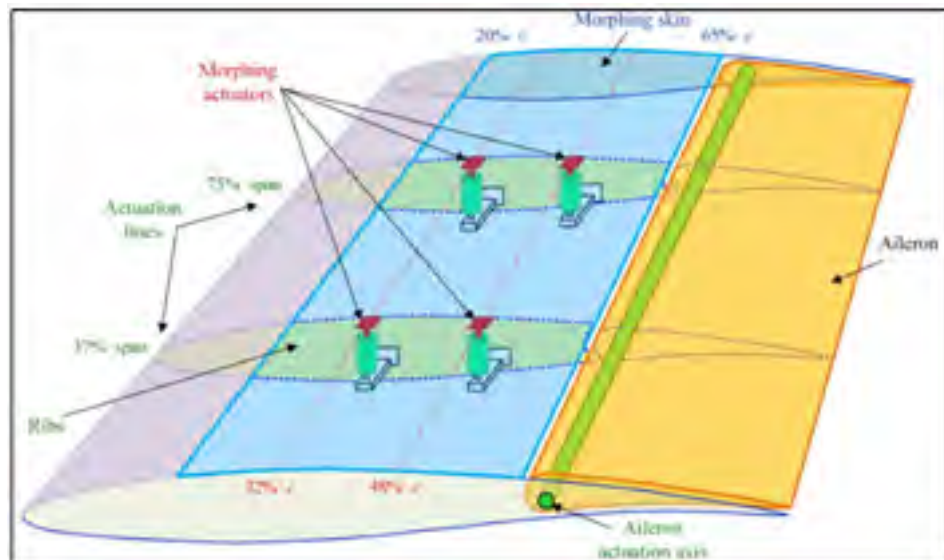

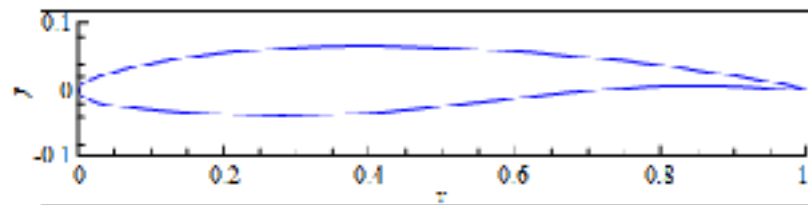Figure 7.1 Morphing Wing architecture

Figure 7.2 Reference airfoil

The aerodynamic performance of the wing was tested in wind tunnel at the National Research Council Canada (NRC). For the wind tunnel tests, ninety seven flow cases were tested: nineteen values for the angle of attack (varied from -3 degree to +3 degree), three values for the Mach number (0.15, 0.2, and 0.25) and thirteen for the aileron deflection angle (varied between -6 degrees an +6 degrees). For the three speeds given before the

corresponding Reynolds numbers were $5.2*10^6$ for Mach number of 0.15, $7.3*10^6$ for Mach number of 0.2 and $8.7*10^6$ for Mach number of 0.25. All Reynolds numbers were calculated using the sea level atmospheric values for pressure (101325 Pa) and temperature (15° C). The ninety seven desired optimized airfoils were obtained by deforming the extrados in the vertical direction according with the four vertical displacements of the actuators obtained during the numerical optimization of the each flow case. The aerodynamic goal was to extend the laminar region by moving the transition point as near as possible to the wing trailing edge with a constant lift. Each of the four morphing actuators was connected to a controller able to vary its output voltage in order to control the position of the actuator. The actuator's controller designed by (Kammegne, Grigorie et al.) modified the actuators linear positions until the real vertical displacements of the morphing skin in the four actuation points equaled the desired vertical displacements of the optimized airfoil resulted for a flow case.
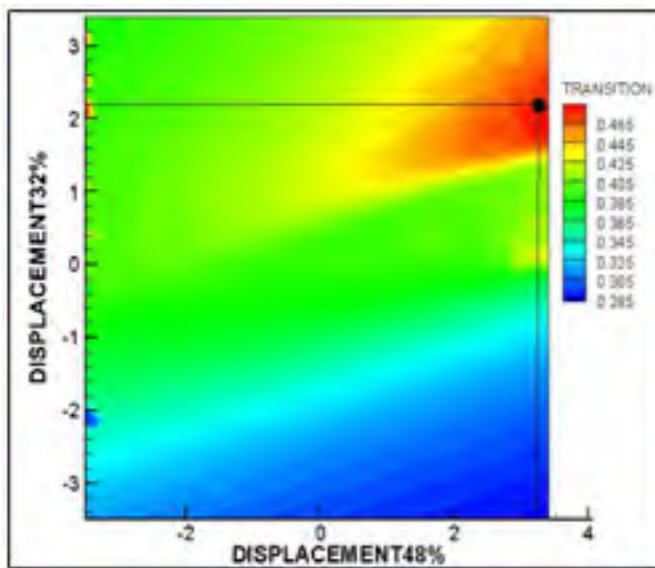

Figure 7.3 Monte Carlo map with optimization results
for M=0.2, α=2°, δ=4° and Reynolds number $7.3*10^6$
flow case

On the flexible skin, 32 high precision Kulite piezoelectric-type sensors for pressure measurement were installed to evaluate the laminar-to-turbulent transition location. These sensors were installed in two staggered lines (with 16 Kulite sensors on each line), situated

respectively at 0.600 m and 0.625 m from the wing root section as presented in (KAMMEGNE, BOTEZ et al.). The pressure signals were logged in parallel while the shape of the airfoil changed. The recorded pressure data were post processed offline to obtain the pressure coefficient distribution curve and the spectral repartition of the pressure. The transition region was characterized by the amplification of the Tollmien-Schlichting waves captured by the Kulite pressure sensors. On the other way, to capture the transition region over the entire wing model surface infra-red (IR) thermography camera visualizations were performed. A Jenoptik Variocam camera, with a resolution of 640×480 pixels, was used to measure the surface temperatures (Merbarki, Mamou et al. 2009).

For the morphing wing control system were developed several variants, based on classic or fuzzy logic techniques. Prior to its design, a nonlinear model was developed for the used miniature actuators. Firstly, a hysteresis current controller and a position controller were developed to control the current in the actuator and to maintain the actuator at a desired position. The controller designed as described in (Kammegne, Grigorie et al.). In an experimental validated approach for the morphing wing control system, the implemented controller by (Kammegne, Khan et al. , Kammegne, Nguyen et al. 2015) was compiled in C language and deployed in the real time hardware system used in this project. The input and output of the controller was configured and mapped so that the controller worked properly. The experimental validation was performed during bench and wind tunnel tests.

The presented work refers here to a special configuration on the control system based on the two loops controlling the actuator position. This paper emphasizes firstly the necessity to control the same variable with two loops and the details of the methods used to post process the raw acquired pressure data signals.

7.3 Two Position Loops Efficiency

The actuator used for this project and placed inside the wing to morph the wing locally has been designed and assembled by the mechanical team in collaboration with the control team. Different parts have been bought separately and brought later together. Consequently, some small plays were accumulated inside the actuators because there were small differences in

term of sizing between the mechanical parts. To evaluate the integration of the actuators inside the wing structure and their functionality under a load producing a wing bending, the structural team of the project realized a successful 1g structural static test.

Therefore, the reason of using this control strategy with two position control loops was to compensate these mechanical plays inside the actuators from the position control point of view and to don't alter the aerodynamic performance of the morphing wing in various flow conditions. The feedback signals from the actuators in terms of linear displacements were provided by four Linear Variable Differential Transducers (LVDT) used as position sensors and having axes parallel to the actuators axes, and simultaneously, by the encoders integrated inside the motors equipping the actuators in terms of the rotor angular position.
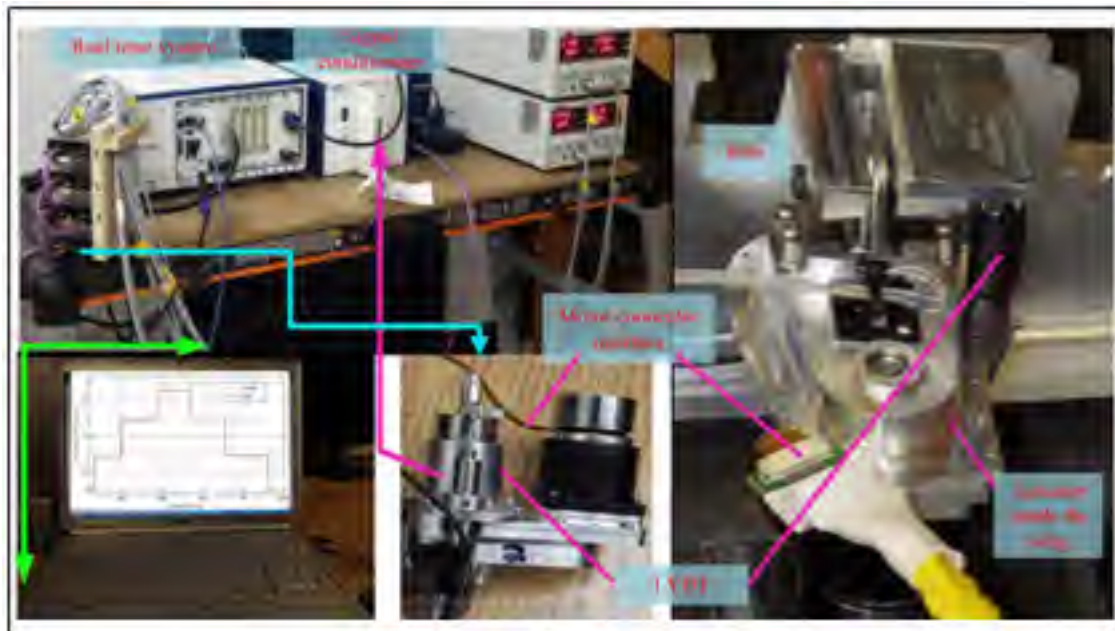

Figure 7.4 Experimental setup

For a better understanding of the necessity to add the loop based on LVDT, it was necessary to perform some bench tests without any feedback from LVDT sensor. In this context, the testing architecture included only the actuator and the associated power amplifier provided by the motor manufacturer; the LVDT signals were just displayed and acquired. The

experimental set up is shown in Figure 4. Models developed with Labview and Simulink on the host personal computer were compiled and the generated ".dll" library files were loaded in the real time system. The architecture of the actuator control system based only on the encoder signal as feedback is shown in Figure 7.5.
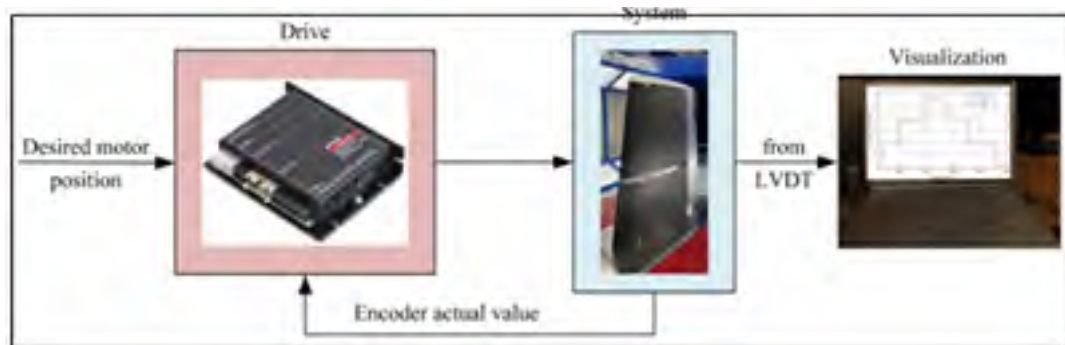

Figure 7.5 Architecture of the open loop control

The desired motor angular position was send from the Graphical User Interface (GUI) and based on the error signal between the desired position and the encoder actual value the appropriated voltage was applied to the motor. In parallel, data (system time, encoder desired position, encoder actual value and LVDT signal) were saved on the hard drive of the real time system. The obtained results for a series of repeated step signals considered as inputs for the control system based encoder feedback are shown in Figure 7.6.

From Figure 7.6 it can be observed that the controller performed very well; there was no overshoot and the static error was cancelled. But there was a significant difference between the static value of the encoder and LVDT. Mechanically, LVDT was fixed or attached to the rest of the system through a nut. It was expected that for a small change of the encoder the LVDT detected that change at the same time not with some delays. The difference between both signals was due to the existing plays inside the system. From the behavior observed in Figure 7.6 (difference between encoder and LVDT signals) it was concluded that a loop based on the LVDT feedback was necessary because firstly LVDT had to be used to sense the displacement of the flexible skin and secondly plays inside the system would be compensated. The encoder signal was not reliable in term of skin displacement value, for instance, from Figure 7.6, if LVDT values was supposed to be the real skin displacements,

186

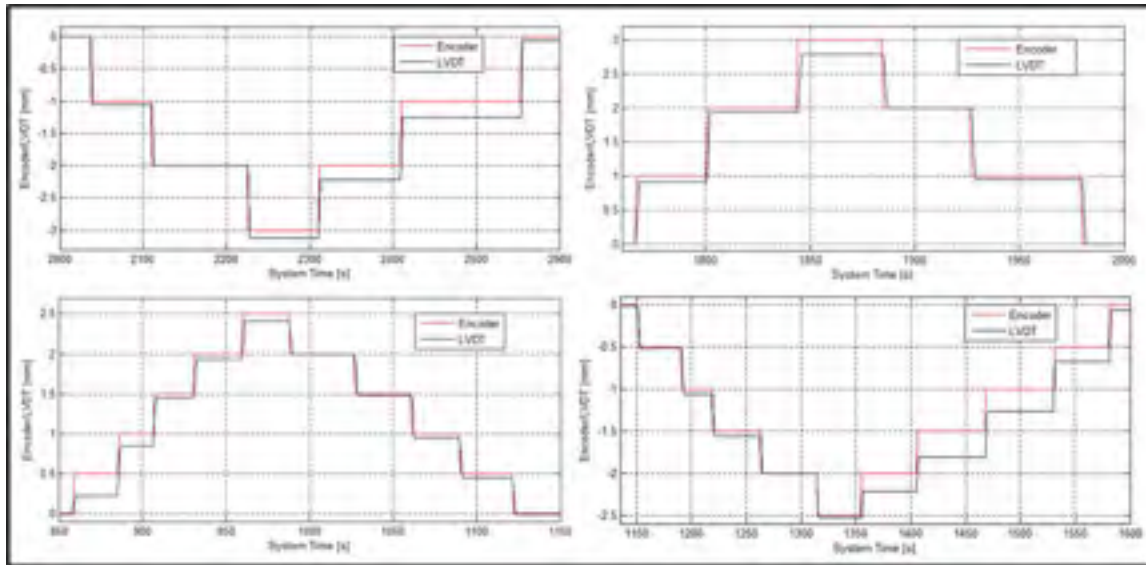encoder gave back values different from the expected ones.

Figure 7.6 Encoder/LVDT data

7.4 Wind Tunnel Test Results

7.4.1 Double Loop Control of the Actuators Position

In the wind tunnel the system was tested in open loop configuration because the pressure sensors signals were not used as feedback for the control system. During the tests, the real time pressure data were recorded for further analyses. Two Graphical User Interfaces were also tested; the first one was used to control all the equipment (aileron drive, actuators power boards) (Figure 7.7 adapted from (KAMMEGNE, BOTEZ et al.)), while the other one was used for the real time displaying of the pressure data results (Figure 7.8 adapted from (KAMMEGNE, BOTEZ et al.).

According to Figure 7.9, the first position control loop used as feedback signal the motor encoder position while the second position control loop used the LVDT signal as feedback signal. Thus, for one actuator two positions sensors (Encoder and LVDT) were used. So, it was expected that both sensor signals gave the same output in term of actuator displacement. To convert the motor revolution, expressed in degrees, in actuator linear displacement, expressed in millimeters, the factor 2400 was used as indicated in the next equation

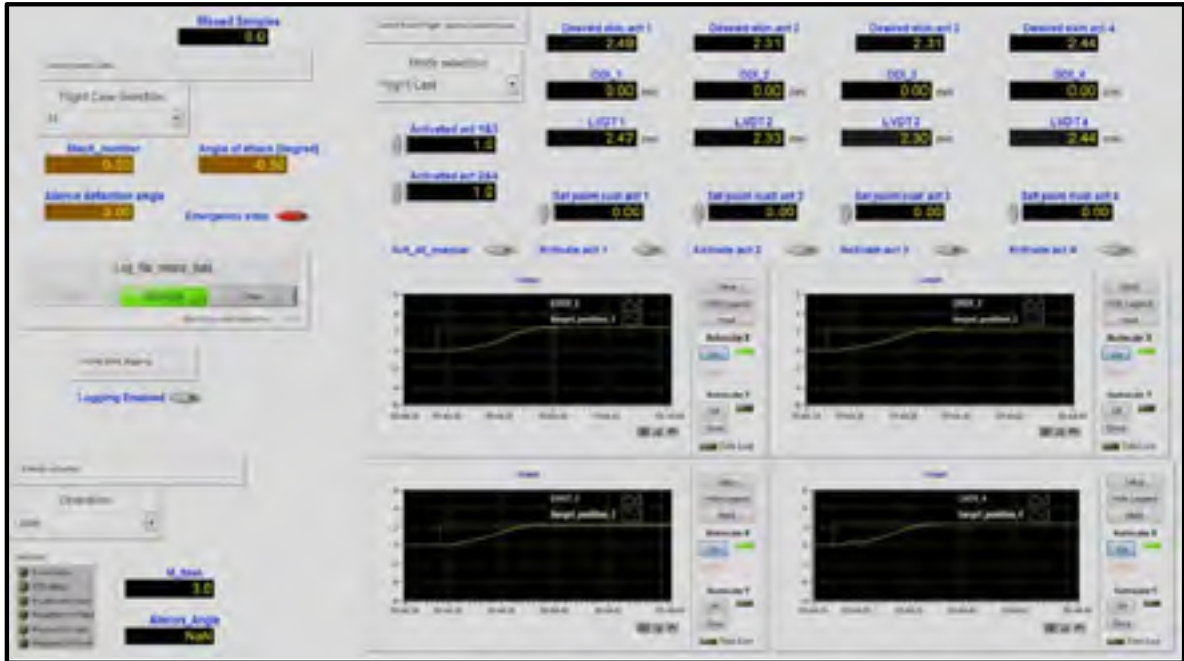$$X\,[\text{mm}] = N\,[\text{Motor revolution}]\,/\,2400. \tag{1}$$

Figure 7.7 Graphical User Interface (GUI) for wind tunnel tests

Therefore, to measure 1 mm vertical displacement of the flexible skin, the motor had to do 100 revolutions or 2400 pulses. During wind tunnel testing, motor encoders data for all actuators were recorded. The recorded data in pulses were converted in millimeters for a better comparison with the LVDT recorded data. An example can be seen in Figure 7.10. Because of the linear relationship between LVDT and encoder it was expected to observe both signals superposed. The outer position loop compensated all plays inside the actuator by forcing the inner loop to count more pulses to achieve the desired skin displacement. For actuators #2 and #4 it could be observed that the LVDT value remained the same for few seconds while the encoder value continued to increase. It was due to the fact that the actuator was in the plays; see the red circle in Figure 7.10. Small overshoots were also observed.
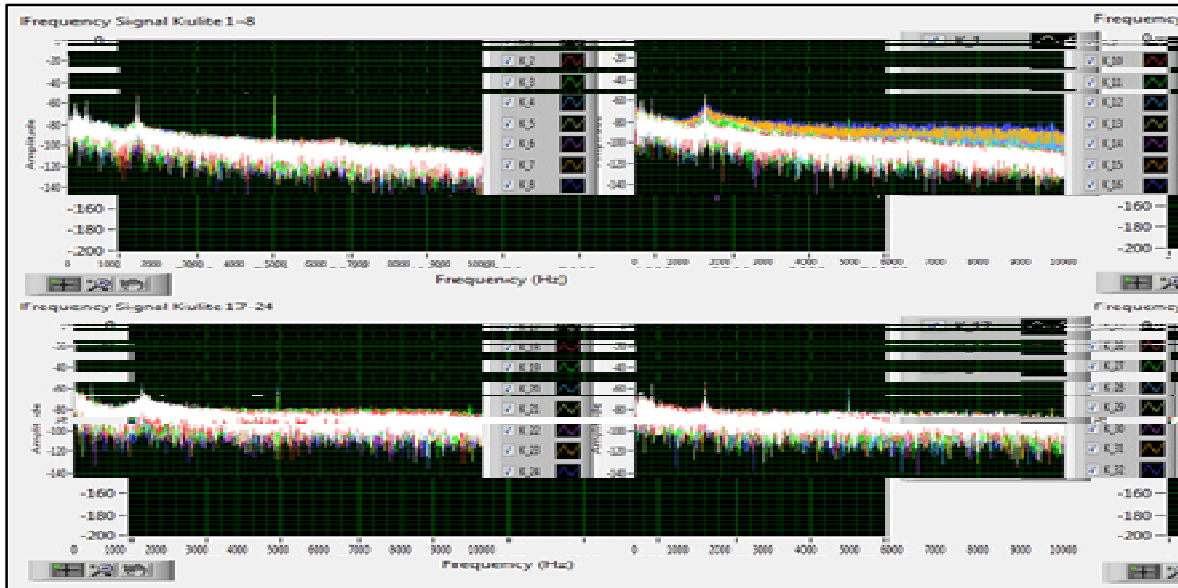
Figure 7.8 Real time Fast Fourier Transforms (FFT) for an acquisition sequence associated to the pressure sensors
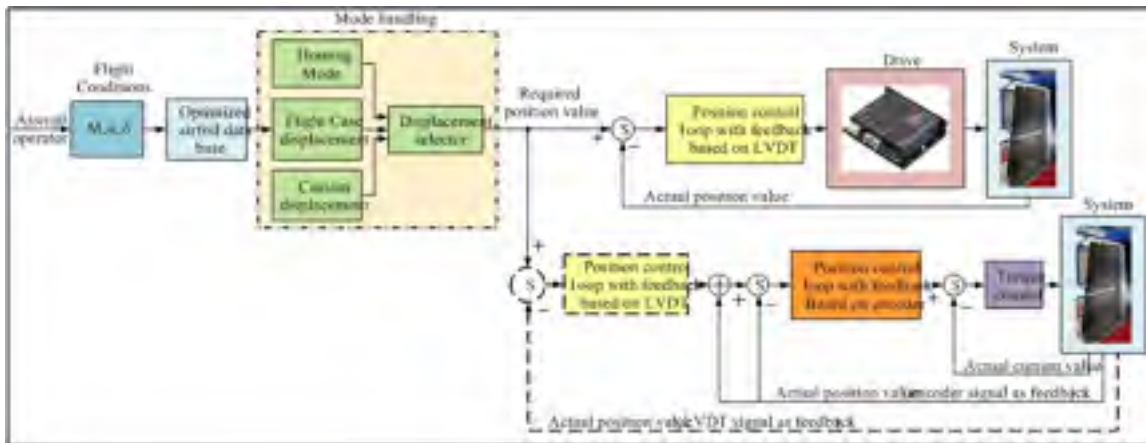

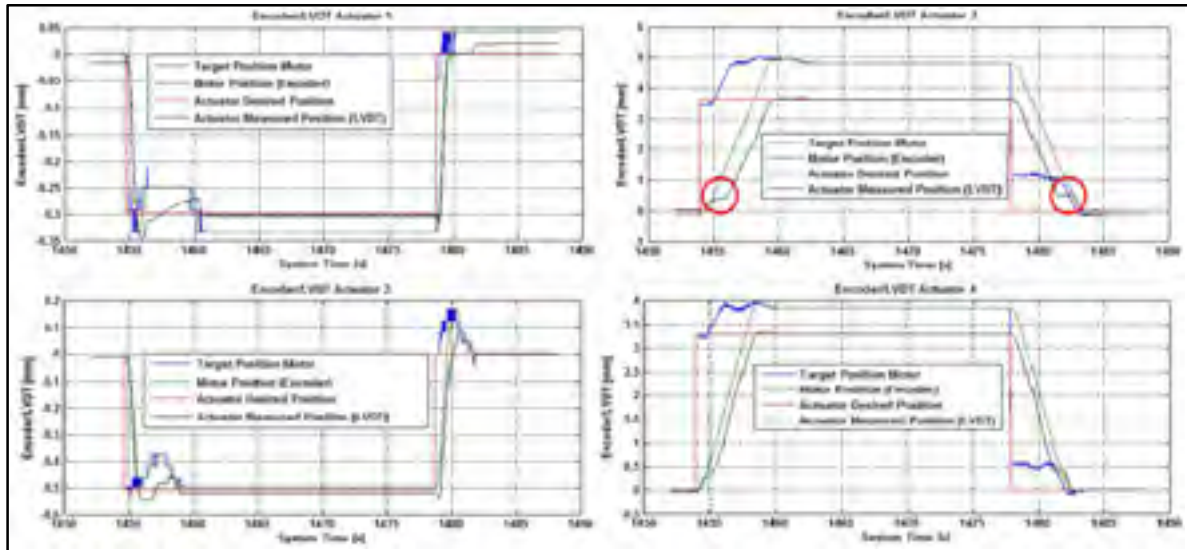Figure 7.9 Control system architecture

Figure 7.10 Encoder/LVDT with feedback on LVDT

7.4.2 Evaluation of the Aerodynamic Gain Brought by the Wing Controlled Morphed Shapes

7.4.2.1 Monitoring of the Pressure over the Wing Upper Surface

The air flowing over wings creates a boundary layer. As can be observed in Figure 7.11, the airflow across an airplane wing is characterized by two distinct different regions. The lead region, which extends from the leading edge to the transition location, is dominated by laminar flow; however, the aft region is completely turbulent, characterized by rapid variation of the pressure in space and time as explained by (Jayantha 1998). The aft region contributes more to drag increase. Because the pressure fluctuations are supposed to be much more intense in the turbulent flow than in the laminar one, the method of determining the transition area with pressure sensors is mainly based on the difference in fluctuation amplitude.
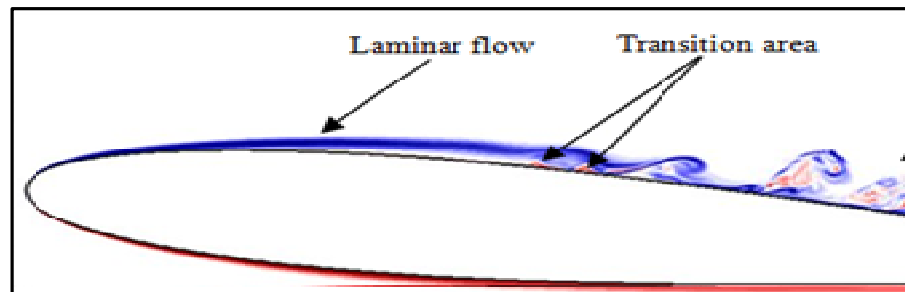
Figure 7.11 Wing airflow
(Adapted from http://aeguana.com/blog/introduction-to-aerodynamics-part-2/)

Based on the previous considerations, to evaluate the laminar-to-turbulent transition location for the wing demonstrator, 32 Kulite pressure sensors were arranged on two closes chord lines (40% of the span and 41.7% of the span, i.e. at 0.600 m and 0.625 m from the wing root section) in order to sense the whole pressure variations with the least possible interaction between two successive sensors. They were disposed from 28% to 68% of the chord as shown on Figure 7.12; for each sensor, a chord percentage was affected. The sensors can sense up to 5 Psi of pressure amplitude on a frequency range of 20 kHz, with an uncertainty of +/-0.25psi.

Figure 7.12 Kulite sensors disposition on the wing

The data processing was made individually for each sensor, and the results were plotted on the same graphs, according to the chords percentage of the sensors. The graphs were finally interpreted conforming to the theory.

7.4.2.2 Data Processing and Evaluation

The waveforms acquired during the wind tunnel tests contained pressure data, which were recorded at the rate of 20 kHz for ninety-seven flow cases with the morphing applied on the

wing and without any morphing. The data processing was mainly based on the estimation of the power spectrum and the standard deviation of the pressure data recorded.

For the visualization of the power spectrum of every sensor data, the Fast Fourier Transform algorithm was applied on consecutive packages of 1024 data points. Each 1024 data package was divided into 25 segments before computing the PSD. The obtained PSDs were averaged following Welch's Method described in (MathWorks, 2015) in order to reduce the variance of the Power Spectrum Density estimate of the entire package.

The standard deviation was a measure that quantifies the amount of variation of a set of values around their average point. Before computing the standard deviation the raw signal was high pass filtered at 1 kHz with the aim of erasing the noises caused by either the wind tunnel or the motor of the aileron actuator. We considered as noise each peak that appeared on every pressure sensor (not necessarily with the same amplitude) regardless of the angle of attack, the morphing of the wing and sometimes the aileron deflection (see Figure 7.13).
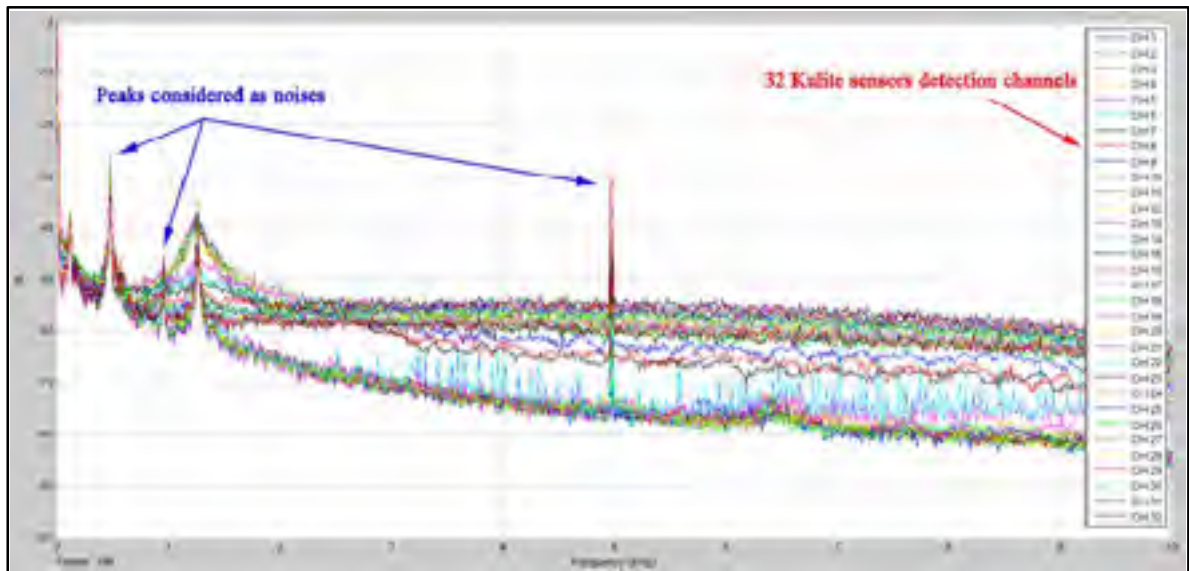

Figure 7.13 Noise representation on the 32 pressure sensors spectrums

Figure 7.14 showed all the data processing procedures which were described herein. To have a satisfactory correlation between the Power spectrum and the standard deviation, both were computed instantaneously for every data package (1024 data points per package). To be sure

that the 1024 data points' package chosen for interpretation was representative enough of all the recorded points, we computed on one side the STD of all the recorded data points (average STD), and compared them with the instantaneous ones (previously saved) by the means of a mean square error algorithm. We chose for interpretation the instantaneous STD, which is the closest to the average one, and the corresponding Power spectrum graph.
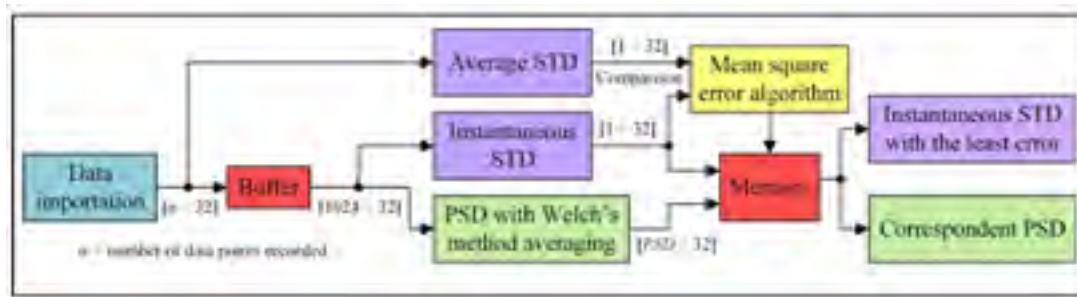

Figure 7.14 Block diagram of data processing

For the interpretation of the obtained FFT and STD curves, we considered the flow to be transitional on the chord region delimited by two distinct sensors. The first was the sensor from which the power spectrum amplitude started to be greater than that amplitude of the previous one, showing the increase in the pressure fluctuations. This sensor position represented the beginning of the transition area. The second sensor was given by the maximum of the standard deviation plot, showing the maximum fluctuation of the flow and the end of the transition area (beginning of the turbulent region).

From Figure 7.15, the standard deviations of the pressure data acquired for the flow case 18 (Mach=0.15, α=-2˚, δ=-2˚) are presented for both un-morphed (reference) and morphed airfoils, it can be observed that the transition for un-morphed airfoil started on the presure sensor #16 positioned at 50.8% of the chord, while the transition for morphed airfoil started on the presure sensor #19 positioned at 53.5% of the chord. Also, for un-morphed airfoil the maximum value of the standard deviation was found on sensor #20 positioned at 54.6% of the chord, while for morphed airfoil the maximum value of the standard deviation was found on sensor #22 positioned at 56.9% of the chord.

The FFT plots associated to the same flow case for un-morphed airfoil (Figure 7.16) and for morphed airfoil (Figure 7.17) show the 32 pressure detection channels as follow: the first four pictures in each figure depicted the results for four groups of 8 channels starting from the leading edge, "CH1÷CH8", "CH9÷CH16", "CH17÷CH24", "CH25÷CH32", the fifth picture in each figure depicted the results for all 32 channels, a centralized representation performed for an easiest observation of the FFTs curves detachment in correlation with the first four pictures.

Figure 7.15 STD of the pressure data acquired for the flow case 18
(Mach=0.15, α=-2˚, δ=-2˚, Reynolds number $7.3*10^6$)

From Figure 7.16, related to the original (un-morphed) airfoil in flow case 18, can be easily observed that the FFT curve associated to the sensor #17 was easiest detached from the lower FFT curves package, indicating the transition starting. A more visible detachment appeared at the level of the sensors #18 and #19, producing the transition to the upper FFT curves package.

For the morphed airfoil, the FFT curves in Figure 7.17 suggested that the transition started on the sensor #20, and the maximum influenced curves were associated to the sensors #21 to #23. Therefore, the conclusions, starting from the FFT observations, were similar as in the analysis of the STD curves. For this case the laminar region being extended with over 3% of the chord in the Kulite sensors section.

In addition to the visualization of the pressure fluctuations, the Infrared thermography (IR) visualization was also implemented to observe the transition area on the extrados of the wing in order to validate the pressure sensors analysis. The Infrared thermography method was based on the differences temperature between the laminar and the turbulent flow. In fact, the intense mixing of the fluid in turbulent flow increased the heat transfer between the fluid particles, which in turn increased the convection heat transfer coefficient. The turbulent region appeared hotter than the laminar region if the wind temperature was greater than the model temperature, as illustrated by (Gabor, Koreanschi et al. 2016). (Diodati, Ricci et al. 2013) realized study to analyze the morphing capabilities for an adaptive Trailing-Edge device.

Figure 7.16 FFT results for the un-morphed airfoil in the flow case 18
(Mach=0.15, α=-2˚, δ=-2˚, Reynolds number 7.3*10^6)

Figure 7.18 showed the region (from 0% to 70% of the chord) of the extrados measured by the IR for the flow case 18, with and without any morphing applied. The left hand side part of the figure displayed the IR results for un-morphed airfoil, while the right hand side showed the IR results for morphed airfoil. The aft rigid portion of the wing (70% to 100% of the chord) was not considered on the IR measurement.
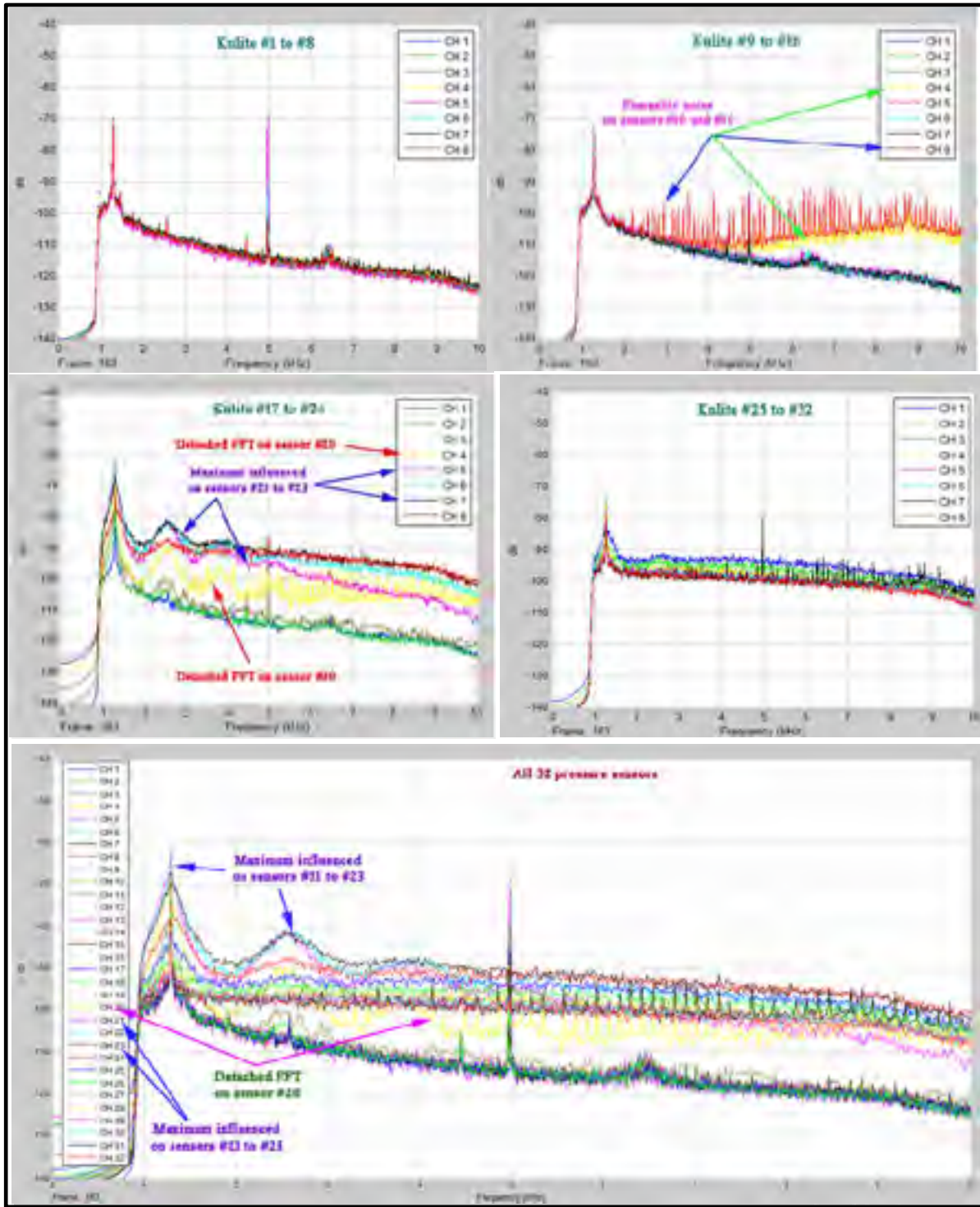
Figure 7.17 FFT results for the morphed airfoil in the flow case 18

(Mach=0.15, α=-2˚, δ=-2˚, Reynolds number 7.3*10⁶)

Figure 7.18 IR visualization of the laminar-to-turbulent transition region
for Mach=0.15, α=2˚, δ=0˚, Reynolds number 7.3*10^6

The wind blows from the left to the right. The blue region indicated the low-temperature area, representing the laminar flow, while the yellow region shows the high temperature area (turbulent flow). The two yellow point lines going from about 30% to 70% of the wing display the Kulite sensors' thermal signature. The transition area of the 3D-wing was averagely and represented by a black line, which is delimited by two white lines along the wing span. To compare the IR thermography with the pressure sensor results, we were only interested in the 2D transition area located on the Kulite chord line. For Mach=0.15, α=-2deg and δ=-2deg, the transition area for the reference configuration was found to be between 47.18% and 59.18% of the chord, and between 53.89% and 59.89% for the optimized airfoil. The IR averaged transition location in this flow case was 53.18% of the chord for the un-morphed airfoil and 56.89% of the chord for the morphed airfoil. Therefore, according to the IR analysis, for this flow case the laminar region was extended with an average value of 3.71% of the chord by using the morphing wing technology.

198

7.5   Conclusions

The paper presented few experimental results obtained during the wind tunnel testing of a morphing wing demonstrator in open loop configuration. Were shown the morphing actuators control results in a special configuration based on the two loops controlling the same variable and the aerodynamic load gain produced by the controlled morphed shapes of the wing. This control configuration was developed starting from the particular requirements imposed by the wing desired structure, which needed to have a behavior similar to a real wing; the morphing actuators placed inside the wing needed to work properly by avoiding their blockage even at the wing extreme bending. The actuators used in the project were designed and manufactured by the mechanical team of the project. Experimentally, it was observed that there were some deviations between the values provided by the LVDT sensors monitoring the linear position of the actuators and the value provided by the encoders included in the actuators' motors monitoring their angular positions. By introducing the position control based on a double loop, those plays were compensated; hence both control loops performed very well during wind tunnel testing. For all tested flow cases the static errors were less than 0.1 mm and the overshoots was less than 5% of the static values. The method of determining the transition area of the flow by using pressure sensors was described and compared with the infrared detection. Furthermore, was observed that the transition area detected by the pressure sensors method was always located before the one indicated by the IR thermography with a neat improvement of the laminar region on the flexible skin.

GENERAL CONCLUSION AND RECOMMANDATION

The goal of this project research was to design, develop and test different control methodologies for an in-house manufactured actuator for a morphing wing application. The different techniques utilized to achieve this objective were presented in five papers published and submitted in peer-reviewed journals. The controller developed for both projects (ATR-42 and MDO 505) showed an excellent behaviour. The numerical aerodynamic results expressed in terms of pressure and infrared transition measurement were validated with this controller.

My main contributions in this thesis were on developing the control design architecture, the hardware, the software implementation and integration and system calibration. The control architecture was validated experimentally with a real time National Instruments system. Thanks to its modular characteristics it was possible to connect all the peripherals with the central unit for the morphing wing.

The network communication between the actuator and the real time system occurred via CANopen protocol, while an Ethernet cable served as the link between the Graphical User Interface and the real time system. All of the software (control, optimized database, communication protocol, emergency function) were deployed into a real-time system and were linked together through a mapping function which was a characteristic of the real-time system.

The differences found between the LVDT response and the Dial Indicator measurements conducted to the development of a new calibration procedure for the controller's system. The purpose of the procedure was to correct the LVDT-demanded values to achieve the desired skin displacement. The software environment dedicated to the real-time system allowed the calibration procedure to be executed automatically.

An algorithm developed with Matlab/Simulink was used to post-process the pressure sensors' data for their comparison with infrared measurements in terms of transition region location. This algorithm was running automatically in view of its implementation in a closed loop control strategy, where pressure data could be used as the feedback signals as a means

to directly control the morphing wing shape. There are differences between numerical and experimental results because of the three dimensional aspect of the flow cannot be captured with the aerodynamic models used in the project. Another reason for the differences is due to the fact there was differences between numerical airfoil used for the aerodynamic optimization and the real manufactured wing airfoil scanned at high resolution by the IAR-NRC team. In addition, there was insufficient information on the wind tunnel calibration such as turbulence rate.

Based on the issues observed during this research over the past four years, the following recommendations can be made for future work:

Within the current configuration, if the actuator falls down, it could damage the linear position sensor. A redesign of the actuator integrating the linear position sensor in the screw axis would be a safety measure for the possible damage of this sensor.

A wave-like deformation of the skin was observed due to the punctual actuation, according to the post-processed data of a wing scan. An array of actuators or a bar placed between two actuators could improve the final morphing wing shape quality.

The actual control architecture integrated within the voltage amplifier allows using only linear control for the torque and position based on encoder as feedback signal. Based on our goal of developing and testing different control methods, it would be interesting to configure the voltage amplifier in the current (torque) mode and to develop a different control algorithm for the position control based on the encoder. This newly-designed controller could be deployed in the real-time system.

ANNEXE I   PRESSURE COEFFICIENT (Cp) VS. PERCENTAGE OF CHORD (X/C)

Figure-A-I 1 Pressure coefficient comparison flight case 2

Figure-A-I 2 Pressure coefficient comparison flight case 43

Figure-A-I 3 Pressure coefficient comparison flight case 78
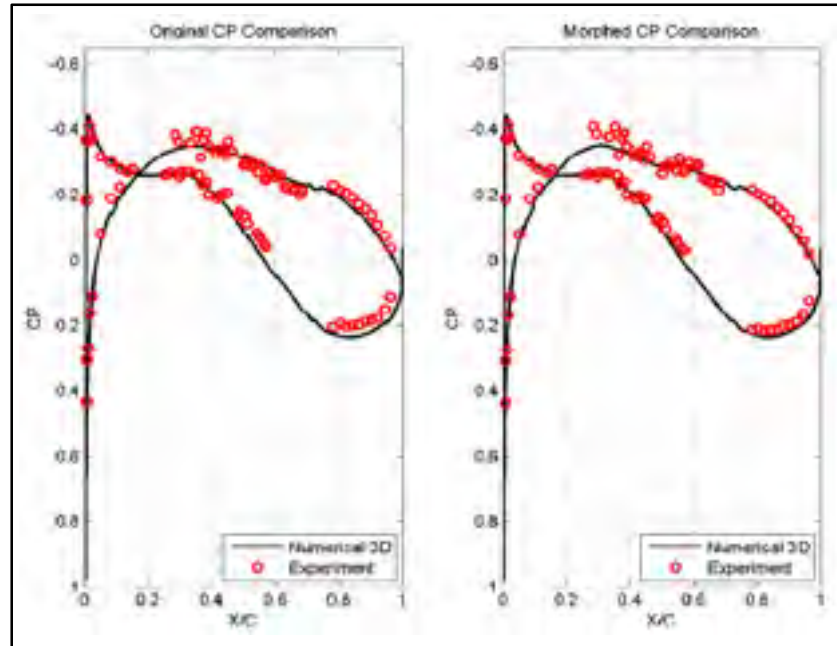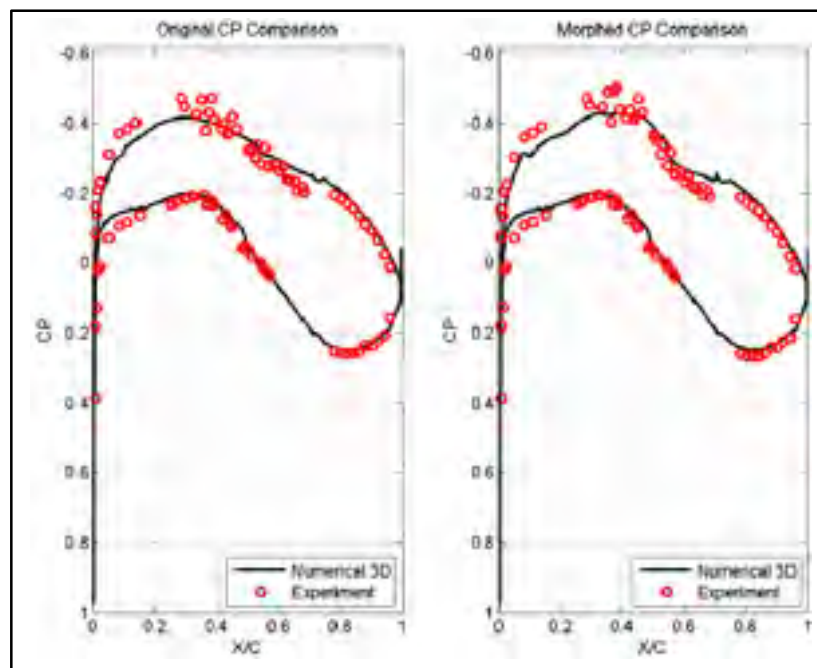

Figure-A-I 4 Pressure coefficient comparison flight case 25

Figure-A-I 5 Pressure coefficient comparison flight case 57

Figure-A-I 6 Pressure coefficient comparison flight case 65

ANNEXE II   TRANSITION POSITION MEASURED

Table A-II 1 Transistion point position determined
with pressure sensors (Morphed case)

Flight Cases	Chord position(%) FFT Morphed	Chord position (%) Rms Morphed	Average transition Morphed
cas 4	41,37%	45,16%	43,26%
cas 18	53,45%	55,71%	54,58%
cas 25	41,37%	43,62%	42,49%
cas 38	39,11%	42,45%	40,78%
cas 40	43,62%	53,45%	48,54%
cas 41	45,16%	54,60%	49,88%
cas 42	41,37%	54,60%	47,98%
cas 43	42,45%	50,79%	46,62%
cas 44	42,45%	45,16%	43,81%
cas 45	41,37%	43,62%	42,49%
cas 47	55,71%	67,72%	61,71%
cas 68	52,70%	54,60%	53,65%
cas 69	50,79%	53,45%	52,12%
cas 70	50,04%	53,45%	51,75%
cas 71	43,62%	45,16%	44,39%
cas 72	43,62%	50,79%	47,21%
cas 80	37,54%	42,45%	40,00%

Table A-II 2 Transistion point position determined
with pressure sensors (non-morphed case)

Flight Cases	Chord position(%) FFT non morphed	Chord position (%) Rms non morphed	Average transition non morphed
cas 4	45,16%	50,04%	47,60%
cas 18	50,04%	54,60%	52,32%
cas 25	42,45%	45,16%	43,81%
cas 38	37,54%	43,62%	40,58%
cas 40	42,45%	45,16%	43,81%
cas 41	41,37%	45,16%	43,26%
cas 42	41,37%	45,16%	43,26%
cas 43	37,54%	43,62%	40,58%
cas 44	37,54%	42,45%	40,00%

cas 45	37,54%	41,37%	39,45%
cas 47	56,87%	62,84%	59,85%
cas 68	43,62%	45,16%	44,39%
cas 69	43,62%	45,16%	44,39%
cas 70	41,37%	45,16%	43,26%
cas 71	39,11%	43,62%	41,37%
cas 72	37,54%	38,25%	37,89%
cas 80	33,41%	37,54%	35,47%

Table A-II 3 Transistion point position determined
with infrared measurements (Morphed and non-morphed case)

Flght Cases	Infra Red morphed	Infra Red non morphed
cas 4	49,54%	50,57%
cas 18	56,89%	53,18%
cas 25	44,89%	43,87%
cas 38	42,12%	41,24%
cas 40	50,67%	47,91%
cas 41	51,12%	48,32%
cas 42	50,44%	48,26%
cas 43	50,42%	47,29%
cas 44	47,65%	45,67%
cas 45	44,11%	43,82%
cas 47	64,95%	64,30%
cas 68	52,97%	51,02%
cas 69	52,13%	50,92%
cas 70	51,68%	49,35%
cas 71	50,76%	43,37%
cas 72	49,34%	42,69%
cas 80	40,39%	38,20%

ANNEXE III ACTUATOR DISPLACEMENTS

Figure-A-III 1 Flight case 1 2nd wind tunnel test (Actuator 1, 2)

Figure-A-III 2 Flight case 1 2nd wind tunnel test (Actuator 3, 4)

Figure-A-III 3 Flight case 2 2nd wind tunnel test (Actuator 1, 2)

Figure-A-III 4 Flight case 2 2nd wind tunnel test (Actuator 3, 4)

Figure-A-III 5 Flight case 10 2nd wind tunnel test (Actuator 1, 2)

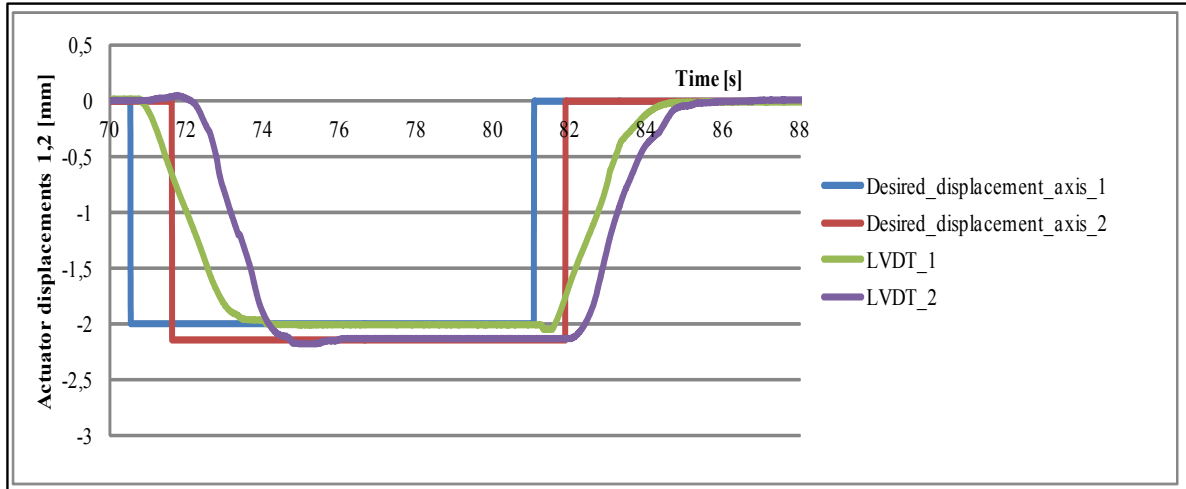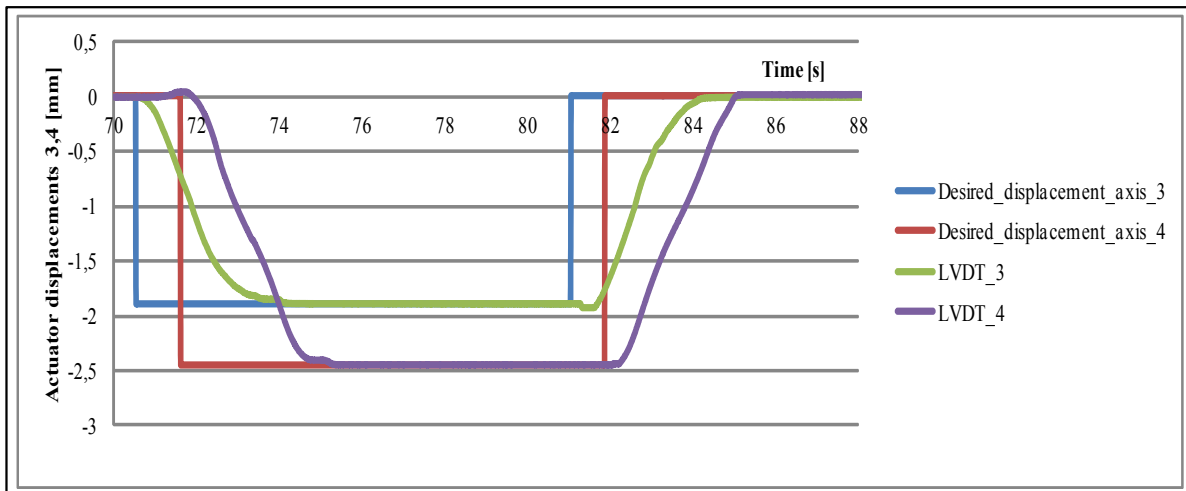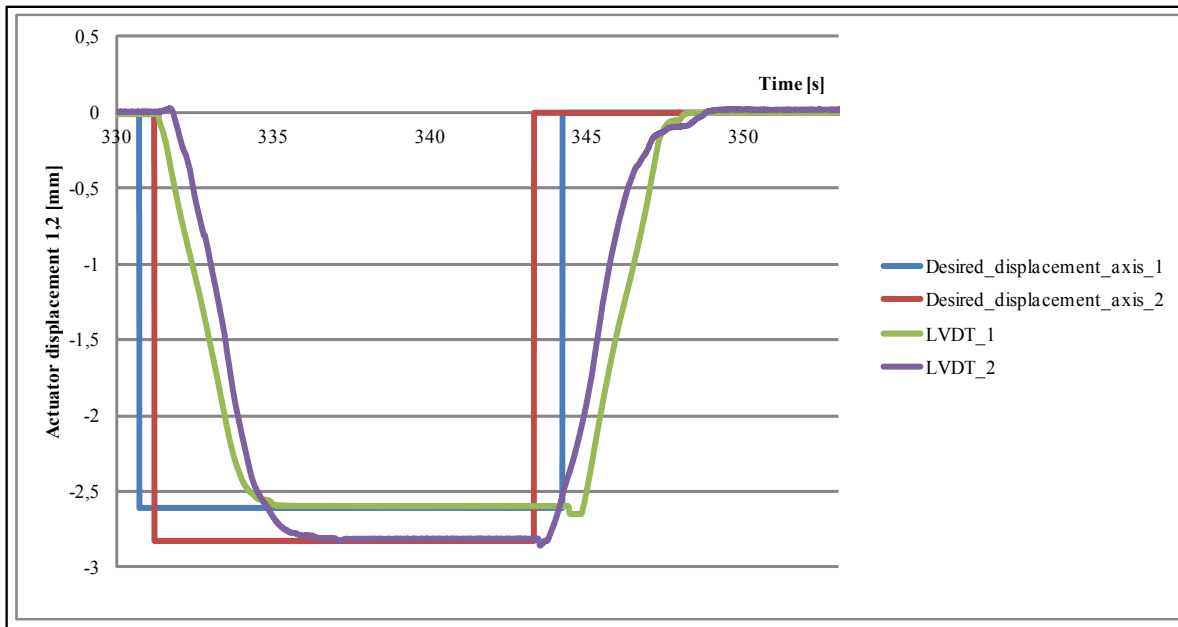Figure-A-III 6 Flight case 10 2nd wind tunnel test (Actuator 3, 4)
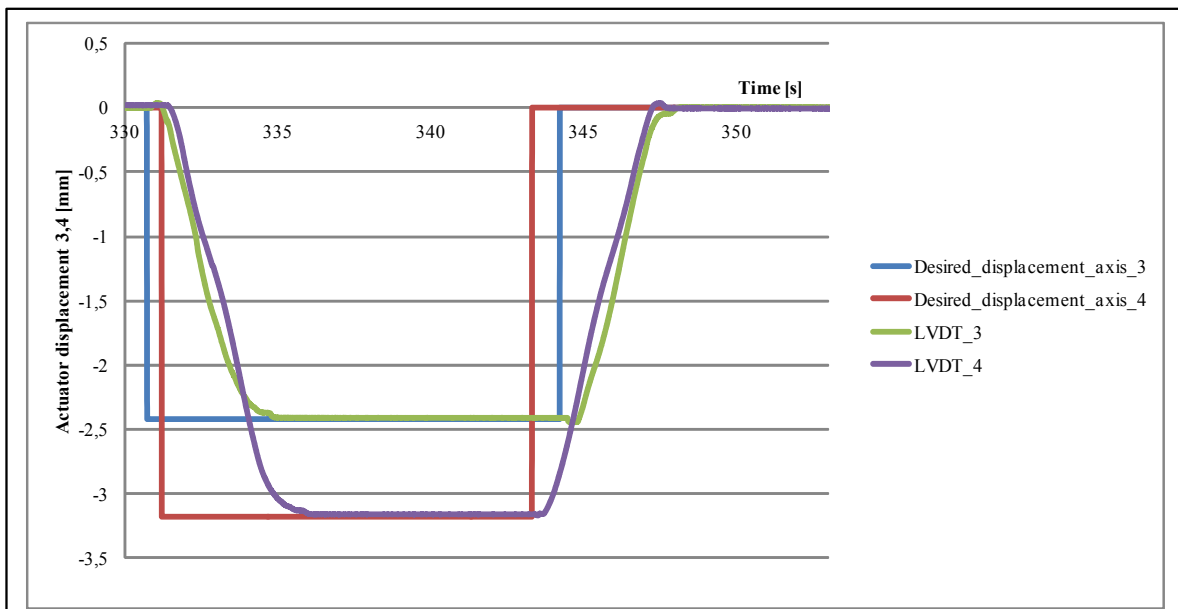
Figure-A-III 7 Flight case 8 2nd wind tunnel test (Actuator 1, 2)

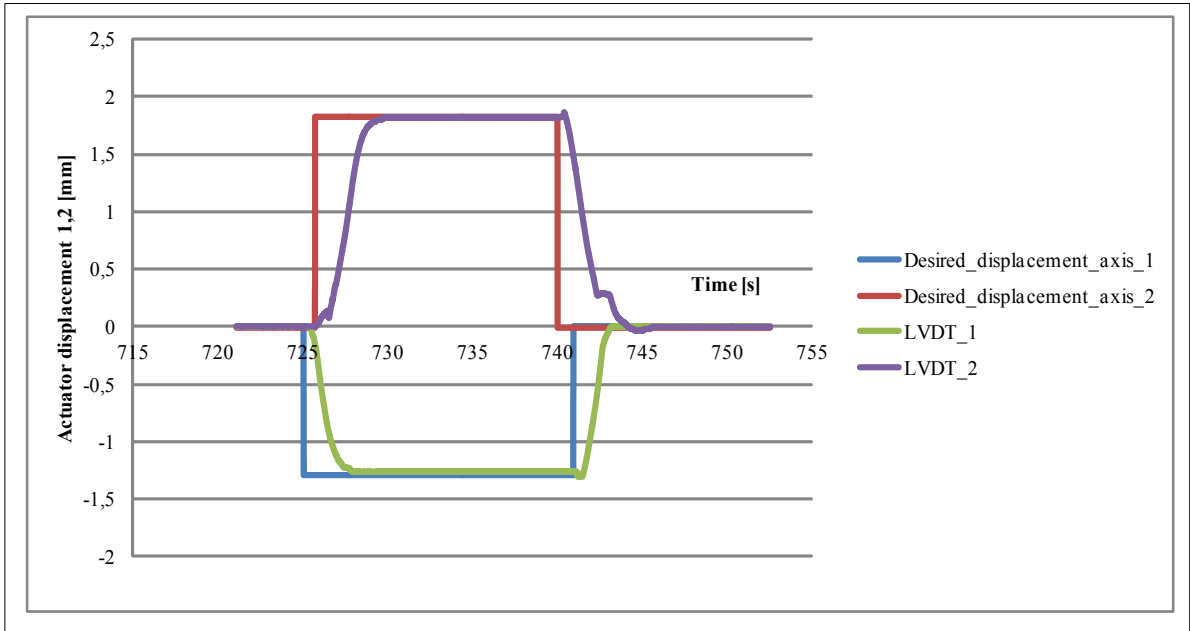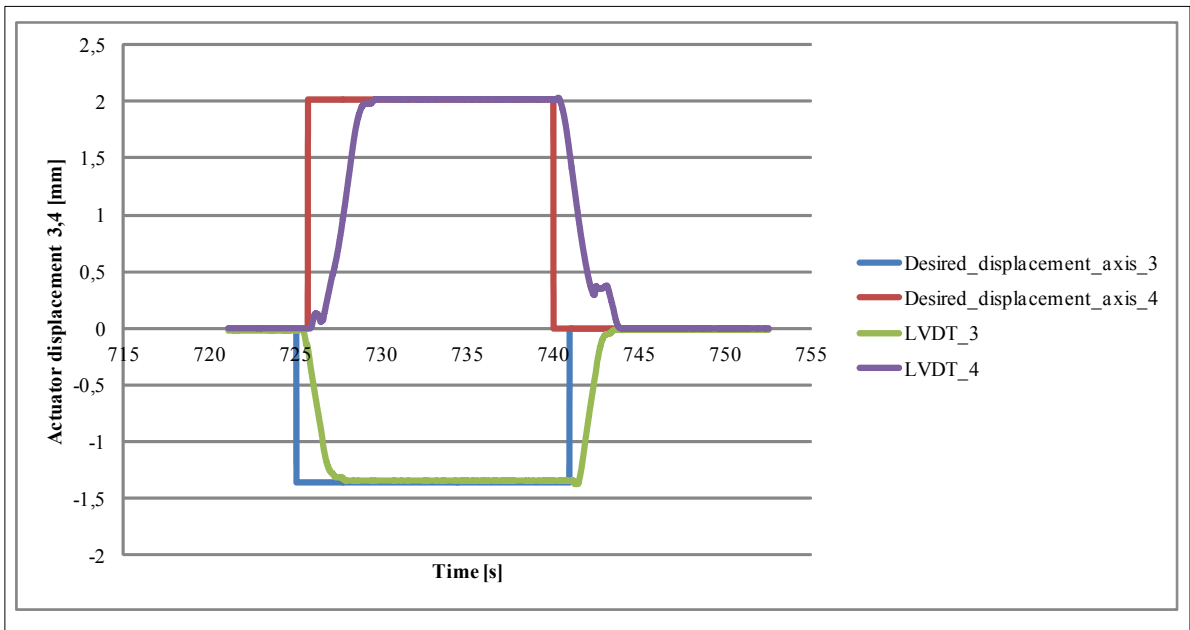Figure-A-III 8 Flight case 8 2nd wind tunnel test (Actuator 3, 4)

BIBLIOGRAPHY

Abe, S., M. Shoyama, S. Obata, T. Ninomiya and T. Zaitsu. 2011. « Pole-Zero-Cancellation Technique for DC-DC Converter », INTECH Open Access Publisher.

Abdullah, E. J., C. Bil and S. Watkins. 2009. « Design of adaptive airfoil control for unmanned aerial vehicles using smart materials ». SAE Technical Paper 2009-01-3272, 2009, doi:10.4271/2009-01-3272..

Abdullah, E. J., C. Bil and S. Watkins. 2009. « Application of smart materials for adaptive airfoil control ». 47th AIAA Aerospace Sciences Meeting Including The New Horizons Forum and Aerospace Exposition.

Abdullah, E., C. Bil and S. Watkins. 2010. « Numerical simulation of an adaptive airfoil system using SMA actuators ». 48th AIAA Aerospace Sciences Meeting Including the New Horizons Forum and Aerospace Exposition (AIAA 2010). (United states 4 - 7 January 2010), pp. 1-10.

Abdullah, E., C. Bil and S. Watkins. 2010. « Adaptive airfoil control system us ing shape memory alloy actuator for unmanned aerial vehicle ». Proceedings of the 21st Australasian Conference on the Mechanics of Structures and Materials. (Netherlands, 7 - 10 December 2010), pp. 141-146. Taylor and Francis publishers

Abdullah, E. J., C. Bil and S. Watkins. 2010. « Testing of adaptive airfoil for uav using shape memory alloy actuators ». 27th International Congress Of The Aeronautical Sciences (ICAS). (Nice, 19 - 24 September 2010)

Abdullah, E., C. Bil and S. Watkins. 2011. « Performance of adaptive airfoil control system using shape memory alloy actuators for UAV ». 11th AIAA Aviation Technology, Integration, and Operations (ATIO) Conference. (Virginia Beach, 20-22 September 2011)

Abdullah, E. J. 2011. « Control system design for a morphing unmanned air vehicle wing using shape memory alloy actuators ». Mémoire de doctorat en génie de fabrication, aérospatial et mécanique, RMIT University, 239 p.

Abdulrahim, M. and R. Lind. 2004. « Flight testing and response characteristics of a variable gull-wing morphing aircraft ». AIAA Guidance, Navigation, and Control Conference and Exhibit. (Rhode Island, 16-19 August 2004).

Alban Dignat : « Premiers vols des frères Wirght». < http://www.herodote.net/17_decembre_1903-evenement-19031217.php>. Consulté le 20 décembre 2015

212

Allison, D. O. and J. R. Dagenhart. 1978. « Design of a laminar-flow-control supercritical airfoil for a swept wing ». AIRCRAFT DESIGN, TESTING AND PERFORMANCE, (United Stated, 01 June 1978), p. 395-408

AMADOR, M. B. 2003. « MORPHING WING DESIGN FOR UAVs: A PROPOSED CONCEPT ». Mémoire de bachelor en génie mécanique et génie industriel, université de Toronto, 98 p

Ameduri, S. and R. Pecora. 2015. « A SMA-based morphing flap: conceptual and advanced design ». Smart Structures and Systems. Vol 16, No. 3, p 555-577.

Baker, D. and M. I. Friswell. 2008. « The design of morphing aerofoils using compliant mechanisms ». 19th international conference on adaptive structures and technologies. (Ascona, October 6-9, 2008)

Baldursson, S. 2005. « Bldc motor modelling and control-a matlab®/simulink® implementation ». Mémoire de maîtrise en génie électrique, Chalmers Tekniska Högskola

Barbarino, S., R. Pecora, L. Lecce, S. Ameduri and E. Calvi. 2009. « A novel SMA-based concept for airfoil structural morphing ». Journal of materials engineering and performance, vol.18, No. 5-6, p 696-705.

Barbarino, S., O. Bilgen, R. M. Ajaj, M. I. Friswell and D. J. Inman. 2011. «A review of morphing aircraft» Journal of Intelligent Material Systems and Structures, vol. 22, No. 9, p 823-877.

Barbarino, S., W. G. Dettmer and M. I. Friswell. 2010. « Morphing trailing edges with shape memory alloy rods » Proceedings of 21st international conference on adaptive structures and technologies (ICAST). (Pennsylvania, October 4-6, 2010)

Benavides, J.C., and Correa, G. « Morphing Wing Design Using Nitinol Wire ». Intelligent Systems Center Research Journal. Vol. 3, No. 1, p. 1–39.

Bil, C., K. Massey and E. J. Abdullah. 2013. « Wing morphing control with shape memory alloy actuators ». Journal of Intelligent Material Systems and Structures, vol.24, No.7, p 879-898.

Bilgen, O., K. Kochersberger and D. Inman. 2009. « Macro-fiber composite actuators for a swept wing unmanned aircraft ». Aeronautical Journal, vol.113, No.1144, p 385-395.

Bilgen, O., K. B. Kochersberger, D. J. Inman and O. J. Ohanian III. 2009. « Novel, Bi-Directional, Variable Camber Airfoil via Macro-Fiber Composite Actuators ». Journal of Aircraft, Vol. 47, No. 1, p. 303-314.

Bilgen, O., K. B. Kochersberger, D. J. Inman and O. J. Ohanian III. 2010. « Macro-fiber composite actuated simply supported thin airfoils » Smart Materials and Structures, vol. 19, No. 5.

Bilgen, O., M. I. Friswell, K. B. Kochersberger and D. J. Inman. 2011. « Surface actuated variable-camber and variable-twist morphing wings using piezocomposites » Proceedings of 52nd AIAA/ASME/ASCE/AHS/ASC Structures, Structural Dynamics, and Materials. Denver, 4(7): 2011-2072.

Bilgen, O., K. B. Kochersberger and D. J. Inman. 2013. « Wing morphing design using macro-fiber composites ». In *Smart Composites: Mechanics and Design*, sous la dir. Rani Elhajjar , Valeria La Saponara , and Anastasia Muliana. p 169-212. CRC Press.

Blondeau, J., J. Richeson and D. J. Pines. 2003. « Design, development and testing of a morphing aspect ratio wing using an inflatable telescopic spar » 44th AIAA/ASME/ASCE/AHS/ASC Structures, Structural Dynamics, and Materials Conference, (Norfolk).

Botez, R. M., P. Molaret and E. Laurendeau. 2007. « Laminar flow control on a research wing project presentation covering a three year period ». En ligne. < https://www.researchgate.net/publication/228618924_Laminar_flow_control_on_a_research_wing_project_presentation_covering_a_three_year_period , consulté le 14/04/2016

Bye, D. R. and P. D. McClure. 2007. « Design of a morphing vehicle ». 48th AIAA Structures, Structural Dynamics, and Materials Conference. (Honolulu, April 23-26, 2007)

Campanile, L. and D. Sachau. 2000. « The belt-rib concept: a structronic approach to variable camber ». Journal of Intelligent Material Systems and Structures vol. 11, No. 3, p 215-224.

Chowdhary, P. V. and R. S. Pant. 2010. « Application of optimization techniques in the conceptual design of morphing aircraft ». Proceedings of 13th AIAA/ISSMO Multidisciplinary Analysis Optimization Conference. (Fort Worth, September 13-15, 2010)

Coutu, D., V. Brailovski, P. Terriault and C. Fischer. 2007. « Experimental validation of the 3D numerical model for an adaptive laminar wing with flexible extrados ».

214

Proceedings of the 18th International Conference of Adaptive Structures and Technologies. (Ottawa, October 3-5. 2007)

Coutu, D., V. Brailovski and P. Terriault. 2009. « Promising benefits of an active-extrados morphing laminar wing ». Journal of Aircraft, vol 46, No. 2, p 730-731.

Coutu, D., V. Brailovski and P. Terriault. 2010. « Optimized design of an active extrados structure for an experimental morphing laminar wing ». Aerospace Science and Technology, vol 14, No.7, p 451-458.

Coutu, D., V. Brailovski, P. Terriault, M. Mamou and Y. Mebarki. 2011. « Aerostructural model for morphing laminar wing optimization in a wind tunnel ». Journal of Aircraft, vol. 48, No. 1, p 66-76.

Da Costa Aleixo, P. M. M. 2007. « Morphing aircraft structures design and testing an experimental UAV ». Mémoire de maîtrise en génie aérospacial, Instituto Superior Tecnico, Universidade Tecnica de Lisboa, Lisbon. p. 65.

De Gaspari, A. and S. Ricci 2011. « A two-level approach for the optimal design of morphing wings based on compliant structures ». Journal of Intelligent Material Systems and Structures, vol. 22, No. 10, p 1091-1111.

Debiasi, M., Y. Bouremel, H. H. Khoo and S. C. Luo. 2012. « Deformation of the upper surface of an airfoil by macro fiber composite actuators ». 31st AIAA Applied Aerodynamics Conference, Fluid Dynamics. (San Diego, June 24-27)

Diaconu, C. G., P. M. Weaver and F. Mattioni. 2008. « Concepts for morphing airfoil sections using bi-stable laminated composite structure ». Thin-Walled Structures, vol. 46, No.6, p 689-701.

Dimino, I., D. Flauto, G. Diodati and R. Pecora. 2014. « Actuation system design for a morphing wing trailing edge ». Recent Patents on Mechanical Engineering, vol. 7, No. 2, p 138-148.

Diodati, G., S. Ricci, A. De Gaspari, F. Huvelin, A. Dumont and J.-L. Godard. 2013. « Estimated performance of an adaptive trailing-edge device aimed at reducing fuel consumption on a medium-size aircraft ». SPIE Smart Structures and Materials, (San Diego, March 10, 2013)

Do Vale, J. L., A. Leite, F. Lau and A. Suleman. 2011. « Aero-structural optimization and performance evaluation of a morphing wing with variable span and camber ». Journal of Intelligent Material Systems and Structures: doi:1045389X11416031.

Dorf, R. C. and R. H. Bishop. 1998. *Modern control systems*.8e édi, Addison-Wesley Longman, Inc, 849 p

Drela, M. (1989). XFOIL: An analysis and design system for low Reynolds number airfoils. Low Reynolds number aerodynamics, Springer: 1-12.

Drela, Mark. 2003. « Implicit Implementation of the Full en Transition Criterion ». In 21st AIAA Applied Aerodynamics Conference. (Orlando, Florida, USA

Elzey, D. M., A. Y. Sofla and H. N. Wadley. 2003. « A bio-inspired high-authority actuator for shape morphing structures ». Proceedings of the SPIE, Volume 5053, p. 92-100 (2003).

Falcão, L., A. A. Gomes and A. Suleman. 2011. « Aero-structural design optimization of a morphing wingtip ». Journal of Intelligent Material Systems and Structures, vol. 22, No. 10, p 1113-1124.

Franklin, G. F., J. D. Powell and A. Emami-Naeini. 1994. Feedback *control of dynamics systems*. Addison-Wesley.

Friswell, M. 2009. « The prospects for morphing aircraft ». Smart Structures and Materials (SMART'09).

Gabor, O. S., A. Koreanschi and R. M. Botez. 2012 . « Low-speed aerodynamic characteristics improvement of ATR 42 airfoil using a morphing wing approach ». IECON 2012-38th Annual Conference on IEEE Industrial Electronics Society, (Montreal, Quebec, Canada), p. 5451-5456. IEEE.

Gabor, O. Ş., A. Koreanschi, R. M. Botez, M. Mamou and Y. Mebarki 2016. « Numerical simulation and wind tunnel tests investigation and validation of a morphing wing-tip demonstrator aerodynamic performance ». Aerospace Science and Technology., vol. 53, p 136-153, March 2016, doi: 10.1016/j.ast.2016.03.014

Gamboa, P., P. Aleixo, J. Vale, F. Lau and A. Suleman. 2007. « Design and Testing of a Morphing Wing for an Experimental UAV ». Meeting Proceedings RTO-MP-AVT-146, (Neuilly-sur-Seine), p 1-30.

Gamboa, P., J. Vale, F. Lau and A. Suleman. 2009. « Optimization of a morphing wing based on coupled aerodynamic and structural constraints ». AIAA journal, vol. 47, no 9, p. 2087-2104

Georges, T., V. Brailovski, E. Morellon, D. Coutu and P. Terriault. 2009. «Design of shape memory alloy actuators for morphing laminar wing with flexible extrados ». ASME Journal of Mechanical Design, vol. 131, n°9.

Giovanni Bisignani. 2009, « IATA Technology Roadmap Report », En ligne. 50 p. https://www.iata.org/whatwedo/environment/Documents/technology-roadmap-

216

2009.pdf. Consulté le 26 mars 2016

Gomez, J. C. and E. Garcia. 2011. « Morphing unmanned aerial vehicles ». Smart Materials and Structures, vol. 20, No.10,

Gomis-Bellmunt, O. and L. F. Campanile. 2009. *Design rules for actuators in active mechanical systems*, Springer Science & Business Media. 205 p

Grigorie, T. and R. Botez. 2009. « Adaptive neuro-fuzzy inference system-based controllers for smart material actuator modelling ». Proceedings of the Institution of Mechanical Engineers, Part G: Journal of Aerospace Engineering, vol. 223, No. 6, p 655-668.

Grigorie, T., R. Botez and A. Popov. 2012. « Design and experimental validation of a control system for a morphing wing ». AIAA Atmospheric flight mechanics conference, (Minneapolis, August 13-16 2012).

Grigorie, T., R. Botez and A. Popov. 2013. « How the airfoil shape of a morphing wing is actuated and controlled in a smart way ». Journal of Aerospace Engineering vol. 28, No. 1, http://dx.doi.org/10.1061/(ASCE)AS.1943-5525.0000372

Grigorie, T., R. Botez, A. Popov, M. Mamou and Y. Mebarki. 2011. « An Intelligent Controller based Fuzzy Logic Techniques for a Morphing Wing Actuation System using Shape Memory Alloy ». 52nd AIAA/ASME/ASCE/AHS/ASC Structures, Structural Dynamics and Materials Conference, (Denver, April 4-7 2011)

Grigorie, T., A. Popov and R. Botez. 2014. « Control strategies for an experimental morphing wing model ». AIAA Atmospheric Flight Mechanics (AFM) Conference, (Atlanta, June 2014)

Grigorie, T., A. Popov, R. Botez, M. Mamou and Y. Mébarki. 2011. « Controller and Aeroelasticity Analysis for a Morphing Wing ». AIAA Atmospheric Flight Mechanics (AFM) Conference. (Portland, August 08-11 2011)

Grigorie, T., A. Popov, R. Botez, M. Mamou and Y. Mébarki. 2011. « A New Morphing Wing Mechanism Using Smart Actuators Controlled by a Self-Tuning Fuzzy Logic Controller ». AIAA Centennial of Naval Aviation Forum" 100 Years of Achievement and Progress". (Virginia, September 21-22 2011)

Grigorie, T., A. Popov, R. Botez, M. Mamou and Y. Mébarki 2011. « On–off and proportional–integral controller for a morphing wing. Part 1: Actuation mechanism and control design ». Proceedings of the Institution of Mechanical Engineers, Part G: Journal of Aerospace Engineering, vol. 226, no 2, p. 131-145.

Grigorie, T., A. Popov, R. Botez, M. Mamou and Y. Mébarki. 2012. « On–off and proportional–integral controller for a morphing wing. Part 2: Control validation–numerical simulations and experimental tests » Proceedings of the Institution of Mechanical Engineers, Part G: Journal of Aerospace Engineering, vol. 226, no 2, p. 146-162.

Grigorie, T. L. and R. Botez. 2010. « Adaptive Neuro-Fuzzy Inference Controllers for Smart Material Actuators ». 51st AIAA/ASME/ASCE/AHS/ASC Structures, Structural Dynamics, and Materials Conference, (Orlando April 12-15 2010)

Grigorie, T. L. and R. M. Botez 2010. « Neuro-Fuzzy Controller for SMAs for a morphing wing application ». 51st AIAA Structures, Structural Dynamics and Materials Conference. (Orlando April 12-15 2010)

Grigorie, T. L. and R. M. Botez. 2010. « New adaptive controller method for SMA hysteresis modelling of a morphing wing » Aeronautical Journal, vol 114, No.1151, p. 1-13

Grigorie, T. L., R. M. Botez and A. V. Popov. 2009. « Adaptive neuro-fuzzy controllers for an open-loop morphing wing system » Proceedings of the Institution of Mechanical Engineers, Part G: Journal of Aerospace Engineering, vol 223, No. 7, p 965-975.

Grigorie, T. L., R. M. Botez, A. V. Popov, M. Mamou and Y. Mébarki 2012. « A hybrid fuzzy logic proportional-integral-derivative and conventional on-off controller for morphing wing actuation using shape memory alloy-Part 1: Morphing system mechanisms and controller architecture design » Aeronautical Journal, vol. 116, No. 1179, p 433.

Grigorie, T. L., R. M. Botez, A. V. Popov, M. Mamou and Y. Mébarki 2012. « A hybrid fuzzy logic proportional-integral-derivative and conventional on-off controller for morphing wing actuation using shape memory alloy, Part 2: Controller implementation and validation ». The Aeronautical Journal vol. 116, No.1179, p 451-465.

Grigorie, T. L., A. Popov and R. Botez 2013. « Control of Actuation System Based Smart Material Actuators in a Morphing Wing Experimental Model » AIAA Atmospheric Flight Mechanics (AFM) Conference. DOI:10.2514/6.2013-4918

Grigorie, T. L., A. V. Popov and R. M. Botez 2012. *Fuzzy logic control of a smart actuation system in a morphing wing*, INTECH Open Access Publisher.

Grigorie, T. L., A. V. Popov, R. M. Botez, M. Mamou and Y. Mébarki 2010. « A Morphing Wing used Shape Memory Alloy Actuators New Control Technique with Bi-positional and PI Laws Optimum Combination-Part 1: Design Phase ». Proceedings of the 7th International Conference on Informatics in Control, Automation and Robotics. (Madeira, June 15-18 2010)

Grigorie, T. L., A. V. Popov, R. M. Botez, M. Mamou and Y. Mébarki. 2011. *Design and experimental validation of a combined PI and Bi-positional laws controller for delaying the transition from laminar flow to turbulent flow over a morphing wing*. Informatics in Control, Automation and Robotics, vol 89, Springer, p 51-76.

Grigorie, T. L., A. V. Popov, R. M. Botez, M. Mamou and Y. Mébarki. 2011. « Smart concepts for actuation system and its control in a morphing wing ». 13th National Conference Caius Iacob in Fluid Mechanics and Technological Applications, INCAS, Bucharest, Roumanie.

He, Y. and S. Guo 2012. « Modeling and experiment of a morphing wing integrated with a trailing edge control actuation system ». Chinese Journal of Mechanical Engineering, vol.25, No. 2, p 248-254.

Heryawan, Y., H. C. Park, N. S. Goo, K. J. Yoon and Y. H. Byun. 2005. « Design and demonstration of a small expandable morphing wing ». Proceedings of the SPIE, Volume 5764, p. 224-231 (2005).

Hutapea, P., J. Kim, A. Guion, C. Hanna and N. Heulitt. 2008. « Development of a smart wing ». Aircraft Engineering and Aerospace Technology, vol. 80, No.4, p 439-444.

Irwin, J., M. P. Kazmierkowski, R. Krishnan and F. Blaabjerg 2002. *Control in power electronics*: selected problems, Academic press.

Janocha, H. 2013. *Actuators: basics and applications*, Springer Science & Business Media. 336 p.

Jayantha, A. S. (1998). «Spectral analysis of pressure fluctuations on bluff bodies placed in turbulent flows», Mémoire de doctorat en genie mécanique, Université technique du Texas,168 p.

Jha, A. K. and J. N. Kudva (2004). « Morphing aircraft concepts, classifications, and challenges » Smart structures and materials, International Society for Optics and Photonics.

Joo, J. J., B. Sanders, T. Johnson and M. I. Frecker. 2006. « Optimal actuator location within a morphing wing scissor mechanism configuration ». Smart Structures and

Materials 2006: Modeling, Signal Processing, and Control. Edited by Lindner, Douglas K. Proceedings of the SPIE, Vol. 6166, pp. 24-35.

Kammegne, M., S. Khan, L. Grigorie and R. Botez. 2015. « New methodology for the controller of an electrical actuator for morphing a wing ». 23nd AIAA/ASME/AHS Adaptive Structures Conference, Science and Technology Forum. (Kissimmee Janvier 5-9 2015)

Kammegne, M. J. T., H. Belhadj, D.-H. Nguyen and R. M. Botez. 2015. « Nonlinear Control Logic for an Actuator to Morph a Wing: Design and Experimental Validation ». IASTED Modelling, Identification and Control Conference. (Innsbruck, Février 2015)

Kammegne, M. J. T., R. M. Botez and T. L. Grigorie. 2016. « Actuation mechanism control in a morphing application with a full-scaled portion of an aircraft wing ». IASTED Modelling, Identification and Control Conference. (Innsbruck, Février 2016)

KAMMEGNE, M. J. T., R. M. BOTEZ, M. MAMOU, Y. MEBARKI, A. KOREANSCHI, O. S. GABOR and T. L. GRIGORIE. « Experimental wind tunnel testing of a new multidisciplinary morphing wing model ». En ligne 8p. http://www.wseas.us/e-library/conferences/2016/venice/MAMUA/MAMUA-14.pdf. Consulté le 14 avril 2016.

Kammegne, M. J. T., L. T. Grigorie and R. M. Botez. 2015. « Design, numerical simulation and experimental testing of a controlled electrical actuation system in a real aircraft morphing wing model ». Aeronautical Journal. Vol.119, No. 1219.

Kammegne, M. J. T., L. T. Grigorie, R. M. Botez and A. Koreanschi. 2014. « Design and Validation of a Position Controller in the Price-Paidoussis Wind Tunnel ». IASTED Modeling, Simulation and Control Conference. (Innsbruck, Février 2014).

Kammegne, M. J. T., L. T. Grigorie, R. M. Botez and A. Koreanschi 2016. « Design and wind tunnel experimental validation of a controlled new rotary actuation system for a morphing wing application ». Proceedings of the Institution of Mechanical Engineers, Part G: Journal of Aerospace Engineering. Vol. 230, No. 1, p 132-145.

Kammegne, M. J. T., D.-H. Nguyen, R. M. Botez and T. Grigorie 2015. « Control validation of a morphing wing in an open loop architecture ». 21st AIAA Modeling and Simulation Technologies Conference, Aviation Forum. (Dallas Juin 22-26 2015)

Koreanschi, A., O. Ş. Gabor, T. Ayrault, R. M. Botez, M. Mamou and Y. Mebarki. 2016. « Numerical Optimization and Experimental Testing of a Morphing Wing with Aileron System » 24th AIAA/AHS Adaptive Structures Conference.(San Diego, Janvier 04-08 2016)

Koreanschi, A., O. Sugar-Gabor and R. M. Botez. 2015. « Numerical and Experimental Validation of a Morphed Wing Geometry Using Price-Païdoussis Wind Tunnel Testing ». 33rd AIAA Applied Aerodynamics Conference. (Dallas, Juin 26 2015)

Kota, S., R. Osborn, G. Ervin, D. Maric, P. Flick and D. Paul. 2009. « Mission adaptive compliant wing–design, fabrication and flight test » RTO Applied Vehicle Technology Panel (AVT) Symposium.

Kovacic, Z. and S. Bogdan. 2005. *Fuzzy controller design: theory and applications,* CRC press.

Krishnan, R. 2001. *Electric motor drives: modeling, analysis, and control*, Prentice Hall.

Krishnan, R. 2009. *Permanent magnet synchronous and brushless DC motor drives*, CRC press.

LeBeau, R., A. Karam, N. Pern and J. Jacob. 2010. « Analysis of low speed flow over an adaptive airfoil with oscillating camber ». 48th AIAA Aerospace Sciences Meeting Including the New Horizons Forum and Aerospace Exposition. (Orlando Janvier 4-7 2010)

Lee, D., K. Srinivas, J. Periaux and E. Oñate. 2012. « Shock-Free Aerofoil/Wing Design Optimisation via Morphing Technique: Leading and Trailing Edge Deformation ». 7th International Conference on Computational Fluid Dynamics. p. 1-10

Leonhard, W. 2001. *Control of electrical drives*, Springer Science & Business Media.

Li, J. and H. Harada. 2013. « Modeling of an SMA actuator based on the Liang and Rogers model » International Journal of Applied Electromagnetics and Mechanics, Vol. 43, No. 4, p 325-335.

Li, M., J. Yuan, D. Guan and W. Chen. 2011. « Application of piezoelectric fiber composite actuator to aircraft wing for aerodynamic performance improvement ». Science China Technological Sciences, Vol. 54, No. 2, p 395-402.

Lim, S. M., S. Lee, H. C. Park, K. J. Yoon and N. S. Goo, 2005. « Design and demonstration of a biomimetic wing section using a lightweight piezo-composite actuator (LIPCA) ». Smart Materials and Structures, Vol. 14, No. 4, p 496.

LU, X.-l., L. Hu, G.-l. WANG and W. Zhe. 2006. « Helicopter sizing based on genetic algorithm optimized neural network ». Chinese Journal of Aeronautics, vol.19, No. 3, p 212-218.

Mahfouf, M., D. Linkens and S. Kandiah. 1999. « Fuzzy Takagi-Sugeno Kang model predictive control for process engineering ». Model Predictive Control: Techniques and Applications. (London,1999), p 4/1-4/4

Majji, M., O. K. Rediniotis and J. L. Junkins. 2007. « Design of a morphing wing: modeling and experiments ». Proceedings of the AIAA Atmospheric Flight Mechanics Conference and Exhibit, Hilton Head, South Carolina, USA.

Martins, A. L. and F. M. Catalano. 1998. « Viscous drag optimization for a transport aircraft mission adaptive wing ». Prog. 21st ICAS Congress, (Melbourne, September 13-18, 1998).

Mason, W. H., H. Robertshaw and D. J. Inman. 2004. « Recent experiments in aerospace and design engineering education ». 42nd AIAA Aerospace Science Meeting and Exhibit. (Reno January 5-8, 2004).

McGowan, A.-M. R., W. K. Wilkie, R. W. Moses, R. C. Lake, J. L. Pinkerton-Florance, C. D. Weiseman, M. C. Reaves, B. K. Taleghani, P. H. Mirick and M. L. Wilbur. 1998. « Aeroservoelastic and structural dynamics research on smart structures conducted at NASA Langley Research Center ». 5th Annual International Symposium on Smart Structures and Materials, International Society for Optics and Photonics. (San Diego Juin 1998)

Michaud, F., S. Joncas and R. Botez. 2013. « Design, Manufacturing and Testing of a Small-Scale Composite Morphing Wing ». 19th International Conference on Composite Materials. (Montréal, July 28-2 August 2013).

Miller, S. J. 2011. « Adaptive wing structures for aeroelastic drag reduction and loadsalleviation ». Mémoire de doctorat en génie mécanique, université de Manchester

Min, Z., V. K. Kien and L. J. Richard. 2010. « Aircraft morphing wing concepts with radical geometry change ». The IES Journal Part A: Civil & Structural Engineering, vol. 3, No. 3, p 188-195.

Mirone, G. 2007. « Design and demonstrators testing of adaptive airfoils and hingeless wings actuated by shape memory alloy wires ». Smart structures and systems, vol. 3, No. 1, p 89-114.

Mohan, N. 2012. *Power electronics: a first course*, 1st ed, Wiley. 288 p.

Monner, H. P., H. Hanselka and E. J. Breitbach. 1998. « Development and design of flexible fowler flaps for an adaptive wing ». 5th Annual International Symposium on Smart Structures and Materials, International Society for Optics and Photonics. (San Diego, Juin 16 1998)

Moosavian, A., F. Xi and S. M. Hashemi. 2013. « Design and motion control of fully variable morphing wings ». Journal of aircraft, vol. 50, No. 4, p 1189-1201.

Mosbah, A. B., M. F. Salinas, R. Botez and T.-m. Dao. 2013. « New Methodology for Wind Tunnel Calibration Using Neural Networks-EGD Approach » SAE International Journal of Aerospace, vol. 6, No. 2, p 761-766.

Munday, D. and J. Jacob. 2001. « Active control of separation on a wing with conformal camber ». 39th AIAA, Aerospace Sciences Meeting and Exhibit. (Reno Janvier 8-11 2001).

Munday, D. and J. Jacob. 2002. « Active control of separation on a wing with oscillating camber » Journal of aircraft, vol. 39, No. 1, p 187-189.

Neal, D., B. Akle and T. Hesse. 2003. « Optimal flight control of an adaptive aircraft wing modeled by NeuroFuzzy techniques ». Intelligent Control. 2003 IEEE International Symposium on, IEEE. (Houston, Octobre 8 2003)

Neal, D. A., M. G. Good, C. O. Johnston, H. H. Robertshaw, W. H. Mason and D. J. Inman. 2004. « Design and wind-tunnel analysis of a fully adaptive aircraft configuration ». 45th Proceedings of AIAA/ASME/ASCE/AHS/ASC SDM, (Palm Springs Avril 19-22 2004).

Ogata, K. 2001. *Modern control engineering*, 4th ed, Prentice Hall.

Ogata, K. 2008. *Matlab for control engineers*, Pearson Prentice Hall.

Paraskevopoulos, P. 2001. *Modern control engineering*, CRC Press. 736 p.

Pecora, R., F. Amoroso, G. Amendola and A. Concilio. 2014. « Validation of a smart structural concept for wing-flap camber morphing ». Smart Structures and Systems, Vol.14, No. 4, p 659-678.

Pecora, R., S. Barbarino, L. Lecce and S. Russo. 2011. « Design and functional test of a morphing high-lift device for a regional aircraft ». Journal of Intelligent Material Systems and Structures, Vol. 22, No. 10, p 1005-1023.

Pecora, R., M. Magnifico, F. Amoroso and E. Monaco. 2014. « Multi-parametric flutter analysis of a morphing wing trailing edge ». Aeronautical Journal, vol. 118, No. 1207, p 1063-1078.

Pendleton, E. W., D. Bessette, P. B. Field, G. D. Miller and K. E. Griffin. 2000. « Active aeroelastic wing flight research program: technical program and model analytical development ». Journal of Aircraft, vol. 37, No. 4, p 554-561.

Perera, M. and S. Guo. 2009. « Optimal design of an aeroelastic wing structure with seamless control surfaces ». Proceedings of the Institution of Mechanical Engineers, Part G: Journal of Aerospace Engineering, vol. 223, No. 8, p 1141-1151.

Perera, M., Y. He and S. Guo. 2010. « Structural and dynamic analysis of a seamless aeroelastic wing ». Proceedings of the 51st AIAA/ASME/ASCE/AHS/ASC structures, structural dynamics, and materials conference. (Orlando, Avril 12-16 2010).

Perkins, D. A., J. L. Reed Jr and E. Havens. 2004. « Adaptive wing structures ». Smart Structures and Materials. (San Diego, March 2004).

Pern, N. and J. Jacob.1999. « Aerodynamic flow control using shape adaptive surfaces ». Proc. 1999 ASME Design Engineering Technical Conferences (Las Vegas, Septembre 12-16 1999).

Phillips, C. L. and R. D. Habor. 1995. *Feedback control systems*, Simon & Schuster.

Poonsong, P. 2004. « Design and analysis of a multi-section variable camber wing ». Mémoire de maîtrise en génie aérospacical, Université de Maryland, 97 p.

Popov, A. V., R. M. Botez and M. Labib. 2008. « Transition point detection from the surface pressure distribution for controller design ». Journal of Aircraft, vol. 45, No. 1, p 23-28.

Popov, A. V., L. T. Grigorie, R. M. Botez, M. Mamou and Y. Mebarki. 2010. « Closed-loop control validation of a morphing wing using wind tunnel tests ». Journal of Aircraft, vol. 47, No. 4, p 1309-1317.

Popov, A. V., L. T. Grigorie, R. M. Botez, M. Mamou and Y. Mébarki. 2010. « Real time morphing wing optimization validation using wind-tunnel tests ». Journal of Aircraft, vol. 47, No. 4, p 1346-1355.

Popov, A. V., T. L. Grigorie, R. M. Botez, Y. Mébarki and M. Mamou. 2010. « Modeling and testing of a morphing wing in open-loop architecture ». Journal of Aircraft, vol. 47, No. 3, p 917-923.

Powers, S. G., L. D. Webb, E. L. Friend and W. A. Lokos. 1992. « Flight test results from a supercritical mission adaptive wing with smooth variable camber ». En ligne.

224

31   p.   http://www.nasa.gov/centers/dryden/pdf/88274main_H-1855.pdf.
    Consulté le 14 Avril 2015

Previtali, F. and P. Ermanni. 2012. « Performance of a non-tapered 3D morphing wing with
    integrated compliant ribs ». Smart materials and structures, vol. 21, No. 5.

Prock, B. C., T. A. Weisshaar and W. A. Crossley. 2002. « Morphing airfoil shape change
    optimization with minimum actuator energy as an objective ». (Atlanta, Sept. 4-
    6 2012)

Ray, C. W., B. A. Batten and J. R. Singler. 2011. « A model based feedback controller for
    wing-twist via piezoceramic actuation ». American Control Conference, 2011,
    IEEE.

Ray, C. W., J. R. Singler and B. A. Batten. 2010. *Feedback control of a bioinspired plate-
    beam system.*

Rioual, J.-L., P. Nelson and M. Fisher. 1994. « Experiments on the automatic control of
    boundary-layer transition ». Journal of aircraft, vol. 31, No. 6, p 1416-1418.

Rodriguez, A. R. 2007. « Morphing aircraft technology survey ». 45th AIAA aerospace
    sciences meeting and exhibit. (Reno, Jan. 8-11 2007)

Roth, B. and W. A. Crossley. 2003. « Application of optimization techniques in the
    conceptual design of morphing aircraft ». 13th AIAA/ISSMO Multidisciplinary
    Analysis Optimization Conference, (Forth Worth Sept.13 - 15 2010)

Roudbari, A. and F. Saghafi. 2014. « Intelligent modeling and identification of aircraft
    nonlinear flight ». Chinese Journal of Aeronautics, vol. 27, No. 4, p 759-771.

RW, W., H. GC, M. AR, P. SL, S. MA, S. RJ and S. JO 1998. « The Aircraft Morphing
    Program ». 39th Structures, Structural Dynamics and Materials Conference and
    Exhibit, (Long Beach April 20-23 1998)

Saggere, L. and S. Kota. 1999. « Static shape control of smart structures using compliant
    mechanisms ». AIAA journal, vol. 37, No. 5, p 572-578.

Sainmont, C., I. Paraschivoiu and D. Coutu, 2009. « Multidisciplinary approach for the
    optimization of a laminar airfoil equipped with a morphing upper surface ». In
    AVT168 NATO Symposium on the Morphing Vehicles. (Evora, Portugal, April
    20-23 2008)

Sainmont, C., I. Paraschivoiu, D. Coutu, V. Brailovski, É. Laurendeau, M. Mamou, Y.
    Mébarki, M. Khalid. 2009. « Boundary Layer Behaviour on a Morphing Airfoil:
    Simulation and Wind Tunnel Tests ». In Canadian Aeronautics and Space

Institute AERO'09 Conference: Aerodynamics Symposium. (Kanata, Ontario, May 7-9 2009).

Sanders, B., F. Eastep and E. Forster 2003. « Aerodynamic and aeroelastic characteristics of wings with conformal control surfaces for morphing aircraft ». Journal of Aircraft, vol. 40, No. 1, p 94-99.

Seow, A., Y. Liu and W. Yeo 2008. « Shape Memory Alloy as Actuator to Deflect a Wing Flap ».49th AIAA/ASME/ASCE/AHS/ASC Structures, Structural Dynamics and Materials Conference(Schaumburg April 7-10 2008)

Sobieczky, H. and W. Geissler. 1999. « Active flow control based on transonic design concepts » AIAA Paper 99-3127

Sobieczky, H., W. Geissler and M. Hannemann. 1999. « Expansion shoulder bump for wing section viscous/wave drag control ». FLOWCON IUTAM Symposium on Mechanics of Passive and Active Flow Control

Sofla, A., S. Meguid, K. Tan and W. Yeo. 2010. « Shape morphing of aircraft wing: status and challenges ». Materials & Design, vol. 31, No. 3, p 1284-1292.

Sommerer, A., T. Lutz and S. Wagner. 2000. « Design of adaptive transonic airfoils by means of numerical optimisation ». Proceedings of ECCOMAS.(Barcelona, Sept. 11-14 2000)

Sommerer, A., T. Lutz and S. Wagner. 2000. « Numerical optimisation of adaptive transonic airfoils with variable camber ». Proceedings of the 22nd International Congress of the Aeronautical Sciences.

Song, G. and N. Ma. 2007. « Robust control of a shape memory alloy wire actuated flap ». Smart materials and Structures, Vol. 16, No. 6.

Sridhar, K., R. Osborn, G. Ervin, P. Flick and D. Paul. 2006. « Mission Adaptive Compliant Wing–Design, Fabrication and Flight Test ». En ligne. 19 p. https://static1.squarespace.com/static/54946b7fe4b04a99c2e3353a/t/5499eb6ce4b0b2582e0c8e47/1419373420162/NATO+Conf+Paper-KOTA.pdf. Consulté le 14 April 2016

Stanford, B., M. Abdulrahim, R. Lind and P. Ifju. 2007. « Investigation of membrane actuation for roll control of a micro air vehicle ». Journal of Aircraft, vol. 44, No. 3, p 741-749.

Stanewsky, E. 2001. « Adaptive wing and flow control technology» Progress in Aerospace Sciences, vol. 37, No. 7, p 583-667.

Strelec, J. K., D. C. Lagoudas, M. A. Khan and J. Yen. 2003. « Design and implementation of a shape memory alloy actuated reconfigurable airfoil ». Journal of Intelligent Material Systems and Structures, vol. 14, p 257-273.

Suzuki, H., K. Rinoie and A. Tezuka. 2010. « Laminar airfoil modification attaining optimum drag reduction by use of airfoil morphing ». Journal of Aircraft, vol. 47, No. 4, p 1126-1132.

Terriault, P. and V. Brailovski. 2011. « Modeling of shape memory alloy actuators using Likhachev's formulation ». Journal of Intelligent Material Systems and Structures: 1045389X11401450.

Tran, D.-M. and C. Liauzun. 2006. *Frequency and time domain fluid-structure coupling methods for turbomachineries. Unsteady Aerodynamics, Aeroacoustics and Aeroelasticity of Turbomachines*, Springer: p. 397-408.

Tutty, O., P. Hackenberg and P. Nelson. 2000. « Numerical optimization of the suction distribution for laminar flow control » AIAA journal, vol. 38, No. 2, p 370-372.

Ursache, N. M., A. J. Keane and N. W. Bressloff. 2006. « On the design of morphing airfoils using spinal structures ». 47th AIAA/ASME/ASCE/AHS/ASC Structures, Structural Dynamics, and Materials Conference. (Newport, May 1-4 2005).

Usher, T. D., K. R. Ulibarri and G. S. Camargo. 2013. « Piezoelectric microfiber composite actuators for morphing wings ». ISRN Materials Science. Vol. 2013, 8 p.

Vos, R., R. Barrett, R. de Breuker and P. Tiso. 2007. « Post-buckled precompressed elements: a new class of control actuators for morphing wing UAVs ». Smart materials and structures, Vol. 16, No. 3.

Wadehn, W., A. Sommerer, T. Lutz, D. Fokin, G. Pritschow and S. Wagner. 2002. « Structural concepts and aerodynamic design of shock control bumps ». En ligne. 10 p. http://www.icas.org/ICAS_ARCHIVE/ICAS2002/PAPERS/P14.PDF. Consulté le 14 April 2016

Weisshaar, T. A. 2006. Morphing aircraft technology-new shapes for aircraft design, . Meeting Proceedings RTO-MP-AVT-141, Overview 1, (Neuilly-sur-Seine, 2006)

Wikipedia, 2016, En ligne. <https://en.wikipedia.org/wiki/Bell_X-5> Consulté le 22 mars 2016.

Wikipedia, 2016, En ligne. <https://en.wikipedia.org/wiki/Grumman_F-14_Tomcat> Consulté le 22 mars 2016.

Xia, C.-l. 2012. *Permanent magnet brushless DC motor drives and controls*, John Wiley & Sons.

Xu, Y.-M., L. Shuo and X.-M. Rong. 2005. « Composite structural optimization by genetic algorithm and neural network response surface modeling ». Chinese Journal of Aeronautics, Vol. 18, No. 4, p 310-316.

Yuan, R. and B. Guangchen. 2011. « New neural network response surface methods for reliability analysis » Chinese Journal of Aeronautics, Vol. 24, No. 1, p 25-31.

Zadeh, L. A. 1978. « Fuzzy sets as a basis for a theory of possibility ». Fuzzy sets and systems, Vol. 1, No. 1, p 3-28.

Zhao, K., J. P. Schmiedeler and A. P. Murray 2012. « Design of planar, shape-changing rigid-body mechanisms for morphing aircraft wings ». Journal of Mechanisms and Robotics, Vol. 4, No. 4, p 041007.

Ziegler, J. G. and N. B. Nichols. 1942. « Optimum settings for automatic controllers ». Transactions of the American Society of Mechanical Engineers, Vol. 64, No. 8, pp. 759–768.

Zingg, D. W., L. Diosady and L. Billing 2006. « Adaptive airfoils for drag reduction at transonic speeds ». AIAA paper, vol. 3656